NUCLEATION AND GROWTH OF SILVER SULFIDE NANOPARTICLES

by

Madeline S. León Velázquez

A dissertation submitted in partial fulfillment of the requirements for the degree of

DOCTOR OF PHILOSOPHY
in
Applied Chemistry

UNIVERSITY OF PUERTO RICO
MAYAGUEZ CAMPUS
2010

Approved by:

_____   _____
Nairmen Mina, Ph.D.   Date
Member, Graduate Committee

_____   _____
Mayra E. Cádiz, Ph.D.   Date
Member, Graduate Committee

_____   _____
Roberto Irizarry, Ph.D.   Date
Member, Graduate Committee

_____   _____
O. Marcelo Suárez, Ph.D.   Date
Member, Graduate Committee

_____   _____
Miguel Castro-Rosario, Ph.D.   Date
President, Graduate Committee

_____   _____
Jeannette Santos, Ph.D.   Date
Representatives of Graduate Studies

_____   _____
Francis Patron, Ph.D.   Date
Chairperson of the Department

ABSTRACT

The synthesis of metal and semiconductor nanoparticles has received widespread attention by the scientific community due to the large number of technological applications they find in nanoscaled systems. The mechanism of nanoparticle nucleation and growth is, in general, still an open question. We have employed transmission electron microscopy (TEM), scanning tunneling microscopy (STM), configuration interaction single calculations (CIS) and real time conductivity and UV-visible absorption measurements of stopped flows of $AgNO_3$ and $(NH_4)_2S$ to study the nucleation and growth for the formation of silver sulfide nanoparticles (Ag_2S NP).

Ionic conductivity measurements provide qualitative information related to the process occurring in the early stages of the reaction but does not provide information related to the identity and chemistry of the clusters or embryos chemistry. These conductivity measurements suggest the formation of non stoichiometric ionic Ag_2S species, rather of neutral Ag_2S, in the early stages of the reaction mixture. Comparison of the calculated absorptions spectra on several silver sulfide clusters with the optical absorption spectra of reaction mixtures obtained in the early stages of the reaction lead us to conclude that the dependence of the optical absorption spectra on time in the first few milliseconds after the flow stops is consistent with formation of AgS^- and Ag_3S^+ cluster ions. Bands that can be attributed to the formation of larger silver sulfide clusters – including Ag_4S_2 and Ag_6S_3 - are observed at longer reaction times: large amounts of the surfactant sodium bis(2-ethylhexyl) sulfosuccinate (AOT) inhibite the nucleation process and stabilize the D_4h Ag_2S_4 cluster.

The UV-visible absorption measurements at longer times revealed that the nucleation and growth process are not well separated in time. The initial nucleation and growth rates are found to increase with initial $[AgNO_3]_0/[(NH_4)_2S]_0$ ratios larger than 1. Silver ions play a central role in the nucleation and growth process. The experimental results suggest that silver-rich-sulfides are involved in the nucleation stage and growth process of Ag_2S NP.

RESUMEN

La síntesis de nanopartículas de metales y semiconductores ha recibido una amplia atención por la comunidad científica debido a la gran cantidad de aplicaciones en la tecnológia de estos sistemas a nanoescala. Sin embargo, el mecanismo de nucleación y crecimiento de nanopartículas sigue siendo una pregunta abierta. Hemos empleado microscopia de transmisión de electrones (TEM), cálculos de interacción de interacción (CIS), microscopia de rastreo de tunelaje (STM), medidas de conductividad y de absorción UV-visible en tiempo real para estudiar la nucleación y crecimiento de la formación de nanopartículas de sulfuro de plata (Ag_2S). Las nanopartículas de Ag_2S son preparadas usando un reactor que permite un mezclado homogéneo de los reactivos iniciales, $AgNO_3$ y $(NH_4)_2S$.

 Las medidas de conductividad iónica proveen información cualitativa relacionada con el proceso que ocurre en las primeras etapas de la reacción, pero no aporta información relacionada con la identidad y química de los aglomerados o embriones. Estas medidas de conductividad sugieren la formación de especies iónicas no estequiométricas de Ag_2S, en lugar de Ag_2S neutrales, en las primeras etapas de la reacción. Comparación de los cálculos teóricos de las estructuras de varios aglomerados de sulfuro de plata con los espectros de absorción óptica de las mezclas de reacción obtenidos en las primeras etapas de la reacción nos llevan a concluir que la dependencia de los espectros de absorción óptica en el tiempo para los primeros milisegundos después de que detiene el flujo son consistentes con la formación de los aglomerados iónicos, AgS^- y Ag_3S^+. Las bandas que se puede atribuir a la formación de grandes aglomerados de sulfuro de plata, incluyendo Ag_4S_2 y Ag_6S_3, se observan en los tiempos de reacción más largos. En adición grandes cantidades del surfactante bis (2-etilhexil) sulfosuccinato de sodio (AOT) inhibe el proceso de nucleación y estabiliza el aglomerado Ag_4S_2 de geometría D_{4h}.

Las medidas de absorción UV-visible en tiempos más largos revelan que el proceso de nucleación y crecimiento no están bien separados en tiempo. Se encontró que la rapidez inicial de nucleación y el crecimiento aumentan cuando la razón de

concentración de los reactivos, $[AgNO_3]_0/[(NH_4)_2S]_0$, es mayor de 1. Los iones de plata desempeñan un papel central en el proceso de nucleación y crecimiento. Los resultados experimentales sugieren que los sulfuros ricos en plata están involucrados en la etapa de nucleación y el proceso de crecimiento de Ag_2S NP.

To My Parents and Sister: Mami, Papi y Marie.
Thanks for your support, your faith in me, your inspiration, your example and strength, for always accompanied me and never leave alone, most of all for your unconditional love. You're the most important persons in my life.
I Love you.

ACKNOWLEDGEMENTS

During my graduate studies in the University of Puerto Rico several persons and institutions collaborated directly and indirectly with my research. Without their support it would be impossible to finish my work. That is why I wish to dedicate this section to recognize their support.

I want to start to thank, first, GOD for always carry me and guide during these years as a graduate student.

My love and respect to my parents and sister I could not have done it without you; and to my aunts and my nieces for the love and encouragement. Thanks for being so special in my life, and for your unconditional support, inspiration and love. Last but not least to Maripí, Frances, Sheila, Sary and Brenda thanks for being my best friends since forever.

I would like to express my sincere gratitude to my advisor; Dr. Miguel E. Castro because he gave me the opportunity to be part of his research group and for his support and guidance for the completion of my dissertation.

My appreciation to my co-advisor; Dr. Roberto Irizarry to open the doors of his laboratory in DuPont Microcircuits Technologies and gave me the opportunity to complete my internship with him, as well for his advice and collaboration during these years.

To my graduate committee: Dr. Mayra Cádiz, Dr. O. Marcelo Suarez and Dr. Nairmen Mina; thanks for you scientific advice, support and confidence in me during this stage of my life.

In addition during my time as graduate student I have the privilege to interact with many persons that enrich my life and fill it with science, laughter, love and friendship. Thank you for made this experience a wonderful journey.

To my lab coworkers and friends: Edmy, Marissa, Eunice, Raquel, Priscila, Miguel, Danny, Sariann, Natasha, Mariana, Wilnia, Zuleyka, Kasandra and Steven. Thanks for always be there for me, help me with the investigation work and for the science I learn from you. In addition I'm appreciative for the hours working hand to hand with you; my work was easier and my research experience amusing because of you.

To my dear friends: Yessenia, Debora, Elvin, Cacimar, Alberto, Yahaira, Leslie and Lolo. Thank you for been my accomplices and share with me the experience of a new beginning. Love you guys!!!!!!!!!!!!

Thanks to my family and friends of SONW and López Lab; especially Ramonita, Samirah, Rosalie, Mario, Carlos R., Carlos N., Rafael, Elddie, Gardy, Ingrid, Daria, Héctor, Josiris, David and Priscila. You are the best.

To my family in North Carolina: Huma, Cludy, Claudia, Laura, Carmen, Olga, Tita and Angel. Your friendship and company is and always will be a blessing. I love you with all my heart.

To my friends in the beauty department: Norma, Jeniffer, Sharon, Patricia, Stella, Ivanna and Viviana; thanks for help me look beautiful in the outside as well as in the inside and for more than a decade of friendship and laugher.

I can't finish my acknowledgments without mentioning two extraordinary persons that help me in a difficult moment of my life, Debora and Dora. I always will be grateful for the company, support and advice.

TABLE OF CONTENTS

TABLE LIST

FIGURE LIST

.

SCHEME LIST

CHAPTER I: INTRODUCTION TO DISSERTATION

Colloidal metal and semiconductor nanostructures find numerous technological applications in biomedicine, electronics, catalysis, sensors, and environmental remediation methods, among others. Although numerous efforts have been paid to understand the chemistry associated with the formation of nanostructures very little is known about the reactions that lead to nuclei formation and their subsequent reactions. In this dissertation we report on the reactions that lead to the formation of silver sulfide nanoparticles (Ag$_2$S NP) in solution: with the objective of (1) contributing to the development of methods to monitor nucleation and growth processes and (2) to provide a chemical perspective to the process of nanoparticles formation. In the context of classical nucleation theory, nanoparticle formation from the reactions among ions in solution maybe visualized as follows:
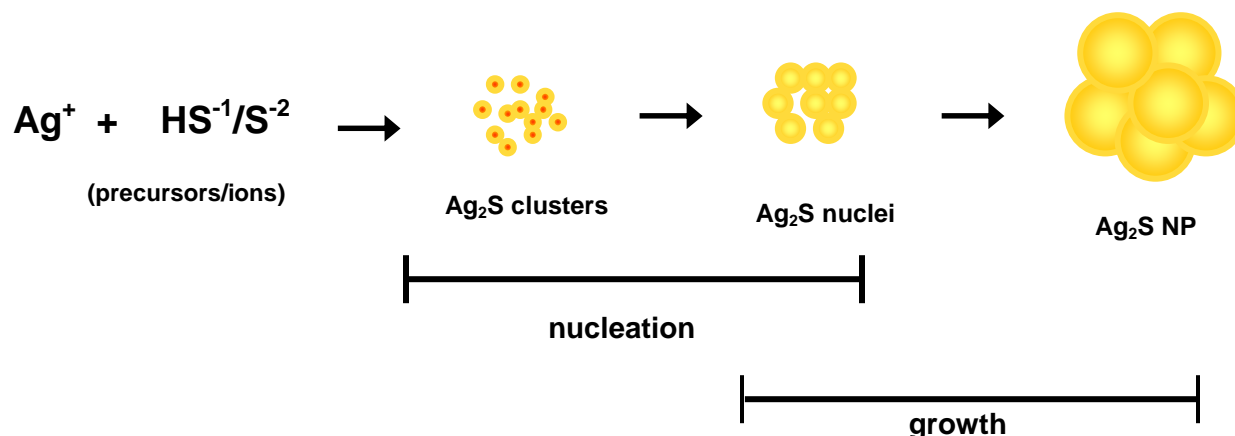
Scheme 1.1: Proposed mechanism for the formation for Ag$_2$S nanoparticles

The synthesis of silver sulfide nanoparticles has been performed by numerous methods, including the use of simple inorganic precursors to molecular beams and lithography. In this study we used a stop flow reactor that allows the formation of a homogeneous mixture of reactants in a flow prior to the reaction: it avoids the formation of concentrations gradients in the solution. AgNO$_3$ and (NH$_4$)$_2$S are used as the source of silver (Ag$^+$) and sulfide ions and (S^{-2}) ions. Even thought (NH$_4$)$_2$S is a strong electrolyte

that dissolve as $NH_4^+{}_{(aq)}$ and $S^{-2}{}_{(aq)}$ ions, the latter can be hydrolyzed to form $HS^-{}_{(aq)}$ and $H_2S_{(aq)}$ depending on the solution pH. The experimental pH value for this reaction mixture is 9.1, at this pH, HS^- is the most likely species in solution.

According to classical nucleation theory, the formation of nuclei is preceded by the formation of an embryonic phase. Little is known about this embryonic phase, although it is generally taken that is consists of clusters that are arranged spatially in such way to resemble the nuclei they are about to form. The lack of knowledge related to the chemistry of this embryonic phase likely results from the fast reactions in which these clusters are involved. We performed real time conductivity and UV-visible absorption measurements, discussed in chapters 4 [1] and 5 [2] respectively, with the hope of learning about the reactions that lead to the formation of these clusters in solution upon mixing the reactants. The conductivity of the solution decreases slightly while the optical absorption spectra experiences significant changes after a flow containing the reactants stops. The small decrease in conductivity is taken as evidence for a small reduction in the number of ions in solution: the amount of the decrease is too small to account for the formation of neutral Ag_2S molecules. Rather, non stoichiometric Ag_2S species - resulting in ionic forms of Ag_2S - are thought to be formed. Configuration interaction single calculations on structures of several silver sulfide clusters optimized at the density functional level were compared with the optical absorption spectra of reaction mixtures obtained in the early stages of the reaction. This comparison lead us to conclude that the dependence of the optical absorption spectra on time in the first few milliseconds after the flow stops is consistent with formation of AgS^- and Ag_3S^+ cluster ions. Bands that can be attributed to the formation of larger silver sulfide clusters – including Ag_4S_2 and Ag_6S_3 - are observed at longer reaction times. In an attempt to isolate and study the species formed in solution prior to nucleation, we studied the effect of a surfactant, AOT (sodium bis(2-ethylhexyl) sulfosuccinate), in the formation of Ag_2S NP. Large amounts of AOT were found to inhibit the nucleation process and stabilize a D_4h Ag_2S_4 cluster.

UV-visible absorption measurements at longer reaction times used to study the nucleation and growth of silver sulfide nanoparticles (Ag_2S NP) are discussed in chapter 6; [3]. Ag_2S NP in the size range of 2 to 10 nm are formed a few seconds after the flow containing the reactants stops. The absorbance near the band edge of the semiconductor nanoparticle is used to monitor the number of particles formed with time and study the nucleation process. Transmission electron microscopy measurements are used to correlate particle size and the indirect band gap energy, determined from the onset of light absorption. A linear relation is established between Ag_2S NP particle size and indirect band gap energy: this is one of the few examples that are now documented in the literature where such relation exists in the size range of the study. The nucleation and growth process are not well separated in time. The initial nucleation and growth rates are found to increase with initial $[AgNO_3]_0/[(NH_4)_2S]_0$ ratios larger than 1. Silver-rich-sulfides are proposed to be involved in the nucleation stage and growth process of Ag_2S NP. Density functional calculations are consistent with this interpretation: Ag_3S^+ is found to have a lower energy than the Ag_2S and AgSH molecules or the AgS^- and Ag_2SH^+ ions

1.1 References

1. León-Velázquez, M. S.; Morales, M.; Irizarry, R.; Castro, M. Conduction in Collodial Systems: A Kinetic Study of Ag_2S Semiconductor. Nanoparticles: Synthesis, Stabilization, Passivation, and Functionalization*, Chapter 15, **2008,** pp 203-213, *ACS Symposium Series*, Volume 996.

2. León-Velázquez, M. S.; Morales, M.; Carbo, M.; Sepúlveda, W.; González, M. Rivera, D.; Irizarry, R.; Castro, M. Inhibition of Ag_2S Nucleation by AOT micelles. Submitted to Materials Letters.

3. León-Velázquez, M.; Irizarry, R.; Castro-Rosario, M. Nucleation and Growth of Silver Sulfide Nanoparticles; *J. Phys. Chem. C*, **2010**, *114*, 5839–5849.

CHAPTER 2: PREVIOUS WORKS

The synthesis and properties of semiconductor particles in the size regime of a few to hundreds of angstroms continue to attract considerable interest in these days due to the impact they may have in the future scientific and technological developments. While excellent progress has been made in the preparation and characterization of materials such as CdS, CdSe, ZnO, and ZnS, very little is known about the properties of small Ag_2S species [1-4]. *Why Ag_2S is interesting?* Ag_2S nanostructures are a promising material for the development of nanoscaled and atomic switching devices with applications in random access memory (RAM) devices, cross bar electronic circuits, as well as fuel cells and batteries based on ionic conductors and H_2S sensing[5-9]. Additionally, the semiconductor silver sulfide, as well as other sulfide alkalines, has promising photoelectric and thermoelectric properties for application in the sensing of biological and chemical systems [10]. Recently Aono and coworkers report the investigation of the electrical properties of individual Ag_2S/Ag heteronanowires (HNWs) by atomic force microscopy (AFM) using a nanoscale-tip electrode. They proposed that reversible resistance switching originates from the creation and rupture of filament-like conducting pathways inside the Ag_2S/Ag HNW [9]. Watanabe and coworkers, on the other hand, performed theoretical calculations where they combine non-equilibrium Green's function technique with density functional theory, electron transport, and structural properties to study an Ag atomic switch through Ag_2S. They found that a spontaneous metallization at the Ag-Ag_2S interface may play an important role in fast switching of the Ag-Ag_2S atomic switch [5]. Despite this, little is known about the chemistry leading to the formation of Ag_2S nanostructures.

The synthesis methods for silver sulfide nanoparticles varies from biology paths [11], ligand and organometallics routes [10], reverse micelles [12] or by using more complicated instruments such as ultrafast photosynthesis [13]. The understanding of their chemistry have increased to the extent that some of them are available for purchase from companies over the world, although information related to chemicals employed in their synthesis is not disclosed of silver sulfide including physical and

chemical methods. One of the most popular physical methods uses molecular beam and lithography techniques obtaining well defined nanostructures [14]. On the other hand, chemical synthesis includes a wide variety of approaches that range from simple precipitation methods to non aqueous complex procedures.

F. Ruiz [15] and Y. Qian [16] used simple precipitation methods for the formation of the silver sulfide nanoparticles. F. Ruiz synthesized the metal sulfide nanoparticle by a precipitation reaction using ammonium sulfide solution with a mixture of silver nitrate solution and a cocktail of protective reagents that included Triton X-100 or 3-mercapto-1,2-propanediol under ambient conditions. These stabilizing agents were used in order to prevent particle growth and agglomeration. The particles obtained were characterized by scanning electron microscopy (SEM), X-ray diffraction (XRD), and transmission electron microscopy (TEM). Samples prepared in the absence of stabilizing agent were found to form the bulk semiconductor material faster than samples prepared in the presence of a stabilizing reactant.

Y. Qian [16] did not use stabilizing agents to control the size of the particles and the resultant particles were nanocrystalline. The Ag_2S particles were made by using trace amounts mol of sublimed sulfur powder in a NaOH aqueous solution to form the sulfide solution. A silver complex solution was prepared by simply dissolving $AgNO_3$ in aqueous ammonia creating a silver nitrate excess. A black precipitate results from the mixing that was filtered and washed with dilute acid HNO_3 followed by drying in vacuum. The characterization was performed by XRD, X-ray photoelectron spectroscopy (XPS) and TEM. The nanoparticle size was calculated by using the Scherrer equation. The above authors attributed the crystallization of the particles to the use of sulfur alkaline solution as the sources for the sulfide ion. The use of an alkaline solution produces two different reactions; the formation of a silver complex and the formation of the nanoparticles. These two reactions cause that the sulfide ion is liberated continuously making a change in the equilibrium of the nanoparticles reactive. In consequence the

silver ions in the complex reaction maintain an excess in the solution that induce crystallization. The estimated size of the synthesized particle was 28 nm.

Y. Ikushima [17] and coworkers produce the silver sulfide quantum dots in an aqueous environment by the reverse microemulsion method. The Ag_2S nanoparticles were synthesized by the reaction between the solutions of $AgNO_3$ and Na_2S in the hydrophilic section of a surfactant. The nanoparticle dispersion was stable for a long time and did not show aggregation or precipitation. The nanoparticles were characterized by the UV-vis spectrum, showing the silver surface plasmon at 330 nm, which was taken as indication of a quantum confined nanoparticles.

 P. Pileni [12] used reverse micelles for the synthesis of Ag_2S nanoparticles. Silver sulfide particles are obtained by mixing two micellar (surfactants) solutions with the same water content: one contains silver solution and the other sodium sulfide, Na_2S. The synthesis is performed at a range of water content. The nanosized particles were characterized by transmission electron microscopy.

S. H. Liu [10] has focused their investigation in the synthesis of silver sulfide nanoparticles using thiol related products as a reactive in the reaction. S. H. Liu synthesized the nanoparticles by dissolving the $AgNO_3$ in a mixture of hyperbranched polyurethane (HP) with N,N-dimethyl formamide (DMF). This mixture is then added to thioacetamide as the sulfur source. Based on TEM, XRD, UV-vis absorption measurements, the above authors concluded that nanoparticles had an average size of about 4-10 nm and a narrow size distribution attributed to the hyperbranched polyurethane used in the formation of the semiconductor nanosize particles.

T. G. Schaaff [18] reports the preparation of Ag_2S nanocrystals, using dodecanethiolate ligands. This type of ligand is proposed to bond to silver (I). Na_2S was added to solutions of $Ag(I)-C_{12}S$ and the formed nanoparticles were characterized with transmission electron microscopy and X-ray diffraction, and laser desorption ionization

mass spectrometry (LDIMS). The above author found that a nanocrystalline structure of about 5.4 nm is formed.

Z. Zhicheng [19] and collaborators developed a reaction method to synthesize metal sulfide (cadmium sulfide (CdS); silver sulfide (Ag_2S); and mercury sulfide (HgS)) nanoparticles. The procedure consists in adding a mixture of ethanol, silver nitrate and a salt solution of polivinylpyrrolidone (PVP) to carbon disulfide. X-ray diffraction, transmission electron microscope, and ultraviolet–visible spectrum revealed that organized metal sulfide nanoparticles can produce using PVP as guide reagent of crystal growth.

Gion Calzaferri [20] synthesized silver sulfide nanoparticles inside the cavities of sodium and calcium zeolite. The sodium and calcium zeolite were dispersed in a solution of silver nitrate to form a loaded zeolite. The zeolite –silver mixture is then exposed to H_2S gas. The nanoparticles were characterized by scanning electron microscopy (SEM) and X-ray powder diffraction (XRD). This is probably the most successful method for the preparation of Ag_2S dots reported in the literature to date. Nearly monodispersed particles were formed inside the pores of the zeolite as revealed by well defined fluorescence bands upon excitation with UV light.

A similar approach was employed by S. Gross [21] and coworkers, who synthesized the metal sulfide nanoparticles in silica. Silica composites containing embedded nanosized silver sulfide-crystallites by a sol–gel process. The systems were then characterized using different analytical tools, including X-ray photoelectron spectroscopy, X-ray-excited Auger electron spectroscopy (XE-AES), X-ray diffraction, secondary-ion mass spectrometry (SIMS), Rutherford backscattering spectrometry (RBS) and transmission electron microscopy. The above authors found that the use of sol-gel provides a good method of controlling both the average size of the nucleating clusters and their average size distribution of the nanoparticle in comparison with other synthesis routes.

R. Guo [22] and collaborators prepared silver sulfide (Ag_2S) nanoparticles by reaction of $AgNO_3$ and Na_2S in the lamellar liquid crystal (LLC) formed by Triton X-100, n-$C_{10}H_{21}OH$ and H_2O. Monodispersed particles, about 2–3 nm in diameter, were formed as determined from transmission electron microscope and X-ray diffraction measurements. Yi Xie, [23] on the other hand, prepared silver sulfide particles using Raney nickel with mixtures of analytically pure $AgNO_3$ and S powder and water. The precipitates were filtered with dilute HCl, ethanol and distilled water.

Other nanostructures based on Ag_2S have been prepared. X. Qian [24] synthesized hollow and concave Ag_2S nanocubes by the reaction of thioacetamide (TAA) and $AgNO_3$ in aqueous solution of carboxymethyl cellulose (CMC). X-ray diffraction, transmission electron microscope, scanning electron microscopy and ultraviolet–visible spectrum were used to characterize the obtained product. Castro and Hernandez [25] synthesized silver nanotubes from mixtures of silver nitrate and an alkyl thiol, a process that results in the formation of silver-sulfur links and have the characteristic $Ag{\leftarrow}S$ charge transfer band at 227 nm. The above authors were not able to point out that optical absorption spectroscopy to distinguish Ag_2S from the silver dimmer, Ag_2, which was proposed to make up the walls of the tubes.

Ya-Ping Sun [11] uses biological methods for the synthesis of the silver sulfide nanoparticles. For this experiment the researchers use bovine serum albumin protein (BSA) and conjugated the nanoparticles to it. The procedure is performed in a special experimental setup in where the solution of $AgNO_3$ in methanol is mixed with liquid ammonia. This solution is heated and converted in a supercritical solution. Then the solution is expanded via a silica capillary nozzle into an ambient aqueous Na_2S solution. The aqueous receiving solution contains BSA protein for conjugating with the Ag_2S nanoparticles produced in the rapid expansion process. UV/vis absorption, X-ray powder diffraction, transmission electron microscopy and atomic force microscopy (AFM) analysis were performed to characterize the nanozise material. The researchers found that the monodispersed nanoparticles in the conjugates are well-coated directly

with the protein. Because the protein undergoes solution pH-dependent association and dissociation, the protein-nanoparticle conjugates also assemble and disassemble with changes in solution pH in a reversible fashion.

In this dissertation we report on the synthesis and reactions that lead to the formation of silver sulfide nanoparticles (Ag_2S NP) in solution: with the objective of (1) contributing to the development of methods to monitor nucleation and growth processes and (2) to provide a chemical perspective to the process of nanoparticles formation.

2.2 References

1. Lakowicz, J. R.; Gryczynski, I.; Gryczynski, Z.; Murphy, C. J. Luminescence Spectral Properties of CdS Nanoparticles. *J. Phys. Chem. B,* **1999**, *103*, 7613-7620.

2. Murray, C. B.; Noms, D. J.; Bawendi, M. G. Synthesis and Characterization of Nearly Monodisperse CdE (E = **S,** Se, Te) Semiconductor Nanocrystallites. *J. Am. Chem. Soc.* **1993**, *115,* 8706-8715.

3. Mu, J.; Gu, D.; Xu, Z. Synthesis and stabilization of ZnS nanoparticles embedded in silica nanospheres. *Applied Physics A –Materials Science & Processing,* **2004.**

4. van Dijken, A.; Meulenkamp, E.A.; Vanmaekelbergh, D.; Meijerink, A. Identification of the transition responsible for the visible emission in ZnO using quantum size effects. Journal of Luminescence, **2000**, 90, 123-128.

5. Wang, Z.; Kadohira, T.; Tada, T.; Watanabe, S. Nonequilibrium Quantum Transport Properties of a Silver Atomic Switch., *Nano Lett.* **2007**, *7*, 2688-2692.

6. Liang, C.; Terabe, K.; Hasegawa, T.; Aono, M. Resistance Switching of an Individual Ag_2S/Ag Nanowire Heterostructure. *Nanotechnology*, **2007**, *18*, 485202-485207.

7. Akai-Kasaya, M.; Nishihara, K.; Saito, A.; Kuwahara, Y.; Aono, M. Quantum Point-Contact Switches Using Silver Particles. *Appl. Phys. Lett.* **2006**, *88*, 23107-23110.

8. Van Ruitenbeek, J. Device Physics: Silver Nanoswitch, *Nature* **2005**, *433*, 21-22.

9. Terabe, K.; Hasegawa, T.; Nakayama, T.; Aono, M. Quantized Conductance Atomic Switch. *Nature* **2005**, *433*, 47-50.

10. Liu, S. H.; Qian, X. F.; Yin, J.; Hong, L.; Wang, X. L.; Zhu, Z. K. Synthesis and Characterization of Ag_2S Nanocrystals in Hyperbranched Polyurethane at Room Temperature. *J Solid State Chem.* **2002**, *168*, 259-262.

11. Meziani, M. J; Sun,Y. Protein-Conjugated Nanoparticles from Rapid Expansion of Supercritical Fluid Solution into Aqueous Solution. *J. Am. Chem. Soc,* **2003**, *125*, 8015-8018.

12. Motte, L.; Pileni, M. P. Influence of Length of Alkyl Chains Used to Passivate Silver Sulfide Nanoparticles in Two- and Three-Dimensional Self-Organization. *J. Phys. Chem. B* **1998**, *102*, 4104-4109.

13. Brelle, M. C.; Zhang, J. Z.; Nguyen, L.; Mehra, R. K. Synthesis and Ultrafast Study of Cysteine- and Glutathione-Capped Ag_2S Semiconductor Colloidal Nanoparticles. *J. Phys. Chem. A,* **1999**, *103,* 10194-10201

14. Eychmüller, A. Structure and Photophysics of Semiconductor Nanocrystals. *J. Phys. Chem. B* **2000**, *104*, 6514-6528.

15. Martinez-Castañón, G. A.; Sanchez-Loredo, M. G.; Dorantes, H. J.;.Martinez-Mendoza, J. R; Ortega-Zarzoza, G.;. Ruiz, F. Characterization of Silver Sulfide Nanoparticles Synthesized by a Simple Precipitation Method. *Mater. Lett.* **2005**, *59*, 529-534.

16. Zhang, W.; Zhang, L.; Hui, Z.; Zhang, X.; Qian, Y. Synthesis of Nanocrystalline Ag_2S in Aqueous Solution. *Solid State Ionics.* **2000,** *130*, 111-114.

17. Liu, J.; Raveendran, P.; Shervania, Z.; Ikushima, Y. Synthesis of Ag_2S Quantum Dots in Water-in-CO_2 Microemulsions. *Chem. Commun.* **2004**, *22*, 2582-2583

18. Schaaff T. G.; Rodinone, A. J. Preparation and Characterization of Silver Sulfide Nanocrystals Generated from Silver (I)-Thiolate Polymers. *J. Phys. Chem. B* **2003,** *107,* 10416-10422.

19. Changqi, X.; Zhicheng, Z.; Qiang, Y. A Novel Facile Method to Metal Sulfide (Metal = Cd, Ag, Hg) Nano-Crystallite. *Mater. Lett.* **2004**, *58*, 1671-1676.

20. Brühwiler, D.; Leiggener, C.; Glaus, S.; Calzaferri, G. Luminescent Silver Sulfide Clusters. *J. Phys. Chem. B* **2002**, *106*, 3770-3777.

21. Armelao, L.; Bertoncello, R.; Cattaruzza, E.; Gialanella, S.; Gross, S.; Mattei, G.; Mazzoldie, P.; Tondelloa, E. Chemical and Physical Routes for Composite Materials Synthesis: Ag and Ag_2S Nanoparticles in Silica Glass by Sol-Gel and Ion Implantation Techniques. *J. Mater. Chem.* **2002**, *12*, 2401-2407.

22. Ding, Y.; Xu, B.; Guo, R.; Shen, M. The preparation of silver sulfide nanoparticles in lamellar liquid crystal and application to lubrication. *Materials Research Bulletin,* **2005**, *40,* 575–582.

23. Xiao, J.; Xie, Y.; Tang, R.; Luo, W. Template-based synthesis of nanoscale Ag_2E (E ~ S, Se) dendrites. *J. Mater. Chem.*, **2002**, *12*, 1148–1151.

24. Wu, M.; Pan, X.; Qian, X.; Yin, J; Zhu, Z. Solution-phase synthesis of Ag_2S hollow and concave nanocubes. *Inorganic Chemistry Communications* **2004**, *7*, 359–362

25. Hernandez, E. ; Posada, B.; Irizarry, R.; Castro, M..E. The role of hydrogen bonding interactions in directing one dimensional-thiol assisted growth of silver based nanofibers *J. Phys. Chem. B,* **2005**, *109,* 7251-7257

CHAPTER 3: EXPERIMENTAL METHODOLOGY

3.1 Synthesis, Characterization and Kinetics Studies of Ag_2S Nanoparticles

The silver solutions employed in the experiments described here was prepared by dissolving the appropriate amount of $AgNO_{3(s)}$ (ACS grade, Fisher) with deionized water, obtained from a Culligan water deionizing system. A 40 % ammonium sulfide, $(NH_4)_2S$, obtained from Alfa Aesar, was diluted with appropriate amounts of deionized water to generate the sulfide containing solutions employed in the mixing experiments described below. The concentration of all solutions employed in the experiments described in this work ranged between 8.0×10^{-2} M and 1.0×10^{-5} M. The mixing experiments were performed in a Biologic stopped-flow reactor model SFM 400. Figure 3.1 represents a simple schematic of the stopped-flow reactor which is intended to guide the readers through the discussion presented here.
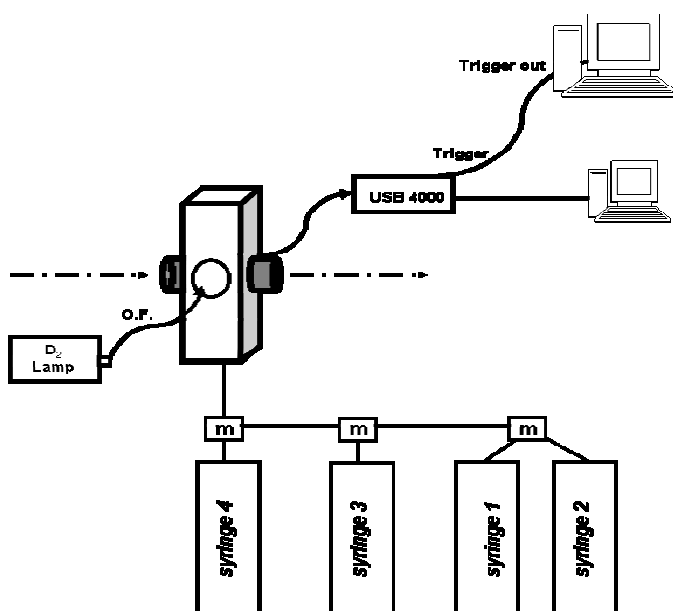
Figure 3.1: Schematic representation of the stopped-flow reactor.

The stopped flow reactor has capabilities to store up to four chemicals in syringes that are coupled to the mixing compartment. Each syringe has a maximum capacity of 10 milliliters. In the experiments described here, syringes 1 and 2 are filled with deionized water which is used to clean the system and dilute the reactants, while syringes 3 and 4 contain silver nitrate and ammonium sulfide solutions. The desired reactant volumes are admitted into the mixer with a minimum dead time of 2.4 milliseconds with a PC controlled injection system. The flow is brought to stop and the reactants mixed in the reaction cell. The reaction cell is made of quartz and allows for UV-visible absorption experiments to be carried out. A high pressure deuterium/ tungsten UV-visible lamp and an Ocean Optics spectrograph models PC 2000 and USB 4000 were employed for the light absorption measurements. UV grade fiber optics (Ocean Optics) are used to guide the light from the lamp and into the reaction cell with the help of a custom made fiber optic coupler placed in the reaction cell holder. A second UV grade fiber optic is used to guide the light transmitted thru the cell into the Ocean Optics spectrograph. Data acquisition by the Ocean Optics spectrograph is triggered by a signal output from the SFM 400 stopped-flow reactor.

The quartz cell is equipped with two carbon glass electrodes that allow for conductivity measurements to be performed. The carbon electrodes are placed perpendicular to the optical light path used in the light absorption measurements. The carbon glass electrodes have a surface area of about 1 mm^2 and are separated by about 1.5 mm, which corresponds to the cell width. Conductivity measurements are triggered by the internal software of the SFM 400 stopped flow reactor.

Transmission electron microscopy (TEM) measurements were performed in a JEOL 2010 model. Negatives of the micrographs were processed using standard techniques and scanned with an EPSON Perfection V750 PRO scanner and stored in the computer for further analysis. Scanning tunneling microscopy (STM) measurements were performed in a Nanosurf easyScan E-STM version 2.1 using a Pt/Ir tip. The STM was calibrated with measurements performed on a commercial gold ruler and with measurements performed on longitudinal features of dry deposits of C_{12}-SH and C_{10}-SH alkyl thiol monolayers that coincided with the expected molecular lengths of these molecules.

CHAPTER 4:

Conductivity measurements as a real time tool to monitor nanostructure synthesis in solution: kinetics considerations of Ag_2S nanostructure formation[29]

4.1 Introduction

Metal and semiconductor nanoparticles nucleation and growth has received widespread attention by the scientific community due to the central role it plays in the synthesis of nanoscaled structures with tailored optical and electronic properties [1-4]. Real time monitoring the formation and growth of nanostructures in situ remains a challenge. Kinetic measurements related to gold nanoparticle formation have relied on the position and structure of the plasmon absorption bands and Mie scattering theory to establish particle size growth kinetics [5-6]. On semiconductor quantum particles, like CdS, the band edge shift has been used to establish nanoparticle size and deduce details associated with the growth mechanism [7-9]. The mechanism of formation of non metallic silver clusters has also been established with light absorption measurements [10-12]. In these cases, the fingerprint associated with light absorption has been used to monitor the formation of particles in real time. In nanostructures that do not have a well established light absorption spectra, there are no simple methods to establish nanoparticle formation kinetics [13].

In this chapter, we present real time conductivity measurements on the formation of Ag_2S nanoparticles. Ag_2S is a semiconductor with important catalytic, optical and electronic properties [14-17]. Ag_2S nanoparticles have an interesting electronic structure and exhibit quantum size effects [18-19]. Ag_2S absorbs light deep in the UV and exhibits visible light fluorescence at low temperatures in the visible [20-26]. These optical properties require access to wavelengths below 300 nm to perform light absorption studies or cryogenic conditions to perform fluorescence measurements, which are not readily available in all laboratories. If successful, conductivity

measurements may be extended to systems that do not have suitable optical absorption bands or do not exhibit fluorescence.

We have focused in the synthesis of Ag_2S from the reaction of silver cations, Ag^+, with sulfide anions, HS^-/S^{-2} according to:

$$2\ Ag^+ + HS^{-1}/S^{-2} \rightarrow Ag_2S \qquad\qquad \textbf{equation 4.1}$$

because the reaction results in the reduction of the number of ions in solution and the formation of the silver sulfide semiconductor. Thus a decrease in conductivity is expected to be observed in reaction mixtures of Ag^+ and S^{-2} as they form Ag_2S.

4.2 Experimental

The silver solutions employed in the experiments described here was prepared by dissolving the appropriate amount of $AgNO_{3(s)}$ (ACS grade, Fisher) with deionized water, obtained from a Culligan water deionizing system. A 40 % ammonium sulfide, $(NH_4)_2S$, obtained from Alfa Aesar, was diluted with appropriate amounts of deionized water to generate the sulfide containing solutions employed in the mixing experiments described below. The concentration of all solutions employed in the experiments described here ranged between 8.0×10^{-2} M and 1.0×10^{-3} M.

A Biologic Stop flow reactor model SFM 400 was employed to prepare the silver sulfide nanoparticles. UV-visible absorption measurements were conducted in situ in a quartz cell. The cell is 5 mm x 7 mm in width and 23 mm long.   The reactor has four syringes. Each syringe has a capacity of 10 milliliters. Each syringe is used to supply the reactants into the mixer. The solutions carrying the reactants are mixed with a dead time of about 2.4 milliseconds. The cell is washed with water after each measurement to remove left over reactants and products from previous experiments. The reaction cell was mounted in a holder equipped with a custom made fiber optic adapter. The UV and

visible light from a high pressure deuterium and tungsten lamps are guided into the cell with UV grade fiber optics. The transmitted light was analyzed with an Ocean Optics PC 2000 spectrograph.

The real time conductivity measurements were performed using the impedance technique [27]. The impedance is defined as the opposition to the flow of alternating current in a circuit (same as resistance in dc current). The impedance is a complex number that includes contributions from the resistance, Z_{re}, which is the real component and the combined capacitance and inductance, Z_{im}, are imaginary components, and is given by:

$$Z = Z_{re} + j\, Z_{im} \hspace{4cm} \text{equation 4.2}$$

The conductance, which is defined as the reciprocal of the resistance, Z_{re}, can be obtained from impedance measurements when the capacitance, Z_{im}, of the solution is significantly smaller than the resistance. The frequency that minimizes the capacitance is obtained from frequency dependent measurements of the impedance with the SFM 400. The conductance is then obtained from measurements of the electrolyte resistance. Experimentally, a circuit that contains a parallel resistor and capacitor is in series with the electrolyte solution (resistor), which is in series with another parallel combination of resistor and capacitor, is employed for conductance measurements. The current drop in the circuit is used to determine the resistor or electrolyte conductance.

The conductance of the solution can be also expressed as the conductivity k and cell constants A and L according to:

$$C = \frac{k\,A}{L} \hspace{4cm} \text{equation 4.3}$$

The values of A and L are obtained from conductance measurements of a standard 1 M KCl solution that has a known conductance value. At high frequencies, the conductivity of the solution depends on the number of ions in solution and is conveniently expressed in terms of the molar conductivity, Λ, is defined as:

$$\Lambda = \frac{k}{M} \qquad \text{equation 4.4}$$

Molar conductivities depends on ion concentration according to Kohlraush's law [28] :

$$\Lambda = \Lambda_o - \alpha \, M^{1/2} \qquad \text{equation 4.5}$$

where Λ_o are limiting ion conductivities and α represents a constant.

4.3 Results and Discussion

The linear dependence of the silver and sulfide ion conductivity on the square root of the corresponding ion concentration was verified experimentally in this work. The upper and lower panels in Figure 4.1 display the dependence of molar conductivity on the square root of the concentration of silver nitrate and ammonium sulfide, respectively.
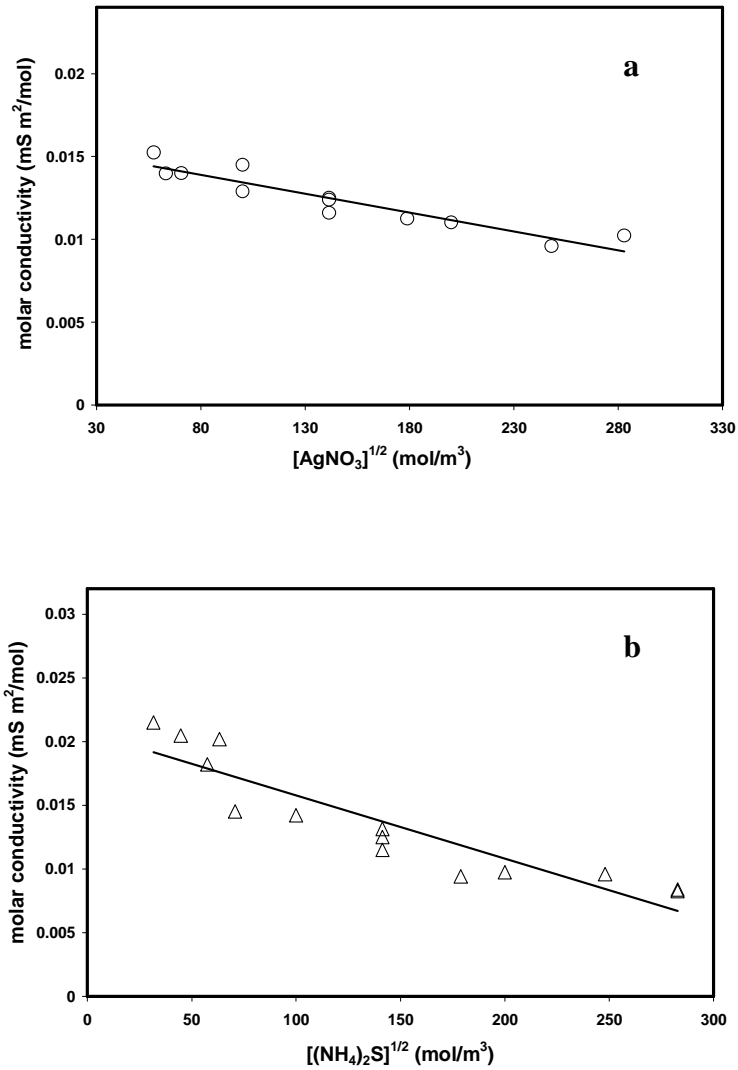
Figure 4.1: Dependence of molar conductivity, Λ, on (a) $AgNO_3$ and (b) $(NH_4)_2S$ concentration.

Within the scatter of the data, the conductivity increases linearly with the square root of the ion concentration due to the increase in charge carriers in solution, as expected from the basis of Kohlraush's law. Linear fits to the dependence of the silver nitrate and

ammonium sulfide molar conductivity on the square root of the ion concentration have correlation factors of 0.98 and 0.97, respectively. The limiting molar conductivity, Λ_o, can be obtained from the intercept of the straight line fit to the data displayed on figure 4.1. Limiting molar conductivities of about 0.0157 and 0.0207 mS·m^2/mol are found for the silver nitrate and ammonium sulfide solutions, respectively.

4.3.1 Real time conductivity measurements

The dependence of conductance on time for a stoichiometric mixture of Ag^+ and S^{-2} is displayed on figure 4.2. A flow mixture is prepared in the SFM stopped flow system and at time t = 0 seconds the flow is brought to a stop. The S^{-2} concentration in the flow is 8 x 10^{-2} M. The optical absorption spectra as a function of wavelength of the reaction mixture is also displayed on figure 4.2. The optical absorption spectra were measured at the times indicated by the arrows. There is no significant absorption of light at times t $\leq$ 0 seconds. Independent experiments on Ag^+ and HS^-/S^{-2} ions exhibit absorption bands at 225 and 240 nm, respectively. Significant changes are observed in the optical absorption spectrum in the first 100 milliseconds of reaction: these spectra are discussed in detail in chapter 5.

The conductance of the equimolar reaction mixture displayed on figure 4.2 exhibits an interesting dependence on time. There is a small decrease in the conductance with time after the flow is brought to a stop at time t = 0 seconds and extends to about 4 seconds. There is a slow decrease in the conductivity with time after t = 4 seconds. The dependence of the conductivity on time is consistent with the observations discussed on the previous paragraphs regarding the optical absorption spectra of the reaction mixture. Accordingly, decrease in the conductance results from the decrease in the number of Ag^+ and $HS-/S^{-2}$ ions in the solution as they form silver sulfides species.
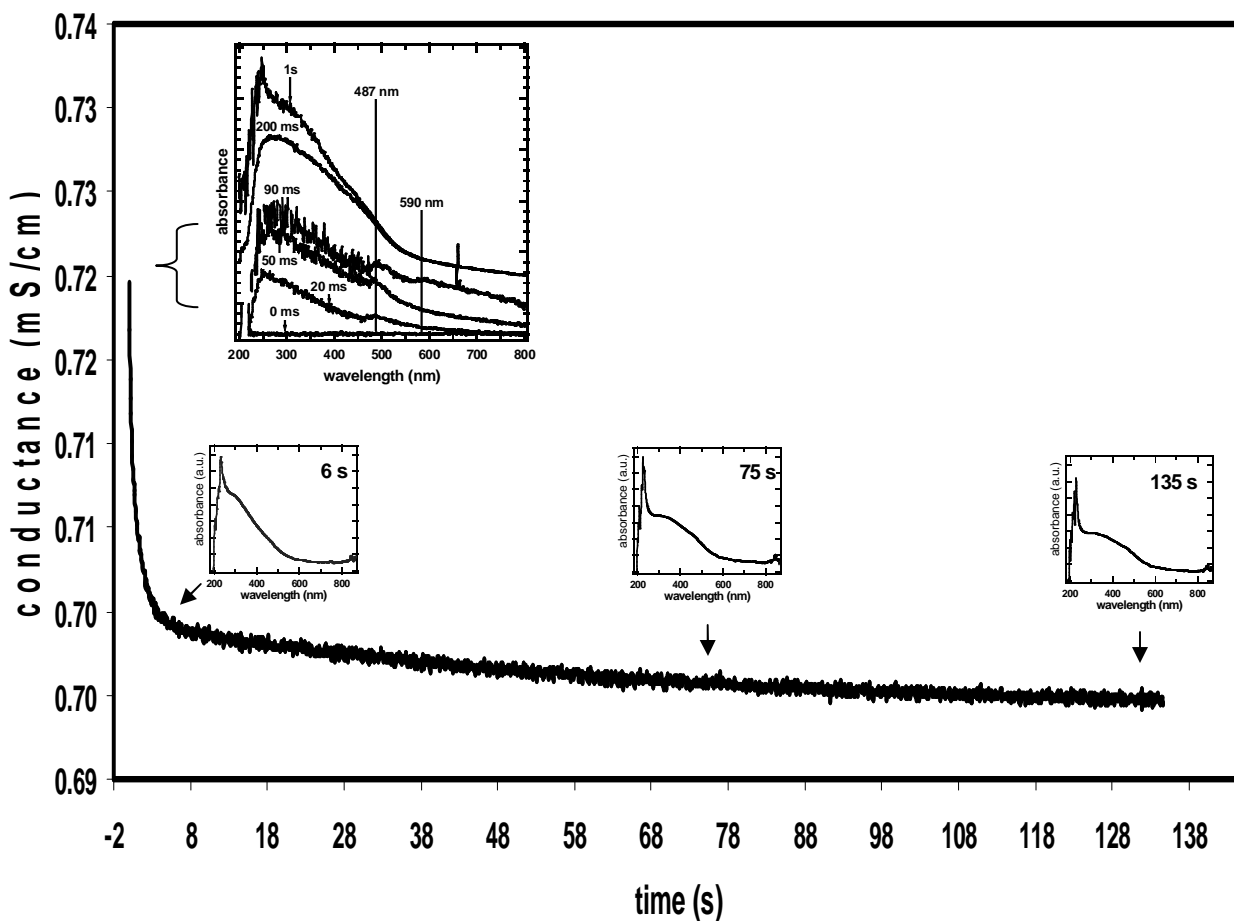
Figure 4.2: Dependence of conductance on time for the reaction mixture of Ag^+ and HS^-/S^{-2}. The inserts represent the optical absorption spectra of the same reaction mixture obtained at the times indicated by the arrows.

Additional measurements were performed to establish if the spectator's ions contribute significantly to the solution conductivity. For this purpose, reaction mixtures of Ag^+ and S^{-2} as a function of time were studied and the solution molar conductivity was determined in the limit of time going to infinity. The molar conductivities of these solutions (circles) are compared with that of a saturated Ag_2S solution (squares), measured under identical experimental conditions. The molar conductivity of this solution is smaller than the one observed for the colloidal Ag_2S prepared here. Displayed on figure 4.3 is the calculated molar conductivity obtained by adding the molar conductivity of all the ions in solution (triangles). In this case, the molar

conductivity measured experimentally is significantly higher than the calculated for the spectator ions in solution, indicating that they can not account for the conductivity of Ag_2S colloid. In synopsis, ionic conductivity measurements provide qualitative information related the process occurring in the early time of the reaction but does not provide information related to the identity of the clusters or embryos chemistry.
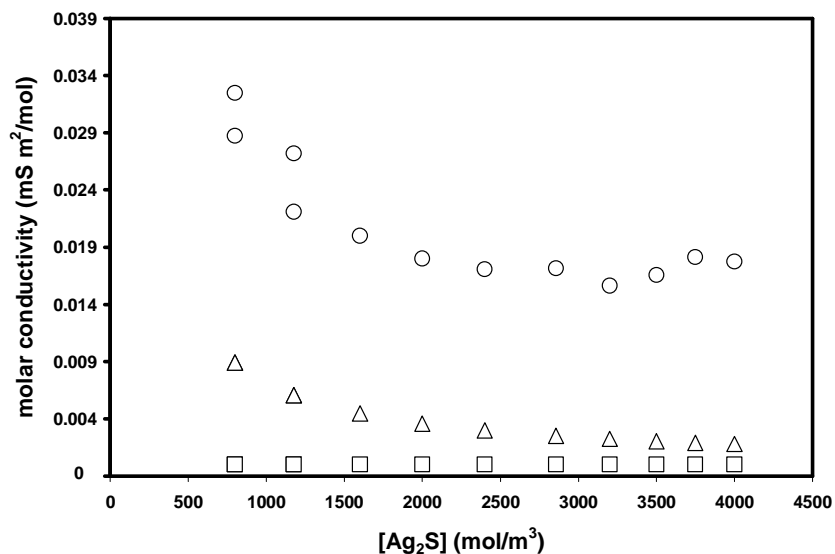
Figure 4.3: Molar conductivity of Ag_2S as a function of colloidal Ag_2S concentration (circles). The triangles and squares represent the ionic conductivity calculated for the spectator ions in solution and for a saturated solution of $Ag_2S_{(s)}$.

4.3.2 Kinetics measurements

Since the Ag_2S solubility product is of the order of 10^{-50}, the formation of silver sulfide may be regarded as irreversible. Thus the increase in Ag_2S concentration with time is proportional to the rate of formation of Ag_2S:

$$r \; \alpha \; \frac{- dm}{dt} \qquad\qquad \textbf{equation 4.6}$$

where r is the reaction rate. To establish the reaction rate, we performed measurements of the dependence of the reaction conductivity on time for various initial Ag^+ and S^{-2} concentrations. The concentration can be related to conductivity of the ions present in solution according to equation 4.5, which allows for reaction rates to be determined. This approach allowed measurements of the dependence of the rate on initial Ag^+ and S^{-2} concentration and to establish the form of the rate law or the reaction that leads to the formation of Ag_2S. From the slope of the plots of the ln(r) as a function of ln (Ag^+) and $ln(S^{-2})$, figure 4.4.a and 4.4.b, we estimate that the order of the reaction with respect to the Ag^+ and S^{-2} ions is -1 and +1, respectively, figure 4.4. These orders where verified in an universal plot of the ln r as a function of the ln $[S^{-2}]/[Ag^+]$, shown in figure 4.4c .
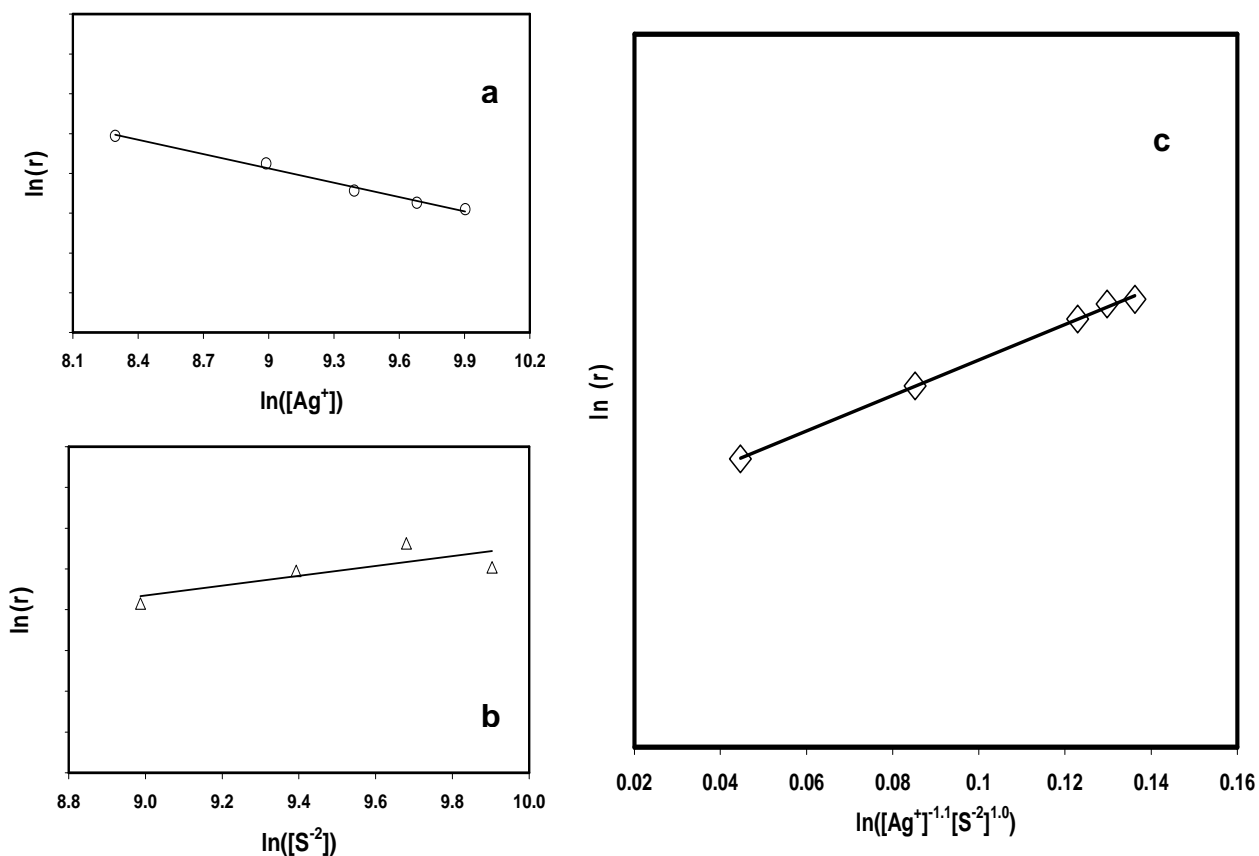
Figure 4.4: a) ln (r) as a function of the ln $[Ag^+]$; b) ln (r) as a function of the $ln[S^{-2}]$; c) ln(r) as a function of the $ln([Ag^+]^{-1.1}[S^{-2}]^{1.0}$

The fact that these reaction orders are markedly different from the stoichiometric numbers described by equation 4.1 indicates that the reaction mechanism involves multiple steps.

4.4 Summary

In summary, we have employed real time time-conductivity and UV-visible absorption measurements of stopped flows of $AgNO_3$ and $(NH_4)_2S$ to study the nucleation and growth for the formation of silver sulfide nanoparticles (Ag_2S NP). The kinetics measurements reveal that the rate law is directly proportional to the S^{-2} concentration while it is inversely proportional to Ag^+ concentration. Conductivity of the solution decreases slightly and the optical absorption spectra experiences significant changes after the flow containing the reactants stops. The small decrease in conductivity is taken as evidence for a small reduction in the number of ions in solution: the amount of the decrease is too small to account for the formation of neutral Ag_2S molecules. Rather, non stoichiometric Ag_2S species - resulting in ionic forms of Ag_2S - are thought to be formed. Ionic conductivity measurements provide qualitative information related to the process occurring in the early stages of the reaction but does not provide information related to the clusters or embryos chemistry. Optical absorption measurements performed in short time scales- in the first few milliseconds after the flow stops- are discussed in the next chapter and support our conclusion that non stoichiometric forms of silver sulfide play a major role in the reactions that lead to the formation of nuclei.

4.5 References:

1. Besson, C.; Finney, E. E.; Finke, R. G. Nanocluster Nucleation, Growth and the Agglomeration Kinetic and Mechanistic Studies: A more general, four-step mechanism involving double autocatalysis. *Chem. Mater.*, **2005**, *17*, 4925-4938.

2. Jana, N. R.; Gearheart, L.; Murphy, C. J. Seeding Growth for Size Control of 5-40 nm Diameter Gold Nanoparticles. *Langmuir*, **2001**, *17*, 6782-6786.

3. Murray, C. B.; Noms, D. J.; Bawendi, M. G. Synthesis and Characterization of Nearly Monodisperse CdE (E = S, Se, Te) Semiconductor Nanocrystallites. *J. Am. Chem. Soc.*, **1993**, *115*, 8706-8715.

4. Privman, V.; Goia, D. V.; Park, J.; Matijevic, E. Mechanism of Formation of Monodispersed Colloids by Aggregation of Nanosize Precursors, *Journal of Colloid and Interface Science*, **1999**, *213*, 36- 45.

5. Murillo, L.E.; Viera, O.; Briano, J. G.; Castro, M. E.; Ishikawa, Y.; Irizarry, R.; Solá, L. Growth kinetics of gold nanoparticles. Proceedings of the International Conference on Computational Nanoscience and Nanotechnology, Chapter 16, *Materials and Nanostructures Studies*, **2002**, 435-438.

6. Njoki, P. N.; Jacob, A.; Khan, B.; Luo, J.; Zhong,C.-J. Formation of Gold Nanoparticles Catalyzed by Platinum Nanoparticles: Assessment of the Catalytic Mechanism, *J. Phys. Chem. B.*, **2006**, *110*, 22503-22509.

7. van Dijken, A.; Meulenkamp, E.A.; Vanmaekelbergh, D.; Meijerink, A. Identification of the transition responsible for the visible emission in ZnO using quantum size effects. *Journal of Luminescence*, **2000**, *90*, 123-128.

8. Lakowicz, J. R.; Gryczynski, I.; Gryczynski, Z.; Murphy, C. J. Luminescence Spectral Properties of CdS Nanoparticles. *J. Phys. Chem. B,* **1999**, *103*, 7613-7620.

9. Qu, L.; Yu, W.; Peng, X. In Situ Observation of the Nucleation and Growth of CdSe Nanocrystals. *Nanoletters*, **2004**, *4*, 465-469.

10. Moskovits, M.; Vlckova, B. Adsorbate-Induced Silver Nanoparticle Aggregation Kinetics. *J. Phys. Chem. B.* **2005**, *109*, 14755-14758.

11. Rodriguez-Sanchez, M. L.; Rodriguez, M. J.; Blanco, M. C.; Rivas, J.; Lopez-Quintela, M. A. Kinetics and Mechanism of the Formation of Ag Nanoparticles by Electrochemical Techniques: A Plasmon and Cluster Time-Resolved Spectroscopic Study. *J. Phys Chem. B.* **2005**, *109*, 1183-1191.

12. Zhang, Z.; Patel, R. C.; Kothari, R.; Johnson, C. P.; Friberg, S. E.; Aikens, P. A. Stable Silver Clusters and Nanoparticles Prepared in Polyacrylate and Inverse Micellar Solutions. *J. Phys. Chem. B*, **2000**, *104*, 1176 -1182.

13. Meneses, C. T.; Flores, W. H.; Sasaki, J. M. Direct Observation of the Formation of Nanoparticles by in situ time-resolved X-ray absorption spectroscopy. *Chem. Mater.* **2007**, *19* , 1024 -1027.

14. Kryukov, A.I.; Stroyuk, A.L.; Zin'chuk, N.N.; Korzhak A.V.; Kuchmii, S.Y.; Optical and catalytic properties of Ag_2S nanoparticles. *Journal of Molecular Catalysis A: Chemical*, **2004**, *221*, 209–221.

15. Meziani, M. J; Sun,Y. Protein-Conjugated Nanoparticles from Rapid Expansion of Supercritical Fluid Solution into Aqueous Solution. *J. Am. Chem. Soc,* **2003**, *125*, 8015-8018.

16. Brelle, M. C.; Zhanga, J. Z. Femtosecond study of photo-induced electron dynamics in AgI and core/shell structured AgI/Ag_2S and $AgBr/Ag_2S$ colloidal nanoparticles. *J. Chem. Phys.*, **1998**, 108, 3119-3126.

17. Wu, M.; Pan, X.; Qian, X.; Yin, J; Zhu, Z. Solution-phase synthesis of Ag_2S hollow and concave nanocubes. *Inorganic Chemistry Communications* **2004**, *7*, 359–362

18. Calzaferri, G.; Brühwiler, D.; Glaus, S.; Schürch, D.; Currao, A.; Leiggener, C. Quantum-Sized Silver, Silver Chloride and Silver Sulfide Clusters. *Journal of Imaging Science and Technology* , **2001**, *45*, 331–339.

19. Kryukov, A. I.; Zin'chuk, N. N.; Korzhak A. V.; Ya. Kuchmil, S. Quantum Size Effects and Nature of Photoprocesses in Nanoparticles of Ag_2S. *Theor. Exp. Chem.* **2001**, *37*, 296-303

20. Brühwiler, D.; Leiggener, C.; Glaus, S.; Calzaferri, G. Luminescent Silver Sulfide Clusters. *J. Phys. Chem. B* **2002**, *106*, 3770-3777.

21. Brühwiler, D.; Leiggener, C.; Calzaferri, G. Luminescence Properties of Ag_2S and Ag_4S_2 in Zeolite A. *J. Mater. Chem.* **2003**, *13*, 1969-1977.

22. Motte, L.; Billoudet, F.; Lacaze, E.; Douin, J.; Pileni, M. P. Self-Organization into 2D and 3D Superlattices of Nanosized Particles by Their Size. *J. Phys. Chem. B* **1997**, *101*, 138-144.

23. Changqi, X.; Zhicheng, Z.; Qiang, Y. A Novel Facile Method to Metal Sulfide (Metal = Cd, Ag, Hg) Nano-Crystallite. *Mater. Lett.* **2004**, *58*, 1671-1676.

24. Liu, J.; Raveendran, P.; Shervania, Z.; Ikushima, Y. Synthesis of Ag_2S Quantum Dots in Water-in-CO_2 Microemulsions. *Chem. Commun.* **2004**, *22*, 2582-2583.

25. Martinez-Castañón, G. A.; Sanchez-Loredo, M. G.; Dorantes, H. J.;.Martinez-Mendoza, J. R; Ortega-Zarzoza, G.;. Ruiz, F. Characterization of Silver Sulfide Nanoparticles Synthesized by a Simple Precipitation Method. *Mater. Lett.* **2005**, *59*, 529-534.

26. Liu, S. H.; Qian, X. F.; Yin, J.; Hong, L.; Wang, X. L.; Zhu, Z. K. Synthesis and Characterization of Ag_2S Nanocrystals in Hyperbranched Polyurethane at Room Temperature. *J Solid State Chem.* **2002**, *168*, 259-262.

27. Electrochemical methods fundamentals and applications, Bard, A. and Faulkner L., 2nd edition (2001), John Wiley & Sons, Inc.

28. Physical Chemistry, Atkins, P. and de Paula J., 7th edition (2002), Oxford University Press Inc., New York.

29. León-Velázquez, M. S.; Morales, M.; Irizarry, R.; Castro, M. Conduction in Collodial Systems: A Kinetic Study of Ag_2S Semiconductor. Nanoparticles: Synthesis, Stabilization, Passivation, and Functionalization*,* Chapter 15, **2008,** pp 203-213, *ACS Symposium Series*, Volume 996.

CHAPTER 5:

Inhibition of Ag$_2$S Nucleation in AOT Micelles [35]

5.1 Introduction

Silver sulfide nanostructures are proposed to play an important role in several emerging technologies [1-7]. In particular, the band gap in bulk Ag$_2$S is about 1 eV [8-9] and can be tuned down to about 2.1 eV [10], making them suitable candidates for the improvement of solar cell technologies.   Silver sulfide nanostructures have been prepared by a variety of methods. These methods pursue control of the organization, size, electronic and morphology to improve Ag$_2$S nanostructure properties.   These synthesis methods include simple precipitation [11], the use of solvation or coordinating agents [10, 12-24] and electrospinning [7], among others. Silica [12], thiols [13-17], polymers [18-19], and surfactants [10, 17, 20-21] are becoming important additives in Ag$_2$S nanostructure synthesis.   Little is known on the effect of surfactants on the chemistry that leads to the nucleation of nanostructures.

The simplest approach to the synthesis of Ag$_2$S NP is thru the reaction of silver and sulfide ions. These ions can react to form a variety of chemical species which may evolve into Ag$_2$S embryos or nuclei. Developing strategies to the characterization of these chemical species is a major challenge of relevance in tailoring nanostructures with the desired morphology and physical properties for specific applications. This can be accomplished by selectively inhibiting different stages in the nucleation and growth process. In this chapter we contribute to the current body of knowledge related to nanoparticle synthesis by studying (1) the optical absorption spectra of the chemical species formed at the early stages of reaction and (2) the effect of a surfactant, sodium bis(2-ethylhexyl) sulfosuccinate (AOT), on the morphology and optoelectronic properties of Ag$_2$S NP. AOT is found to stabilize the clusters formed in the early stages of the nucleation process according to:

$$xAg^+ + yS^{-2} + nAOT \rightarrow Ag_{2x}S_y(AOT)_n \rightarrow Ag_2S\ NP \qquad \text{reaction 5.1}$$
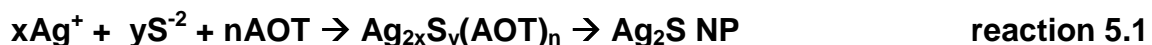
where x and y are the stoichiometric coefficients of Ag^+ and S^{-2} ions and n is the stoichiometric coefficient of AOT molecules required to stabilize this molecular species. Density functional calculation (DFT) and configuration interaction singlet calculations (CIS) are used to determine the physical properties of possible Ag_2S species that may serve as clusters in the nucleation process. We found that AgS^- and Ag_3S^+ species are formed in the first 100 ms of reaction. AOT, on the other hand, is found to inhibit Ag_2S nucleation. UV visible absorption spectroscopy measurements as a function of AOT concentration are consistent with the formation of clusters and nuclei with characteristic absorption features around 300 nm and above 500 nm, respectively. Following our earlier work, the absorption of light at 575 nm is used as a measurement of the number of nuclei in solution [25]. Light absorption at 575 nm is found to decrease non-linearly with initial AOT concentration, a result taken as evidence for the quenching of nuclei formation. Scanning tunneling microscopy measurements on samples that consist predominantly of clusters reveal the existence of particles with dimensions, HOMO and LUMO gap similar to those predicted by DFT calculations for a Ag_4S_2 dimer with D_{4h} symmetry, an interpretation consistent with the light absorption measurements. Transmission electron microscopy and electron diffraction measurements indicate that monoclinic Ag_2S nanoparticles with an average diameter of 4 ± 1 nm are representative of the nuclei formed in the synthesis.

5.2 Experimental

Master solutions of silver nitrate ($AgNO_3$, Fisher) and sodium bis(2-ethylhexyl) sulfosuccinate, (AOT, Alpha Aesar) were prepared by dissolving the appropriate mass of the solid in 100 mL of deionized water. A ammonium sulfide ((NH_4)$_2$S, Alpha Aesar) master solution was prepared by diluting 0.6 μL of a 40-44 % by volume solution in enough water to make a 4×10^{-3} M (NH_4)$_2$S solution.

Two different sets of samples were prepared for the experiments described here. In one set, several aliquots of the $AgNO_3$ and AOT master solutions were mixed to produce a $(AgNO_3)$/AOT solution. This procedure was also performed with the $(NH_4)_2S$ and AOT master solutions to prepare a $(NH_4)_2S$/AOT solution. The $(AgNO_3)$/AOT and $(NH_4)_2S$/AOT solutions were mixed to produce Ag_2S/AOT dispersions. In the second set of samples, the Ag_2S NP were formed by mixing adequate amounts of $AgNO_3$ and $(NH_4)_2S$ in the absence of AOT. The resulting Ag_2S NP dispersion was further diluted with different amounts of the AOT master solution.

UV-visible absorption measurements were conducted using an Agilent Spectrophotometer model 8453. A quartz cuvette with an optical path of 0.25 cm was used for the optical absorption measurements. Scanning tunneling microscopy (STM) measurements were performed in a Nanosurf easyScan E-STM version 2.1 using a Pt/Ir tip. The STM was calibrated with measurements performed on a commercial gold ruler. Measurements performed on longitudinal features of dry deposits of C_{12}-SH and C_{10}-SH alkyl thiol monolayers coincided with the expected molecular lengths of these molecules. A drop of the Ag_2S/AOT dispersion was deposited on a nickel magnetic holder and allowed to dry at open air for several days prior to the measurements. Transmission electron microscopy (TEM) measurements were performed in a JEOL 2010 electron microscope. A carbon coated grid was immersed in the Ag_2S/AOT or in the methanol/Ag_2S dispersion. The samples were out gassed at 10^{-3} torr for several days prior to placing them in the TEM sample compartment. TEM measurements were performed with and acceleration voltage of 120 kV. Negatives of the micrographs were processed using standard techniques and scanned with an EPSON Perfection V750 PRO scanner and stored in a PC computer for further analysis. Theoretical calculations were performed in a Dimension 5500 desktop PC using the 2003 Gaussian and GaussView packages.

5.3 Results and Discussion

5.3.1 Theoretical calculations

We wish to highlight that little information is known about the properties of small silver sulfides, particularly their optical absorption spectrum. In this section with report the results of theoretical calculations. The theoretical calculations on Ag_2S dimers and ions were performed using density functional theory at the B3LYP/DGDZVP or PBEPBE/DGDZVP while the calculations on Ag_2S trimer were performed at the PBEPBE/LANL2MB. Optimized structures at the indicated level of theory are summarized on scheme 5.1. Configuration interaction singlet (CIS) calculations were performed on the optimized structures. The results, including relevant bond lengths and molecule or ion size and HOMO-LUMO gaps, are summarized in table 1. Theoretical calculations of silver sulfide monomers and dimers were performed earlier by Bagatur'yants and co workers [26]. They employed ab initio relativistic pseudo potentials to study the stability of these species. This work complements these previous efforts by extending theoretical calculations to other silver sulfides and provides information about their optical absorption properties.

The average Ag-S bond length in optimized structures is found to be 2.49 $\pm$ 0.12 Å. The sizes of the molecules or ions were estimated using the longest atomic distance. The largest cluster is the trimer, where the distance between an axial silver ion to the farthest sulfide ion located in the opposite extreme of the plane is 5.97 Å. The shortest Ag-S bond distance is found in the AgS^- ion which corresponds to 2.33 Å. The sizes of the silver sulfide dimers range from 3.77 Å in the D_{4h} Ag_4S_2 dimer to 4.35 Å in the C_{2v} and C_{2h} Ag_4S_2 dimers.

Almost all HOMO-LUMO gaps are found to be larger than 1. Ag_2SH^+ is predicted to have a HOMO-LUMO gap of 4.16 eV, the largest found among the species considered. This is significantly larger than the 2.48 eV HOMO-LUMO gap found in the Ag_2S

molecule. The lowest HOMO-LUMO gaps are found in the Ag_4S_2 dimers with D_{4h} and C_{2v} at 0.87 and 0.46 eV, respectively.

AgS⁻ (C∗ᵥ)

$Ag_2S(C_{2v})$

AgSH (C_S)

$Ag_3S^+(C_{3v})$

Ag_4S_2 (C_{2v})

Ag_4S_2 (C_{2h})

Ag_4S_2 (D_{4h})

Ag_6S_3
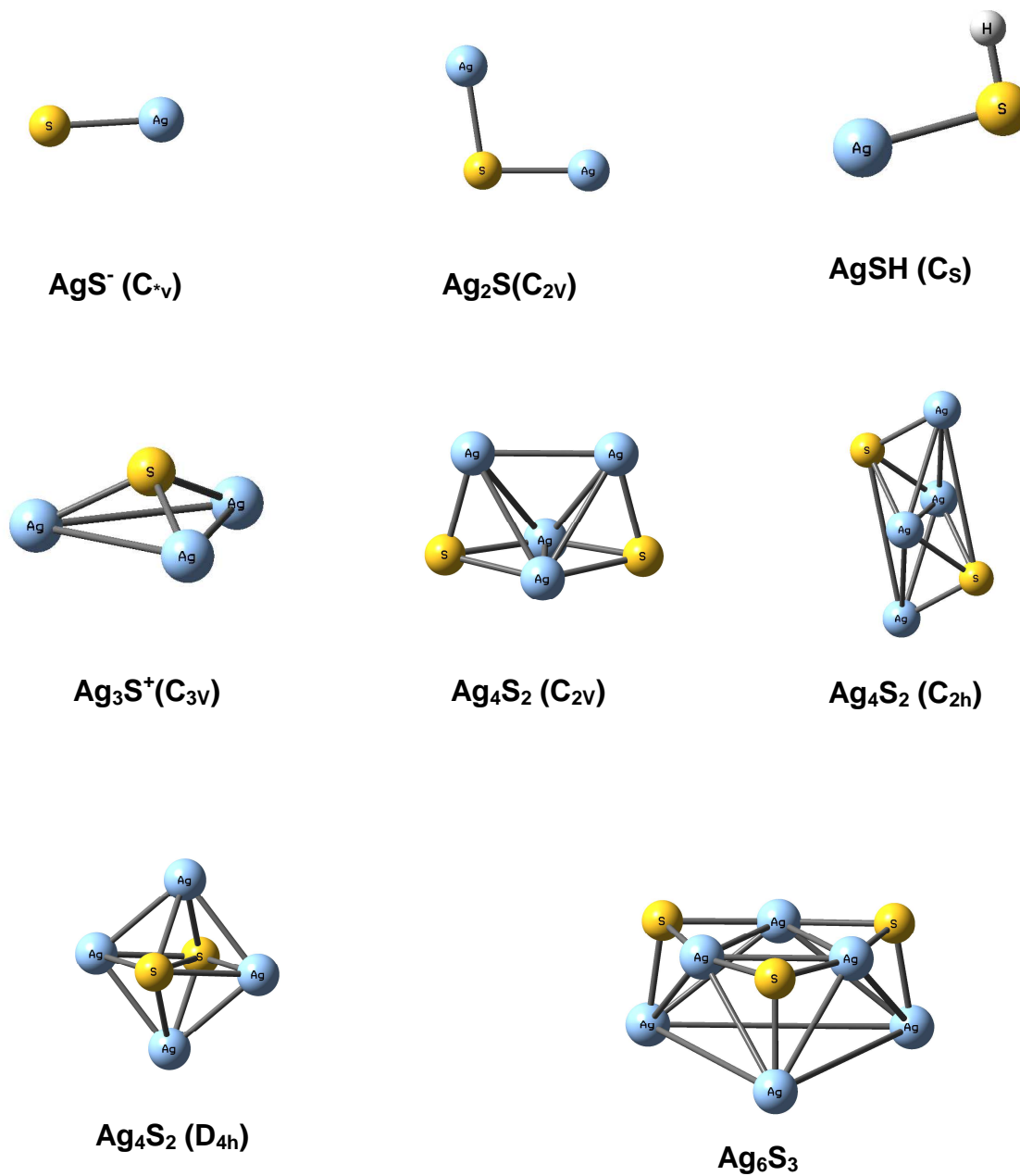
Scheme 5.1: Optimized structures of simple sulfides at the DFT level of theory. See table 5.1 for bond lengths.

Ground State	Level of Theory Functional/ Basis Set	Bond Distances (Å)	Longest Intramolecular Distance(Å)	Homo/Lumo Gap (eV)	CIS Excited State	Energy (nm)	Strength
AgS⁻ C∗v	B3LYP/DGDZVP	(Ag-S) 2.36	2.3350	1.71	1 3 7	1009.8 **482.7** **204.9**	0.0103 0.2930 0.2780
Ag₂S C₂v	B3LYP/DGDZVP	(Ag-S) 2.39 (Ag-Ag) 3.23	3.2254	2.48	1 2 3 5 6 10	781.0 660.1 **410.1** **334.9** **295.2** 207.9	0.010 0.027 0.185 0.172 0.179 0.314
Ag₄S₂ D₄h	PBEPBE/DGDZVP	(Ag-S) 2.72 (Ag-Ag) 2.77 (S-S) 3.77	3.7700	0.87	1 13, 14 16	753.8 **298.3** 293.0	0.0140 0.2890 0.0074
Ag₄S₂ C₂v	PBEPBE/DGDZVP	(Ag6-Ag2) 3.23 (Ag5-Ag6)3.16 (Ag1-Ag2) 2.86 (Ag2-S4) 2.61 (Ag6-S4) 2.41 (S-S) 4.35	4.3500	0.46	6	**368.0**	0.280
Ag₄S₂ C₂h	PBEPBE/DGDZVP	(Ag2-Ag5) 3.25 (Ag1-Ag2) 2.83 (Ag1-S4) 2.60 (S4-Ag5) 2.40 (S4-S6) 4.35	4.3500	1.2	1 4 6 8	488.5 384.9 **360.1** 307.5	0.053 0.074 0.341 0.057

Ground State	Level of Theory Functional/ Basis set	Bond Distances (Å)	Longest Intramolecular Distance(Å)	Homo/Lumo Gap (eV)	CIS Excited State	Energy (nm)	Strength
Ag$_6$S$_3$	PBEPBE/LANL2MB	(Aga - S) 2.48 (Aga - Aga) 5.81 (Aga - Agp) 3.73 (Agp - Agp) 2.57 (Agp - S) 2.57	5.9730 (Aga-Sp)	1.5	1	615.6	0.008
					2	478.0	0.021
					4	446.9	0.041
					5	**393.5**	0.496
					6	373.6	0.019
					7	371.3	0.021
					8	**345.1**	0.449
					9	332.9	0.059
					10	272.1	0.006
AgSH C$_s$	B3LYP/DGDZVP	Ag-S (2.42) S-H (1.35) Ag-H (2.87)	2.8737	3.37	3	546.97	0.0074
					4	**401.37**	0.2441
					10	**244.13**	0.1022
Ag$_3$S$^+$ C$_{3v}$	B3LYP/DGDZVP	(Ag-S) 2.47 (Ag-Ag) 3.86	3.8618	3.56	1	651.6	0.0122
					2	593.54	0.0264
					3	**340.49**	0.2877
					4	322.43	0.0104
					6	296.58	0.0098
Ag$_2$SH C$_s$	B3LYP/DGDZVP	(Ag-S) 2.51 (Ag-H) 2.99 (Ag-Ag) 4.21	4.2117	4.16	-	-	-

Table 5.1: Predicted ground state HOMO-LUMO gap and relevant CIS wavelength dependent-oscillator strengths of optimized structures.

Brühwiler and coworkers reported the formation of Ag$_2$S monomers and dimers inside the cages of zeolites [27]. These authors have claimed that Ag$_2$S monomers are

formed when the number of Ag^{+} ions per zeolite cage is 0.01 [22, 27-28]. A mixture of the monomer and dimer is formed upon increasing the Ag^{+} ion content. The Ag_2S dimmers become the dominant species when the amount of silver ions inside the zeolite cage is about 2. The spectrum of the monomer shows a broad absorption between 200 nm to 350 nm with a tail that extends to 700 nm. We estimate shoulders around 270 nm and 340 nm and a long wavelength tail above 400 nm in the spectrum of the monomer reported in the work of Brühwiler [27]. These results are in general agreement with the predictions of the configuration interaction singlet (CIS) calculations summarized table 5.1.
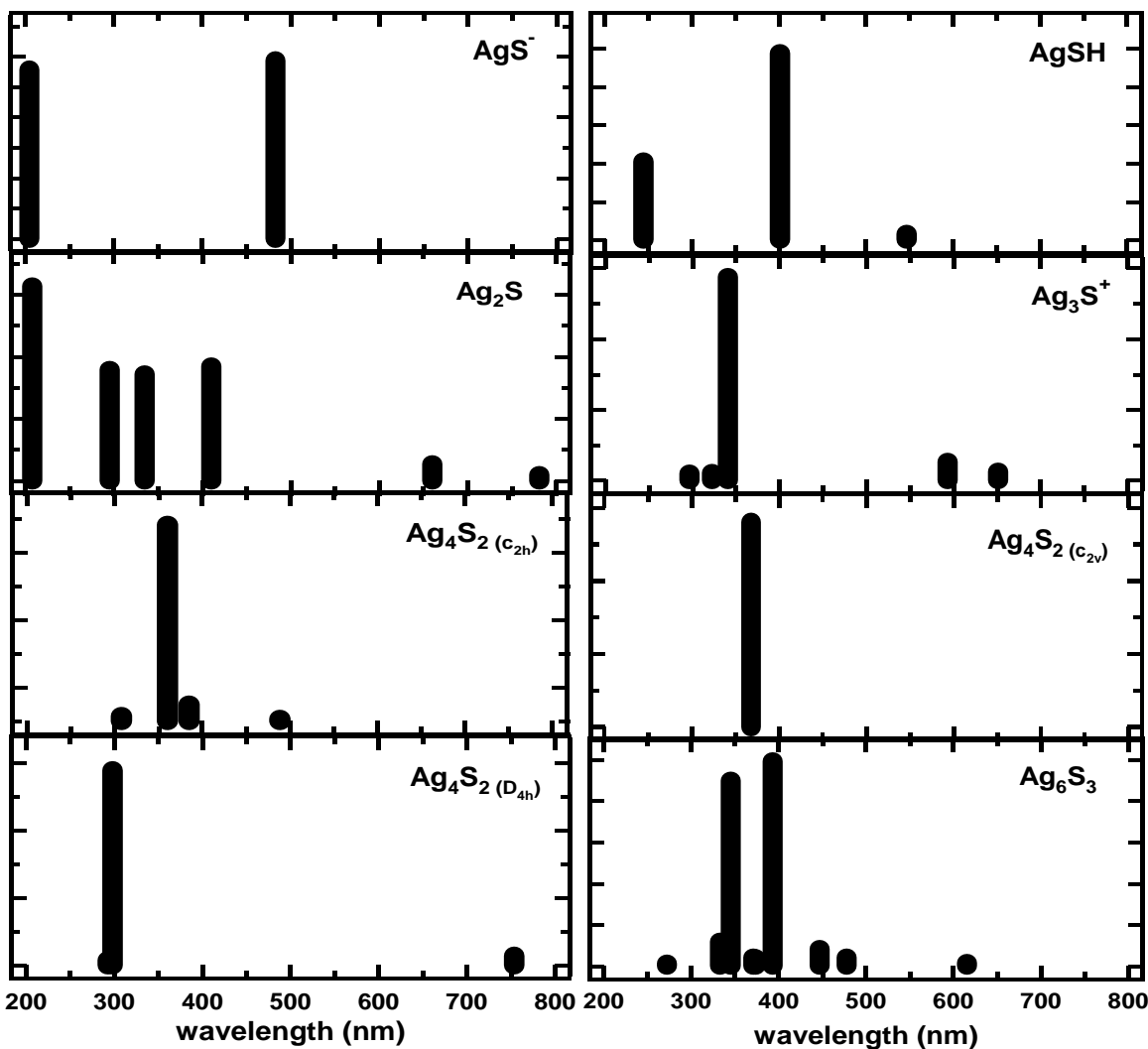
Figure 5.1: Predicted UV-visible absorption lines for the different silver sulfides clusters and ions considered in the CIS calculations.

Since the absorption coefficient is directly proportional to the oscillator strength, it is expected that those transitions with the highest oscillator strength will exhibit the strongest bands in the optical absorption spectra. The predicted UV-visible absorption lines for the different clusters and ions considered in the calculations documented here are displayed on figure 5.1. Considering only those transitions above 250 nm, the Ag_2S monomer is expected to have three strong bands in 295.2 nm, 334.9 nm and 410.1 nm in close agreement with the experimental observations reported by Brühwiler [27]. Each dimer is predicted to have at least one strong transition. The C_{2h} and C_{2v} dimers are predicted to have transitions at 360 nm and 368 nm, respectively. The dimer with D_{4h} symmetry is predicted to have a single transition at 298 nm. The trimer, on the other hand, is calculated to have strong transitions at 345 nm and 393 nm. The AgSH molecule is predicted to have a band near the 250 nm and a stronger band at 401 nm. The ion AgS^- is expected to have a band at 483 nm and Ag_3S^+ ion two bands at 340 nm and 590 nm. Our results suggest that the multiple absorption bands reported by Brühwiler may reflect the existence of a mixture of all these species in the cage of zeolites.

5.3.2 UV-visible absorption spectroscopy measurements.

5.3.2.1 UV-visible absorption spectroscopy measurements. Early stages of the reaction

UV-visible absorption spectra of $AgNO_3$ and $(NH_4)_2S$ reaction mixtures in the early stages of the reaction are displayed on figure 5.2. The spectrum obtained 20 ms after the flow stops is characterized by a broad band deep in the UV and a small feature around 487 nm. The intensity of the bands increases with time and a broad absorption feature around 590 nm is observed at about 90 seconds. The spectrum obtained around 100 ms is very similar in structure to the one observed at 1 second with small differences in light absorption intensity and a tail towards the visible. The theoretical

predictions discussed previously allow us to propose that the band at 487 nm and 590 nm results from the light absorption by AgS^- and Ag_3S^+ ions. The broad absorption between 250 nm and 400 nm, on the other hand, may result from the coexistence of other clusters or nanoparticles, as discussed in further detail below.
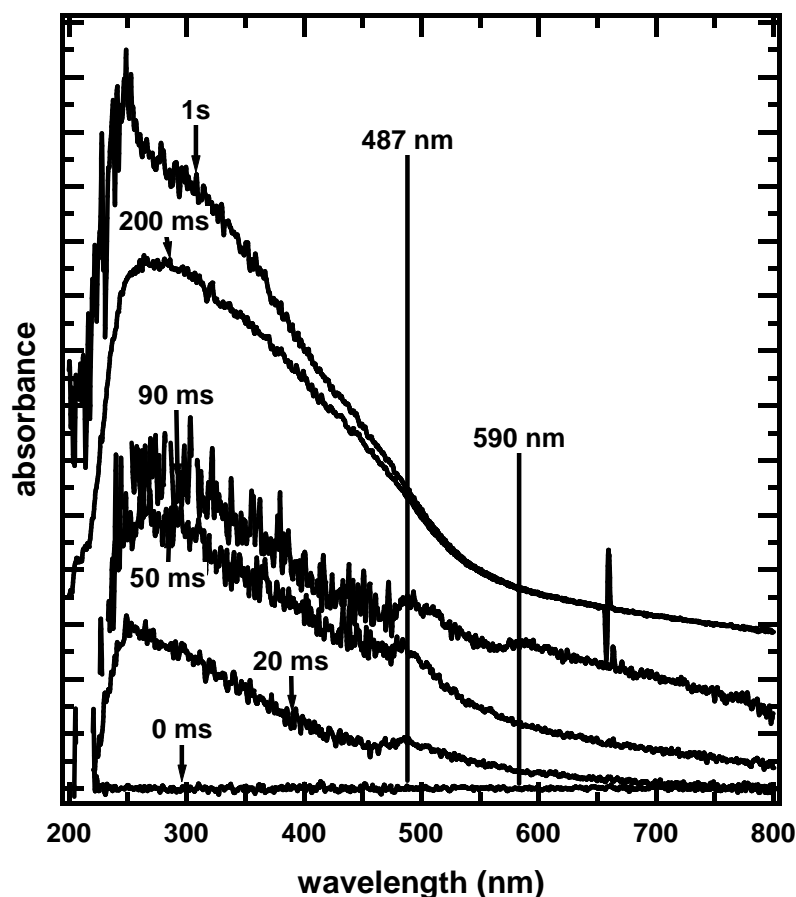
Figure 5.2. UV-visible absorption spectra of $AgNO_3$ and $(NH_4)_2S$ reaction mixtures in the early stages of the reaction.

5.3.2.2   UV-visible absorption spectroscopy measurements: Effect of AOT

The UV-visible absorption spectra of aqueous dispersions of Ag_2S/AOT formed from mixing $AgNO_3$/AOT and $(NH_4)_2S$/AOT solutions are displayed on figure 5.3. The number of moles of $AgNO_3$ and $(NH_4)_2S$ in all the solutions are identical while the concentration

of AOT increases in going from the spectrum labeled 'a' to the spectrum labeled 'f'. In the absence of AOT, the spectrum of the mixture reveals a broad absorption band between 250 nm with a long wavelength tail that extends above 800 nm with noticeable features around 300 nm and 500 nm. The absorbance of the band at 300 nm and long wavelength tail is decreases gradually for $[AOT]_o$ below 4.8×10^{-4} M. This decrease in absorbance is more noticeable when the $[AOT]_o$ is above 1.5×10^{-3} M.
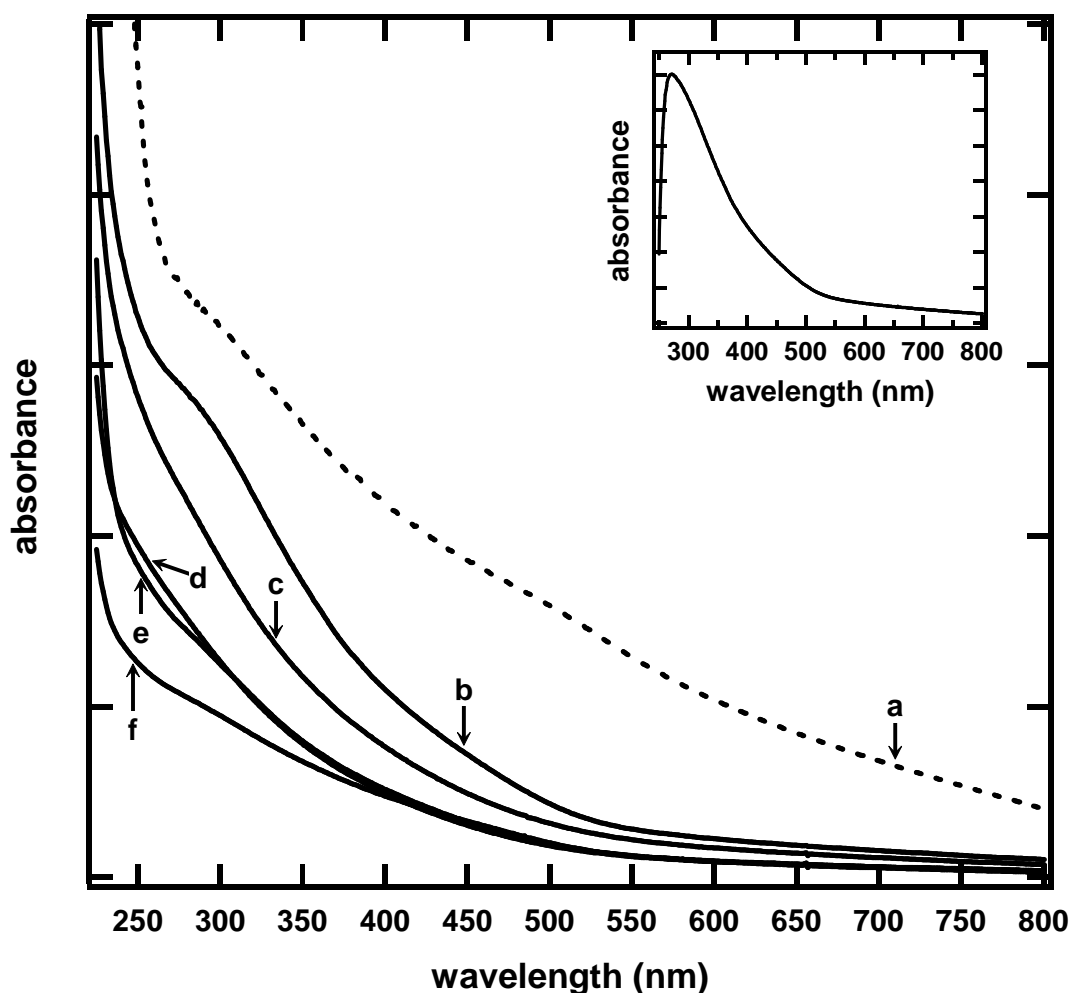
Figure 5.3: Dependence of the absorbance on wavelength for the dispersion of Ag_2S/AOT: a) Ag_2S nanoparticles, b) Ag_2S/AOT $[AOT]_o$ = 1.4×10^{-3} M, c) Ag_2S/AOT $[AOT]_o$ = 2.7×10^{-3} M, d) Ag_2S/AOT $[AOT]_o$ = 3.2×10^{-3} , e) Ag_2S/AOT $[AOT]_o$ = 3.5×10^{-3} M, and f) Ag_2S/AOT $[AOT]_o$ = 3.7×10^{-3} M. The insert represents the absorption spectrum of the Ag_2S/AOT solution containing the largest quantity of AOT after the spectra corresponding to the initial reactants was subtracted.

Quantitative measurements of the absorbance of the 300 nm and 575 nm bands were performed to establish the effect of $[AOT]_o$ in the nucleation of Ag_2S. The closed and open circles in the upper panel of figure 5.4 represent the dependence of Ag_2S absorbance at 300 nm and 575 nm, respectively, as a function of the predicted $[Ag_2S]$ (lower horizontal axis) and $[AOT]_o$ (upper horizontal axis) concentration. Light absorption of bands between 300 nm and 350 nm were observed to track each other with $[AOT]_o$ indicating that they result from a common species. Similarly, the absorbance between 500 nm and 575 nm were observed to track each other with $[AOT]_o$ also indicating that they result from light absorption from a common species. Light absorption at 300 nm and 575 nm exhibited a different dependence on $[AOT]_o$ indicating that they represent two different chemical species.
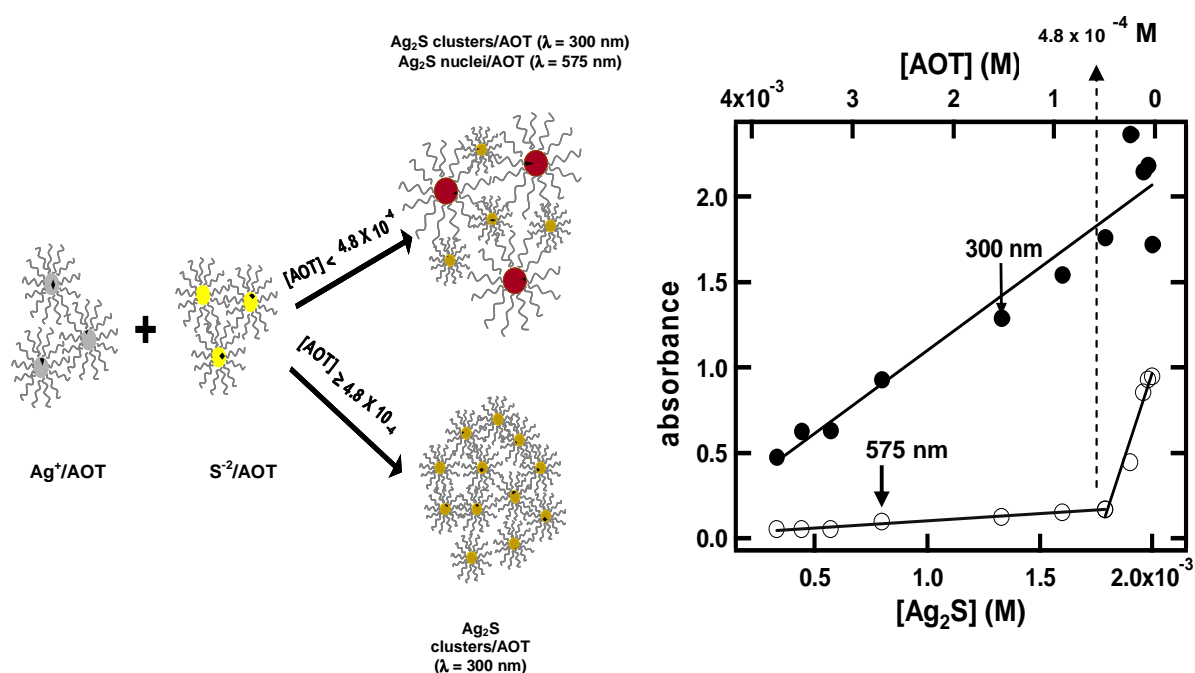
Figure 5.4: Dependence of Ag_2S absorbance as a function of Ag_2S and AOT concentration at 300 and 575 nm. The scheme in the left size of the figure represents the suggested mechanism of Ag_2S cluster formation in experiments Ag_2S NP /AOT.

Based on the CIS calculation presented on table 5.1, we attribute the band at 300 nm to light absorption by Ag_2S clusters while the absorbance at 575 nm is taken as a measure of the number of Ag_2S nuclei.[25] The absorbance at 300 nm decreases linearly with $[AOT]_o$. The absorbance at 575 nm, on the other hand, exhibits a non linear decrease with $[AOT]_o$.
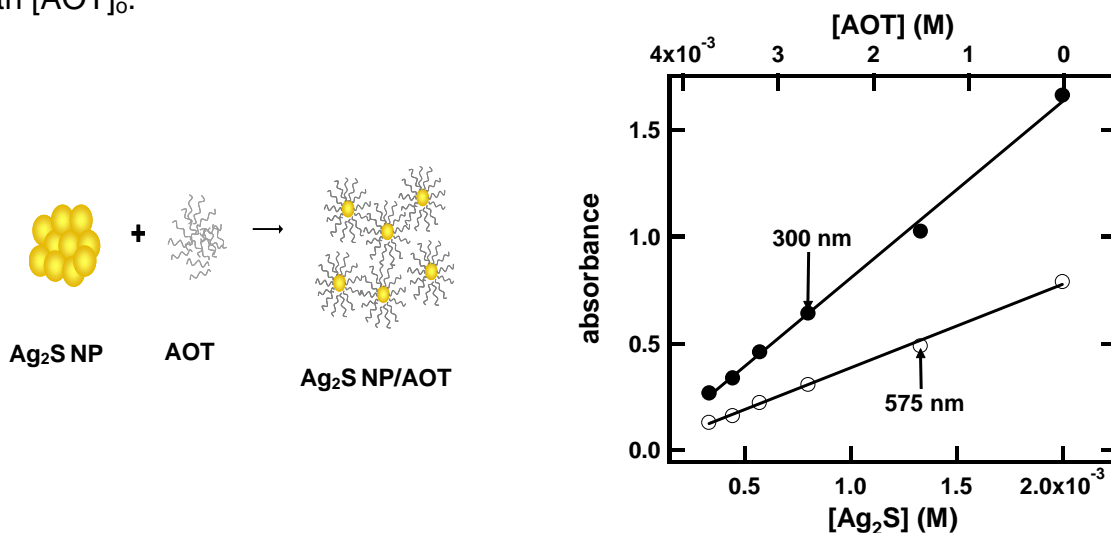
Figure 5.5: Dependence of Ag_2S absorbance as a function of Ag_2S and AOT concentration at 300 and 575 nm. The Ag_2S NP formed in the absence of AOT are diluted with aqueous solutions containing different amounts of the surfactant. The scheme left size of the figure represents the suggested mechanism of Ag_2S cluster formation in the experiment describes above.

Controlled experiments were performed to determine if the strong dependence of the absorbance on initial $[AOT]_o$ discussed above resulted from solubility effects, or alternatively, deviations of the Beer-Lambert's law.[29] In these experiments, the Ag_2S NP, formed the absence of AOT, were further diluted with aqueous solutions containing different amounts of the surfactant. The dependence of the absorbance at 300 nm and 575 nm in the control experiment is displayed on figure 5.5: the absorbance at both wavelengths decreased linearly with the $[AOT]_o$ concentration. Thus neither solubility effects or a deviation from Beer Lambert's law can account for the strong dependence of the absorbance at 575 nm on initial $[AOT]_o$ discussed in the previous paragraph. We

further tested the possibility that the nucleation was halted by a reduction in the number of collisions due to dilution effects. Attempts to model the dependence of the absorbance at 575 nm on initial reactant concentration using a collision model failed to reproduce the experimental observations summarized on figure 5.4.

The dependence of the 575 nm absorbance of $AgNO_3$/AOT and $(NH_4)_2$S/AOT reaction mixtures on $[AOT]_o$ displayed on figure 5.4 can be broken into two regions. The first region extends from $[AOT]_o = 0$ to about 4.8×10^{-4} M while the second region extends to $[AOT]_o$ larger than 4.8×10^{-4} M: in this range of $[AOT]_o$ the formation of Ag_2S nuclei is negligible based on the amount of light absorbed at 575 nm. The absorbance at 575 nm decreases to 15 % of its original value when the $[AOT]_o$ reaches 4.8×10^{-4} M. At this [AOT], the ratio of the number of moles of the surfactant to the total number of silver and sulfide ions is 10^{-3} indicating that one AOT molecule inhibits the reaction between nearly 1000 Ag^+ and S^{-2} ions. We propose that AOT stabilizes the clusters formed upon mixing $AgNO_3$ and $(NH_4)_2S$ solutions. These clusters are involved in the reactions that ultimately results in the formation of Ag_2S nuclei. Since the number of moles per unit volume of AOT is always smaller than the number of moles per unit volume of the initial reactants, such stabilization effect can only result if the AOT stabilizes more than one chemical species at a time. Trapping these clusters in AOT micelles is a very attractive explanation for the inhibition in the Ag_2S nucleation observed here. The critical micelle concentration of AOT is a value that depends, among other factors, on the nature and concentration of the ions in solution. [30-31] Micelles are known to form in AOT/water solutions with a critical micelle concentration of 1.5×10^{-3} M. [30] Previous studies have shown that the surface tension (γ) of electrolyte solutions is a sensitive diagnostic of the formation of surfactant micelles [30-33]. Typically, such plots exhibit a decrease in γ with surfactant concentration followed by a region in which γ remains constant: the surfactant concentration at this point is usually referred to as the critical micelle concentration. Figure 5.6 shows the dependence of γ on $[AOT]_o$ for the $AgNO_3$ and $(NH_4)_2S$ solutions employed in the synthesis of Ag_2S NP. The value of γ decreases with initial surfactant concentration in both cases until a $[AOT]_o$ of about 2×10^{-4} M is

obtained: γ remains nearly constant thereafter. The dependence of γ illustrated on figure 5.6 is very similar to the one found for other surfactant-electrolyte solutions where micelles are known to form. The dependence of the absorbance at 575 nm and surface tension on $[AOT]_o$ lead us to conclude that micelles are responsible for the inhibition of Ag_2S nucleation reported here.
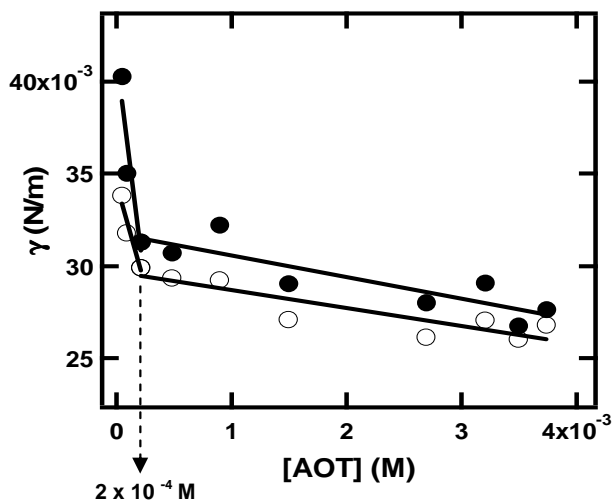
Figure 5.6: Dependence of the surface tension of the reactant solutions employed for Ag_2S NP preparation as a function of surfactant concentration. The closed circles represent the $AgNO_3$/AOT solutions and open circles represent $(NH_4)_2S$/AOT solutions.

It is of interest to compare the optical absorption properties predicted for the different Ag_2S clusters and cluster ions discussed in section 5.3.1 with the absorption spectra summarized on figure 5.3 to assign the provide an interpretation in terms of the different chemical species involved in the Ag_2S synthesis. The CIS calculations predict transitions between 200 and 1000 nm for several of the sulfides considered. Many of the optical transitions predicted by theory have small oscillator strengths will likely be hidden under the absorption spectra displayed on figure 5.3. Since the absorption coefficient is directly proportional to the oscillator strength, it is expected that those transitions with the highest oscillator strength will exhibit the strongest bands in the optical absorption spectra. Those transitions with oscillator strengths larger than 0.10

are highlighted in boldface in table 5.1. The D_{4h} Ag_2S structure is identified as the one with predicted transitions that most closely resembles the one observed experimentally in the aqueous Ag_2S/AOT solutions.

5.3.3 Microscopy measurements

The results discussed in the previous section point out to the existence of a well defined range of concentrations where clusters or nuclei are the dominant species in solution. AOT likely plays a major role in providing stabilization to the clusters as they are formed. In our measurements this is reflected by the dependence of the absorption around 300 nm on initial AOT concentration: at the largest AOT concentrations Ag_2S clusters are likely to be the dominant species while nuclei become important at lower AOT concentrations.

5.3.3.1 STM measurements on clusters

Representative scanning tunneling microscope image of a dry deposit obtained from the Ag_2S/AOT solution containing the highest $[AOT]_o$ employed in the UV-visible absorption measurements (5.3 f) is displayed in the left half of figure 5.7. The image is dominated by nanoscaled chain array of clusters: these features are not observed in STM measurements of the sample holder or in deposits of AOT alone. The average cluster size is 0.39 $\pm$ 0.06 nm with a range of sizes from 0.27 nm to 0.59 nm. The cluster to cluster distance is of the same order of magnitude as the size of cluster itself while the depth varies among the different areas examined. Ag_2S NP prepared in the absence of AOT, on the other hand, results in larger particles – up to about 50 nm- as illustrated in the 200 x 200 nm^2 image displayed in the right half of figure 5.7.

Results obtained from the measurements of the tunneling current as a function of bias voltage performed on top of the clusters shows that the tunneling current increases with bias voltage. This is not an artifact, since measurements performed on areas between

clusters results in a negligible tunneling current over the range of bias voltages employed. In the bulk, Ag_2S is a semiconductor with a band gap of 1 eV: the band gap has been found to decrease from 2.1 eV to 1.7 eV with an increase in the particle size from 2.2 nm to 8 nm. The Ag_2S clusters that make up the deposit are too small to have a well defined semiconductor band structure. Rather, it is likely that the region where the tunneling current is nearly zero reflects the HOMO-LUMO gap of the cluster. The average gap observed experimentally on top of the different aggregates is about 0.6 $\pm$ 0.2 eV. The size and band gap determined experimentally for these aggregates is consistent with the theoretical predictions for the Ag_4S_2 D_{4h} cluster.
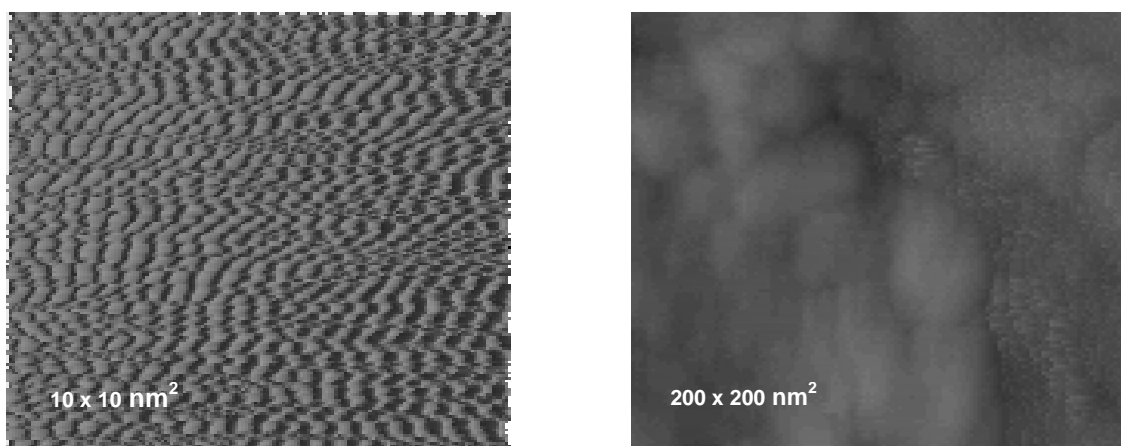
Figure 5.7: The left panel represents 10 x 10 nm^2 image of Ag_2S deposit prepared from the reaction of 0.008 M Ag_2S and 0.004 M $(NH_4)_2S$ solution with $[AOT]_o = 3.7x\ 10^{-3}$ M. The measurement is performed in the constant current mode and a bias voltage of 2.4 V. The right panel represents 200 x 200 nm^2 image of Ag_2S deposit prepared from the reaction of 0.008 M Ag_2S and 0.004 M $(NH_4)_2S$ solution in the absence of a stabilizer.

5.3.3.2 TEM measurements on Ag_2S nuclei

We attempted to obtain TEM images of the nuclei that are formed from a dry deposit prepared from solutions of Ag_2S/AOT ($[AOT]_o = 2.7 \times 10^{-3}$ M). However, we found it to be difficult to attain a good vacuum and the quality of the images was poor. Better

results were obtained when methanol was used as the stabilizer. The absorption spectra were found to be dominated by a broad absorption band from the UV to the visible wavelengths: the absorption band at 300 nm claimed in the previous section is no longer observed in the spectrum of the Ag_2S NP formed in methanol. Thus the sample is largely dominated by Ag_2S nuclei.
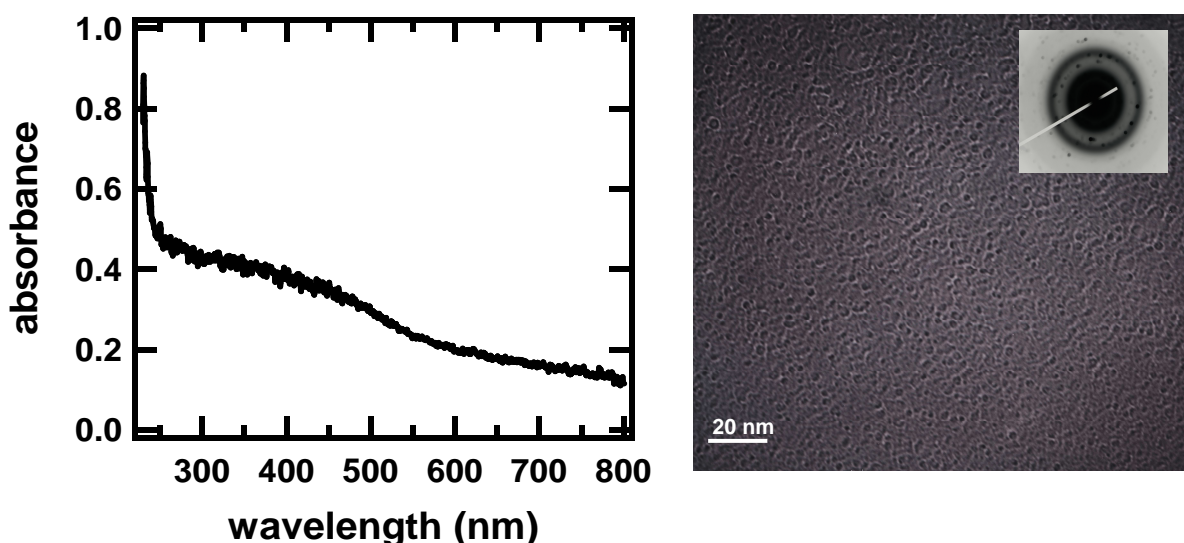
Figure 5.8: The left graph illustrates the dependence of absorbance as a function of wavelength for Ag_2S suspension dispersed in methanol. The right panel displays the TEM image of the corresponding dry deposited from Ag_2S suspension dispersed in methanol. Insert show the electron diffraction pattern obtained for Ag_2S nanoparticles in methanol.

Representative TEM images of the deposit are illustrated on figure 5.8 and 5.9. Regions containing scattered nuclei as well as agglomerates of these nuclei are identified in the images. The average diameter of the Ag_2S nuclei is (4 $\pm$ 1) nm, with a range of sizes between 1 nm and 9 nm, while agglomerates as large as 20 nm can be spotted in the images. After a week sitting inside the TEM chamber we found that most of the agglomerates have formed well defined particles like those displayed in figure 5.9b. Representative diffraction pattern of the Ag_2S nuclei and the larger particles are indicated in the inserts of figures 5.8. The pattern is consistent with the formation of the

monoclinic form of the semiconductor [34]. In this arrangement the sulfide ion is surrounded by six silver ions. The Ag-S bonds distance when the Ag atom is located near the S is between 2.5 Å to 3.1 Å: the Ag-S bond distance estimated from our measurements is in agreement with this range of values for Ag_2S.
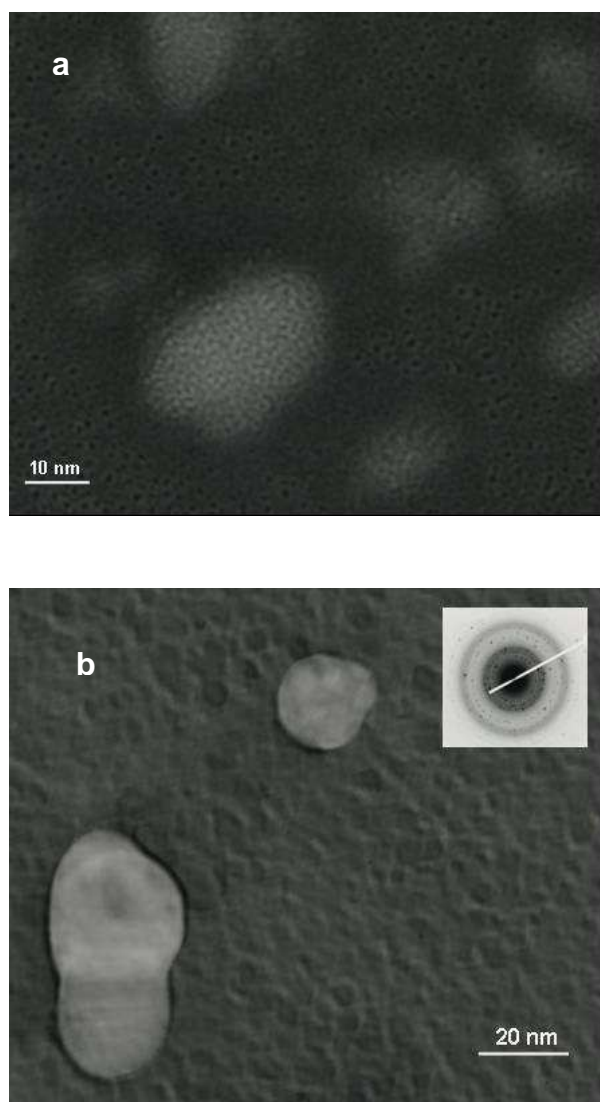
Figure 5.9: Representative TEM images of Ag_2S suspension dispersed in methanol. a) Image acquired immediately after sample preparation. b) Image obtained after a week sitting inside the TEM chamber a week. Insert show the electron diffraction pattern obtained for Ag_2S nanoparticles in methanol.

5.4. Summary

In summary, CIS calculations on structures of several silver sulfide clusters optimized at the density functional level were compared with the optical absorption spectra of reaction mixtures obtained in the early stages of the reaction. This comparison lead us to conclude that the dependence of the optical absorption spectra on time in the first few milliseconds after the flow stops, bands at 487 nm and 590 nm, results from the light absorption by AgS^- and Ag_3S^+ ions. The broad absorption between 250 and 400 nm, on the other hand, may result from the coexistence of other clusters or nanoparticles. In addition, Ag_2S NP were prepared from the reaction of $AgNO_3$, and $(NH_4)_2S$ in the presence of AOT. UV- visible absorption measurements of these Ag_2S/AOT dispersions as a function of AOT concentration are consistent with bands at 300 nm and a broad absorption tail that extends above 700 nm. The absorbance at 300 nm was found to decrease linearly with $[AOT]_o$ while the absorbance at 575 nm decreased monotonically and leveled off when the $[AOT]_o$ reached about 4.8×10^{-4} M. The decrease in the absorbance at 575 nm is attributed to quenching of the formation of nuclei. The physical properties of the embryos and nuclei isolated under our experimental conditions were established by STM and TEM microscopy, respectively. Comparison of the physical properties determined experimentally and the theoretical calculations lead us to propose that a Ag_4S_2 cluster with D_{4h} symmetry is likely responsible for the spectroscopic and physical properties determined for the embryos. A monoclinic form of Ag_2S, on the other hand, appears to be the dominant nuclei formed from the reaction of silver and sulfide ions in the presence of AOT.

5.5 References

1. Nayak, A.; Tamura, T.; Tsuruoka, T.; Terabe, K.; Hosaka, S.; Hasegawa,T.; Aono, M. Rate-Limiting Processes Determining the Switching Time in a Ag_2S Atomic Switch. *J. Phys. Chem. Lett.* **2010**, *1*, 604–608.

2. Wang, Z.; Kadohira, T.; Tada, T.; Watanabe, S. Nonequilibrium Quantum Transport Properties of a Silver Atomic Switch, *Nano Lett.* **2007**, *7*, 2688-2692.

3. Liang, C.; Terabe, K.; Hasegawa, T.; Aono, M. Resistance Switching of an Individual Ag_2S/Ag Nanowire Heterostructure. *Nanotechnology* **2007**, *18*, 485202-485207.

4. Akai-Kasaya, M.; Nishihara, K.; Saito, A.; Kuwahara, Y.; Aono, M. Quantum Point-Contact Switches Using Silver Particles. *Appl. Phys. Lett.* **2006**, *88*, 23107-23110.

5. Van Ruitenbeek, J. Device Physics: Silver Nanoswitch, *Nature* **2005**, 433, 21-22.

6. Terabe, K.; Hasegawa, T.; Nakayama, T.; Aono, M. Quantized Conductance Atomic Switch. *Nature* **2005**, *433*, 47-50.

7. Lu, X.; Li, L.; Zhang, W.; Wang, C. Preparation and characterization of Ag_2S nanoparticles embedded in polymer fibre matrices by electrospinning. *Nanotechnology.* **2005**, *16*, 2233 - 2237.

8. Núñez Rodriguez, A.; Nair, M.T.S.; Nair, P. K. Structural, Optical and Electrical Properties of Chemically Deposited Silver Sulfide Thin Films, *Semicond. Sci. Technol.* **2005**, *20*, 576-585.

9. Meherzi-Maghraoui, H.; Dachraoui, M.; Belgacem, S.; Buhre, K. D.; Kunst, R.; Cowache, P.; Lincot, D. Structural, Optical and Transport Properties of Ag_2S Films Deposited Chemically from Aqueous Solution. *Thin Solid Films* **1996**, *288*, 217-223.

10. Motte, L.; Billoudet, F.; Pileni, M. P. Self-Assembled Monolayer of Nanosized Particles Differing by Their Sizes. *J. Phys. Chem. B* **1995**, *99*, 16425-16429.

11. Zhang, W.; Zhang, L.; Hui, Z; . Zhang, X.; Qian, Y. Synthesis of Nanocrystalline Ag_2S in Aqueous Solution. *Solid State Ionics.* **2000,** *130*, 111-114.

12. Armelao, L.; Bertoncello, R.; Cattaruzza, E.; Gialanella, S.; Gross, S.; Mattei, G.; Mazzoldie, P.; Tondelloa, E., Chemical and Physical Routes for Composite Materials Synthesis: Ag and Ag_2S Nanoparticles in Silica Glass by Sol-Gel and Ion Implantation Techniques. *J. Mater. Chem.* **2002**, *12*, 2401-2407.

13. Tian, C.; Kang, Z.; Wang, E.; Mao, B.; Li, S.; Su, Z.; Xu, L. 'One-step' controllable synthesis of Ag and Ag_2S nanocrystals on a large scale. *Nanotechnology.* **2006**, *17*, 5681 – 5685.

14. Martinez-Castañón, G. A.; Sanchez-Loredo, M. G.; Dorantes, H. J.;.Martinez-Mendoza, J. R; Ortega-Zarzoza, G.;. Ruiz, F. Characterization of Silver Sulfide Nanoparticles Synthesized by a Simple Precipitation Method*. Mater. Lett.* **2005**, *59*, 529-534.

15. Gao, F.; Lu, Q.; Zhao, D. Controllable Assembly of Ordered Semiconductor Ag_2S Nanostructures. *Nano Lett.* **2003**, *3*, 85-88.

16. Schaaff T. G.; Rodinone, A. J. Preparation and Characterization of Silver Sulfide Nanocrystals Generated from Silver (I)-Thiolate Polymers. *J. Phys. Chem. B* **2003,** *107,* 10416-10422.

17. Motte, L.; Pileni, M. P. Influence of Length of Alkyl Chains Used to Passivate Silver Sulfide Nanoparticles in Two- and Three-Dimensional Self-Organization. *J. Phys. Chem. B* **1998**, *102*, 4104-4109.

18. Liu, S. H.; Qian, X. F.; Yin, J.; Hong, L.; Wang, X. L.; Zhu, Z. K. Synthesis and Characterization of Ag_2S Nanocrystals in Hyperbranched Polyurethane at Room Temperature. *J Solid State Chem.* **2002**, *168*, 259-262.

19. Changqi, X.; Zhicheng, Z.; Qiang, Y. A Novel Facile Method to Metal Sulfide (Metal = Cd, Ag, Hg) Nano-Crystallite. *Mater. Lett.* **2004**, *58*, 1671-1676.

20. Motte, L.; Billoudet, F.; Lacaze, E.; Douin, J.; Pileni, M. P. Self-Organization into 2D and 3D Superlattices of Nanosized Particles by Their Size. *J. Phys. Chem. B* **1997**, *101*, 138-144.

21. Pileni, M. P.; Motte, L.; Billoudet, F.; Lacaze, E.; Mahrt, J.; Willig, F. Nanosized Silver Sulfide Particles: Characterization, Self-Organization into 2D and 3D Superlattices. *Mater. Lett.* **1997**, *31*, 255-260.

22. Brühwiler, D.; Leiggener, C.; Glaus, S.; Calzaferri, G. Luminescent Silver Sulfide Clusters. *J. Phys. Chem. B* **2002**, *106*, 3770-3777.

23. Ding, Y.; Xu, B.; Guo, R.; Shen, M. The Preparation of Silver Sulfide Nanoparticles in Lamellar Liquid Crystal and Application to Lubrication. *Mater. Res. Bull.* **2005**, *40*, 575-582.

24. Liu, J.; Raveendran, P.; Shervania, Z.; Ikushima, Y. Synthesis of Ag_2S Quantum Dots in Water-in-CO_2 Microemulsions. *Chem. Commun.* **2004**, *22*, 2582-2583.

25. León-Velázquez, M.; Irizarry, R.; Castro-Rosario, M. Nucleation and Growth of Silver Sulfide Nanoparticles; *J. Phys. Chem. C*, **2010**, *114*, 5839–5849.

26. Bagatur'yants, A. A.; Safonov, A. A.; Stoll, H.; Werner, H. J. Ab Initio Relativistic Pseudopotential Study of Small Silver and Gold Sulfide Clusters $(M_2S)_n$, n=1 and 2. *J. Chem. Phys.* **1998**, *109*, 3096-3108.

27. Brühwiler, D.; Leiggener, C.; Calzaferri, G. Luminescence Properties of Ag_2S and Ag_4S_2 in Zeolite A. *J. Mater. Chem.* **2003**, *13*, 1969-1977.

28. Leiggener, C.; Calzaferri, G. Synthesis and Luminescence Properties of Ag_2S and PbS Clusters in Zeolite A. *Chem. Eur. J.* **2005**, *11*, 7191 -7198.

29. Harris, D. C. *Quantitative Chemical Analysis,* 6th Ed., W.H. Freeman, New York, NY, **2002.**

30. Bujan, M.; Sikiric, M.; Filipovic-Vincekovic, N.; Vdovic, N; Garti, N., Furedi-Milhofer, H. Effect of Anionic Surfactants on Crystal Growth of Calcium Hydrogen Phosphate Dihydrate, *Langmuir,* **2001,** *17,* 6461-6470.

31. Chatterjee, A.; Moulik, S. P.; Sanyal, S. K.; Mishra, B. K.; Puri, P. M. Thermodynamics of Micelle Formation of Ionic Surfactants: A Critical Assessment for Sodium Dodecyl Sulfate, Cetyl Pyridinium Chloride and Dioctyl Sulfosuccinate (Na Salt) by Microcalorimetric, Conductometric, and Tensiometric Measurements, *J. Phys. Chem. B,* **2001,** *105,* 12823-12831.

32. Fan, Y.; Li, Y.; Yuan, G.; Wang, Y.; Wang, J.; Han, C. C.; Yan, H. Comparative Studies on the Micellization of Sodium Bis(4-phenylbutyl) Sulfossuccinate and Sodium Bis(2-ethylhexyl) Sulfosuccinate and Their Interaction with Hydrophobically Modified Poly(acrylamide). *Langmuir*, **2005**, *21*, 3814-3820.

33. Datwani, S. S.; Stebe, K. J. Surface Tension of an Anionic Surfactant: Equilibrium, Dynamics, and Analysis for Aerosol-OT. *Langmuir*, **2001**, *17*, 4287-4296.

34. Kashida, .S.; Watanabe, N.; Hasewaga, T.; Iida, H.; Mori, M.; Savrasov, S. Electronic structure of Ag_2S, band calculation and photoelectron spectroscopy. *Solid State Ionics*. **2003**, *158*, 167- 175.

35. León-Velázquez, M. S.; Morales, M.; Carbo, M.; Sepúlveda, W.; González, M. Rivera, D.; Irizarry, R.; Castro, M. Inhibition of Ag_2S Nucleation by AOT micelles. Submitted to Materials Letters.

CHAPTER 6:

Nucleation and growth of silver sulfide nanoparticles [59]

6.1 Introduction

Colloidal metal and semiconductor nanostructures find numerous technological applications. The chemistry associated with the formation of nanostructures has been subject of a few studies. [1-7] The formation of nanostructures is a chemical process initiated by the reactions of molecules or ions that serve as precursors to nuclei. Nuclei undergo growth or further reactions to form nanostructures. Detailed understanding of the chemistry associated with nuclei formation and growth is important in controlling several physical properties of nanostructures, including size and shape. [8-9]

In this chapter we report on the reactions that lead to the formation of silver sulfide nanoparticles (Ag_2S NP) in solution. Ag_2S nanostructures are a promising material for the development of nanoscaled and atomic switching devices with applications in random access memory (RAM) devices, cross bar electronic circuits, as well as fuel cells and batteries based on ionic conductors and H_2S sensing.[10-14] Despite this, little is known about the chemistry leading to the formation of Ag_2S nanostructures.

Silver sulfide nanoparticles have been prepared by numerous methods that include the use of simple inorganic precursors, providing Ag^+ and S^{-2} ions, to molecular beams and lithography. [15-17] While a simple $AgNO_3$ salt is typically used as the silver source, various organic and inorganic sulfides are used to provide S^{-2} ions, including $(NH_4)_2S$, H_2S and alkyl thiols.[15,18-24] Surfactants, on the other hand, are used to form micelles or microemulsions in chemical synthesis with the purpose of controlling particle size and shape. [25-27]

In this work we report on the nucleation and growth of Ag_2S nanoparticles in a stopped flow reactor. [28-31] $AgNO_3$ and $(NH_4)_2S$ are used as the source of silver and sulfide ions, the latter initially present as hydrosulfide ions in solution. [36-39] The mixer allows the formation of a homogeneous mixture of reactants in a flow prior to the reaction, which is taken to start at the time the flow stops. UV-visible light absorption measurements are used to monitor the nucleation and growth process in real time. Transmission electron microscopy measurements are used for the ex situ characterization of the Ag_2S NP. We found that the nucleation and growth process are not well separated in time. Silver ions play a central role in the nucleation and growth process. The initial nucleation and growth rates are found to increase with initial $[AgNO_3]_0/[(NH_4)_2S]_0$ ratios larger than 1. The experimental results suggest that silver-rich-sulfides are involved in the nucleation stage and growth process of Ag_2S NP. Density functional calculations are consistent with that interpretation: Ag_3S^+ is found to have a lower energy than the Ag_2S and $AgSH$ molecules or the AgS^- and Ag_2SH^+ ions. The results are discussed in terms of classic nucleation and growth theory and the possible growth mechanisms are discussed.

6.2. Experimental

Silver solutions were prepared by dissolving silver nitrate (ACS grade Fisher) in deionized water, obtained from a Culligan system. Sulfide solutions were prepared using ammonium sulfide solutions (Alfa Aesar) in deionized water. The concentration solutions employed in the experiments described here ranged from 2.4×10^{-2} M to 0.5×10^{-3} M.

A Biologic Stop flow reactor model SFM 400 was employed to prepare the silver sulfide nanoparticles. UV-visible absorption measurements were conducted in situ in a quartz cell. The transmitted light was analyzed with an Ocean Optics USB 4000 spectrograph. Transmission electron microscopy measurements were performed in a JEOL 2010 model. Negatives of the micrographs were processed using standard techniques and

scanned with an EPSON Perfection V750 PRO scanner and stored in the computer for further analysis.

6.3. Results and Discussion:

6.3.1 TEM measurements

A TEM image of a deposit prepared from a solution of the Ag_2S NP formed a few seconds after a flow containing 17 μL of a 8 x 10^{-3} M $AgNO_3$ solution and 17 μL of a 4 x 10^{-3} M $(NH_4)_2S$ solution stopped is displayed on figure 6.1. The deposit was prepared by immersing a carbon coated grid in a solution of the Ag_2S NP dispersed in methanol for about 10 seconds and out gassed at 10^{-3} torr for about 24 hours. The deposit was out gassed for an additional 24 hours inside the high vacuum environment of the TEM prior to the measurements. The TEM measurements reveal that the reaction between $AgNO_3$ and $(NH_4)_2S$ results in the formation of nanoparticles, in excellent agreement with previous works.[15] Quantitative measurements of TEM images like the one shown on figure 6.1 obtained in several regions of the grid to include about 500 NP resulted in the particle size distribution histogram displayed on the lower panel of figure 6.1. The average diameter of the Ag_2S NP is 4 nm. The Ag_2S nanoparticles exhibit a broad distribution, with nanoparticle diameters in the size range of 2 to 9 nm. Over 70% of the nanoparticles have diameters between 2 and 5 nm. TEM images collected 10 minutes after a flow containing the same initial reactant concentrations has stopped reveal a similar average particle size but a broader distribution, with nanoparticle diameters in the 1 to 48 nm size range. We conclude that most of the Ag_2S NP forms in the first few seconds after the flow stops and growth results in the formation of particles with a broad size range.
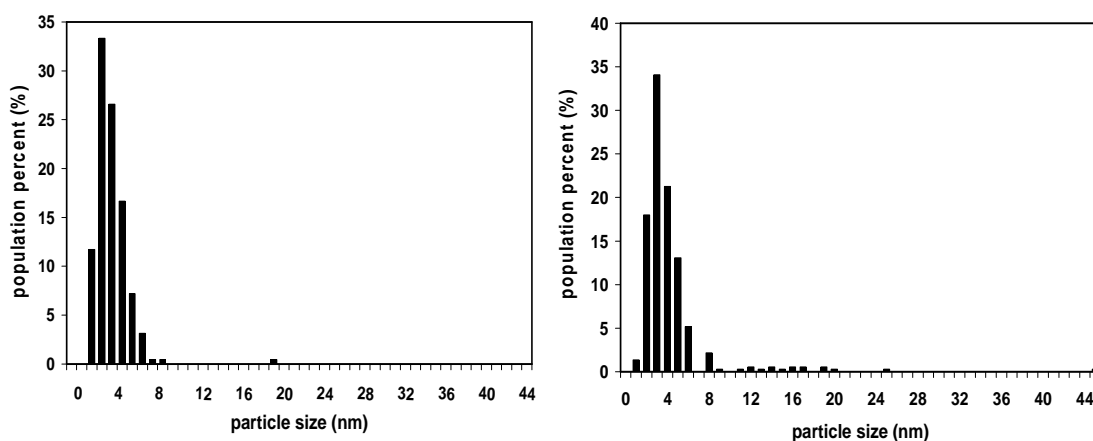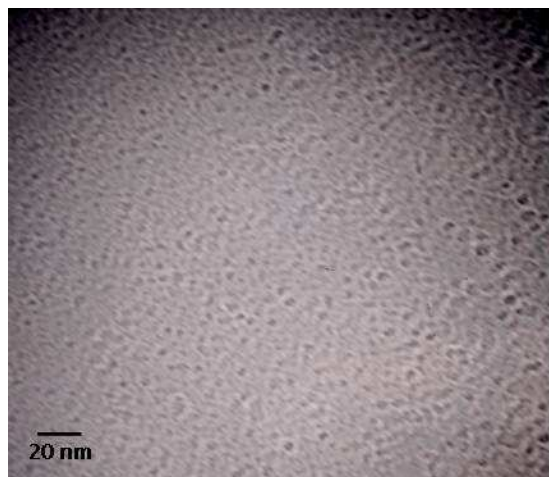
Figure 6.1: TEM image of Ag$_2$S NP formed from the reaction of 8.0 x 10^{-3} M AgNO$_3$ and (NH$_4$)$_2$S 4.0 x10^{-3} M solutions in a stopped flow reactor. Particle size distributions obtained from analysis of TEM images corresponding to (a) the first 10 to 15 seconds and (b) about 10 minutes after the flow stopped is displayed on the bottom of the figure.

6.3.2 UV-visible absorption spectroscopy measurements

With the purpose of learning the role played by the ions in the formation of Ag$_2$S NP we performed UV-visible absorption measurements as a function of initial silver ion concentration. UV-visible absorption spectra of reaction mixtures containing an initial

[(NH$_4$)$_2$S]$_o$ of 4 x 10^{-3} M and different initial silver concentrations are displayed on figure 6.2.
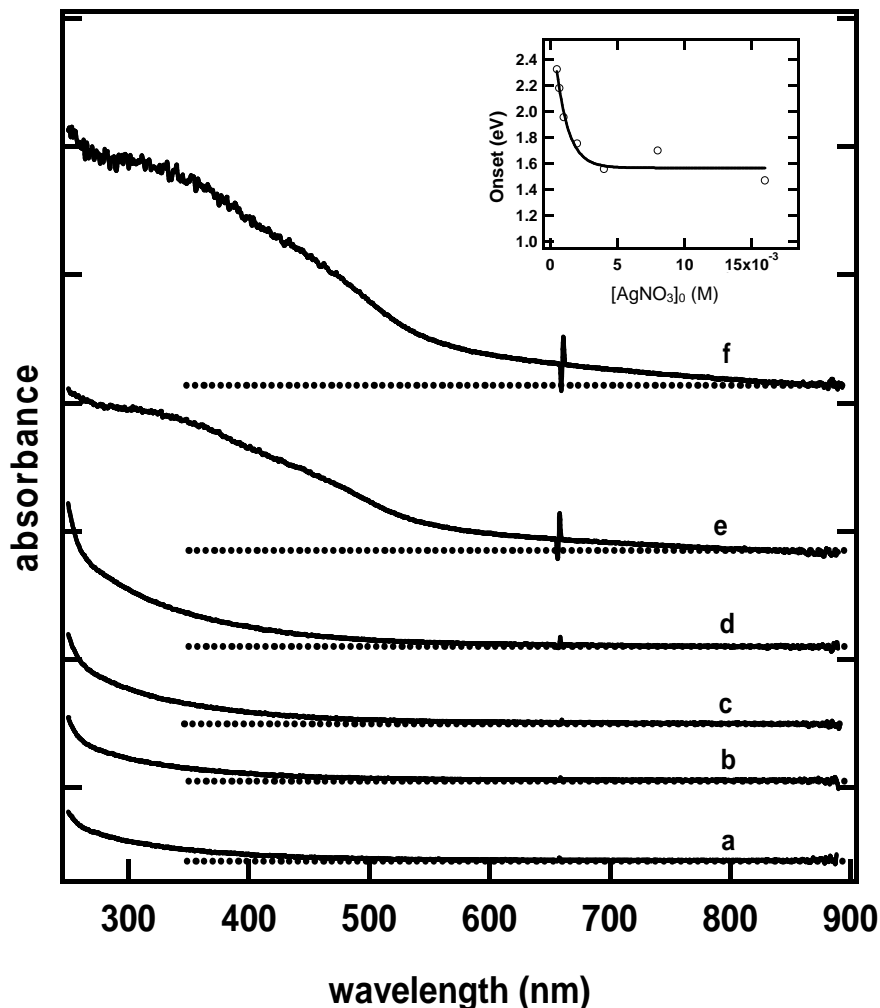
Figure 6.2: UV visible absorption spectra of Ag$_2$S NP as a function of initial silver concentration. The initial [(NH$_4$)$_2$S]$_o$ is 4 x 10^{-3} M in throughout. The spectra were obtained about 5 seconds after the flow stops. The initial [AgNO$_3$]$_o$ concentrations are (x 10^{-3} M): (a) 0.5, (b) 0.67, (c) 1, (d) 2, (e) 4 and (f) 16. The onset of light absorption as a function of initial AgNO$_3$ concentration is illustrated in the inset of figure 6.2. The solid line is to guide the eye and does not represent a fit to the data.

The spectra were obtained about 5 seconds after the flow containing the reactants stopped. The spectrum corresponding to an initial [AgNO$_3$]$_o$ concentration of 5 x 10^{-4} M is characterized by an onset in light absorption around 530 nm and an increase in

absorbance with decreasing wavelength from the visible to the ultraviolet region. The wavelength at which the absorbance has fallen to the baseline value were used as a measure of the onset of light absorption: the reader is referred to section 6.3.5 for a detailed description of a more rigorous treatment of the data to estimate the onset of light absorption. The onset in light absorption shifts toward longer wavelengths with increasing initial reactant concentration: it is found around 565 and 630 nm when the initial $[AgNO_3]_o$ is further increased to 7×10^{-4} and 1×10^{-3} M, respectively. A marked change in the appearance of the absorption spectrum of the Ag_2S NP is observed when the initial silver concentration is equal to or higher than the initial $(NH_4)_2S$ concentration. The spectrum labeled 'e' in figure 6.2 corresponds to a stopped flow with $[AgNO_3]_o$ and $[(NH_4)_2S]_o$ of 4×10^{-3} M. The spectrum is dominated by a band between 310 and 320 nm and a high wavelength shoulder that extends above 500 nm. The absorbance of the band at 310 nm and the high wavelength shoulder increases when the initial silver concentration is further increased to 1.6×10^{-2} M.

The insert in figure 6.2 summarizes the band gap energy as a function of initial $[AgNO_3]_o$ concentration. Band gap energies are estimated from the onset in light absorption of the spectra displayed on figure 6.2. There is a small shift toward lower band gap energies with $[AgNO_3]_0$ concentration. Previous works have reported quantum confinement effects on Ag_2S NP in the size range of 3 to 8 nm. Motte and coworkers [32] have reported a small decrease in the indirect band gap with increasing Ag_2S NP size from 3.2 up to 5.8 nm. Chen [33], on the other hand, has reported gap energy of 1.71 eV for 8.4 nm Ag_2S nanoparticles formed upon exposure of 7.4 nm Ag NP to H_2S gas. These particle size dependent band gap energies reported in previous works are higher than the corresponding bulk value of 1 eV (1239.8 nm) [8,34-35]. The onset in light absorption summarized in the insert displayed on figure 6.2 corresponds to band gap energies that are higher than the 1 eV band gap reported for bulk Ag_2S. This lead us to conclude that the Ag_2S NP formed in the initial stages of the reaction between $AgNO_3$ and $(NH_4)_2S$ in the concentration range of our work exhibit quantum confinement effects.

6.3.3 Time dependent UV-visible absorption spectra

The time profile of the UV-visible absorption spectra of stopped flows with two different $[AgNO_3]_o/[(NH_4)_2S]_0$ ratios are summarized on figures 6.3 and 6.4, respectively. The absorption spectra of $AgNO_3$ and $(NH_4)_2S$ are indicated in figure 6.3. The spectra of $AgNO_3$ and $(NH_4)_2S$ are dominated by a single band centered at 225 and 237 nm, respectively. The spectra of $AgNO_3$ and $(NH_4)_2S$ were obtained in independent measurements by averaging 50 scans between between 200 and 300 nm. Since $(NH_4)_2S$ is a strong electrolyte, it is likely dissolved into S^{-2} and NH_4^+ ions in aqueous solution. Depending on pH, $S^{-2}_{(aq)}$ ions hydrolyze to form $HS^-_{(aq)}$ and $H_2S_{(aq)}$. The pH of solutions formed upon mixing 8×10^{-3} M $AgNO_3$ and 4×10^{-3} $(NH_3)_4S$ solutions is 9.1. At this pH, HS^- is the most likely species in solution. [36-37] Thus the band around 235 nm in the spectra of the solutions of $(NH_4)_2S_{(aq)}$ employed likely results from HS^- in solution. This interpretation is consistent with the UV-visible absorption spectrum of HS^- reported by previous investigators. [36-39]

Exciting changes are observed in the time profile of the UV-visible absorption spectra of a reaction mixture with initial 8×10^{-3} M $AgNO_3$ and 4×10^{-3} M $(NH_4)_2S$ concentrations displayed on figure 6.3. The spectrum of the solution that results a second after the flow containing the $AgNO_3$ and $(NH_4)_2S$ reaction mixture has stopped is dominated by a broad band with strong absorption between 200 and 300 nm and a long wavelength tail that extends above 500 nm. The strong absorption between 200 and 300 nm decreases to about 50 % of its initial value at t=2 seconds and the band at 310 nm starts to develop. There is also an increase in the absorbance at longer wavelengths, which is reflected by the increase in absorbance between 400 and 575 nm and a shift toward longer wavelengths in the onset of light absorption with time. On the other hand, the most significant changes in the UV-visible absorption spectra displayed on figure 6.4, corresponding to a stopped flow containing a $[AgNO_3]_o/[(NH_4)_2S]_o = 0.5$, is a shift toward longer wavelengths in the onset of light absorption with time.
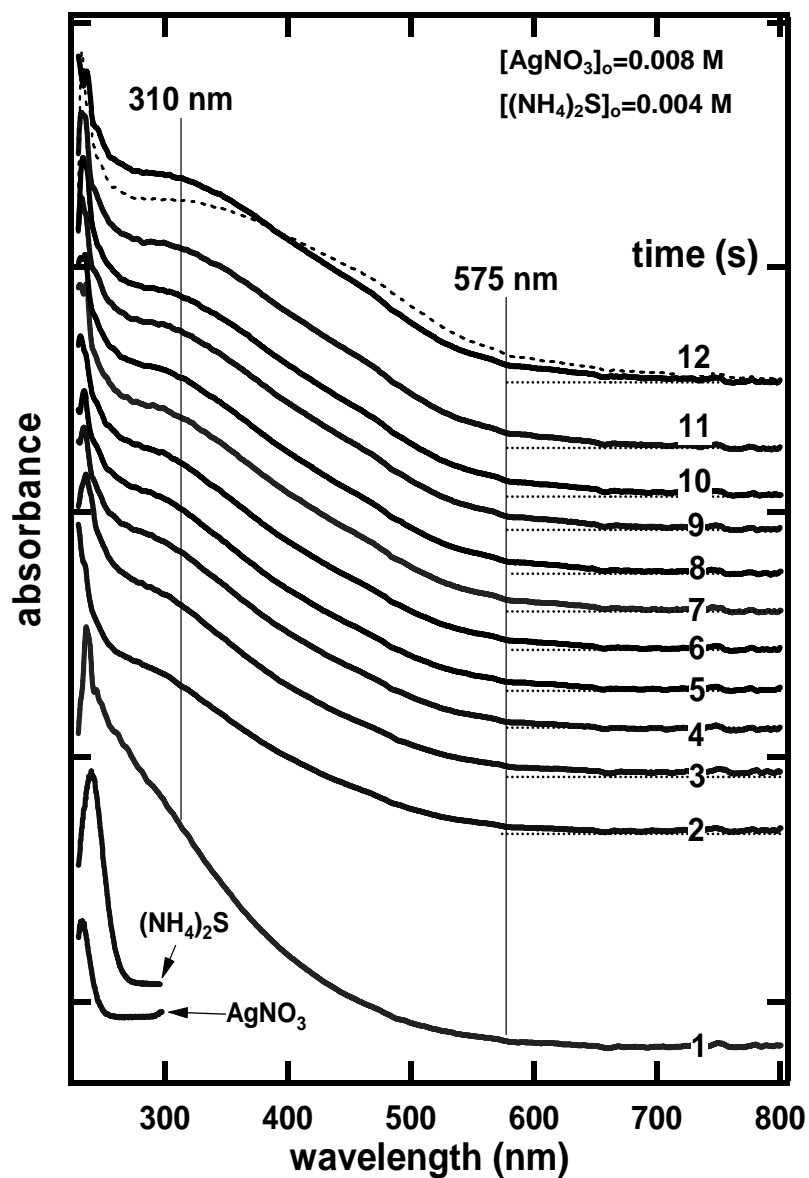
Figure 6.3: Time dependent UV-visible absorption spectra of a stopped flow with the indicated initial $[AgNO_3]_o$ and $[(NH_4)_2S]_o$ concentrations. The absorption spectra of the $AgNO_3$ and $(NH_4)_2S$ used are indicated in the figure. The dotted line represents the spectrum obtained 45 seconds after the flow stopped.
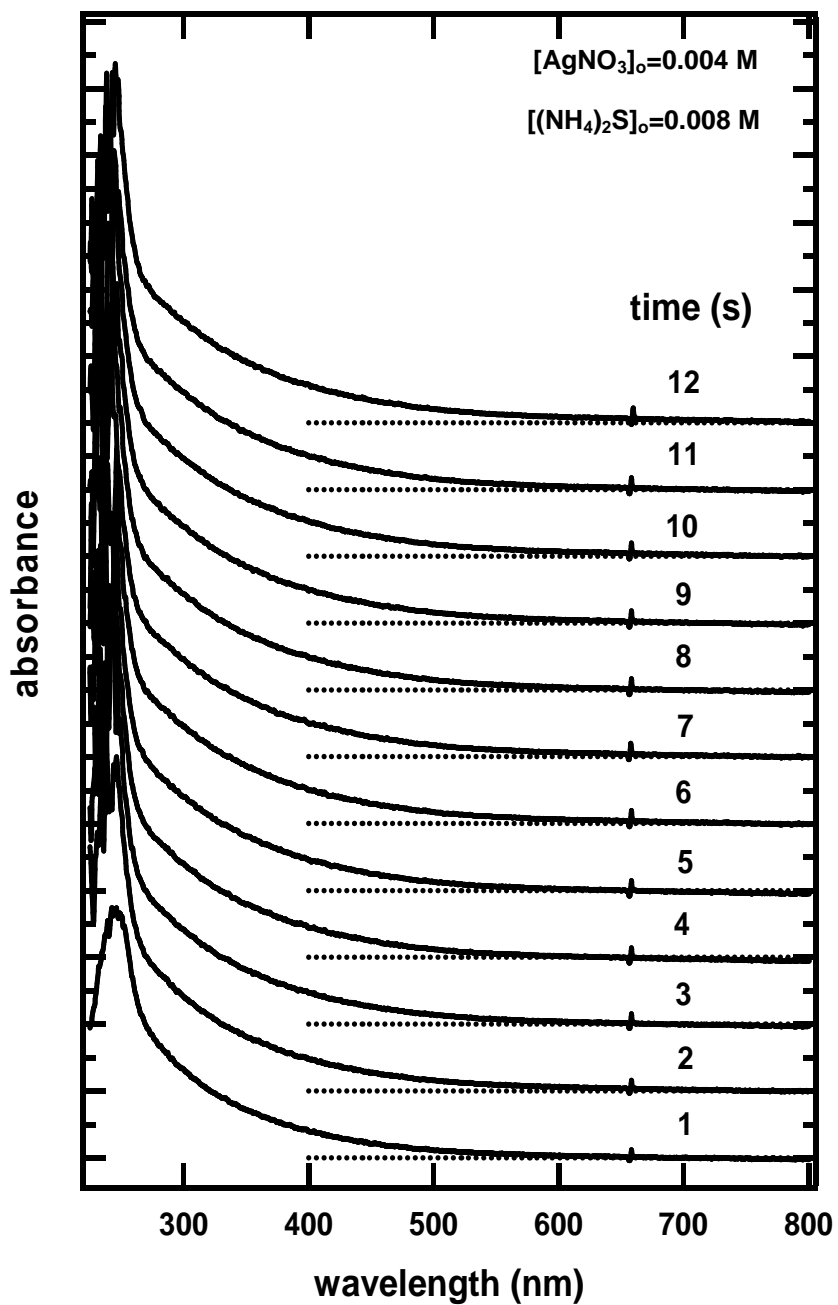
Figure 6.4: Time dependent UV-visible absorption spectra of a stopped flow with the indicated initial $[AgNO_3]_o$ and $[(NH_4)_2S]_o$ concentrations.

6.3.4 Ag$_2$S NP nucleation

The onset in light absorption in semiconductor nanoparticles results from transitions from the valence to the conduction band [32-33, 40]. The absorbance (A) is related to particle concentration,[N], according to Beer-Lambert law :

$$A= \alpha \ell \, [N] \qquad\qquad \text{equation 6.1}$$

where α and ℓ represent the absorptivity coefficient and cell width. We have used the absorbance near the band edge to establish the effect of initial [AgNO$_3$]$_o$ and [(NH$_4$)$_2$S]$_o$ on the rate of nuclei formation [32-33,40]. The dependence of the absorbance near the band edge at 575 nm for several initial [AgNO$_3$]$_o$ with a constant [(NH$_4$)$_2$S]$_o$ of 4 x 10^{-3} M is illustrated in the upper panel of figure 6.5. For the lowest [AgNO$_3$]$_o$ there is no significant increase in the absorbance at 575 nm in the time scale of the measurements. For an initial [AgNO$_3$]$_o$ of 8 x 10^{-3} M, the absorbance at 575 nm increases to reach a value of 0.18 in the first 8 seconds after the flow stops: it increases slightly, to about 0.20 at t=14 seconds.

A noticeable increase in the absorbance at 575 nm occurs in the first 6 seconds after the flow stops when the initial [AgNO$_3$]$_o$ reaches 1.6 x 10^{-2} M. When the [AgNO$_3$]$_o$ is 2.4 x 10^{-2} M, the absorbance reaches a value of about 0.45 in the first 6 seconds after the flow stops and increases by a little more than 10 % when the reaction has reached 15 seconds. The dependence of the absorbance near the band edge at 575 nm for several initial [(NH$_4$)$_2$S]$_o$ with a constant [AgNO$_3$]$_o$ of 4 x 10^{-3} M is illustrated in the lower panel on figure 6.5. The absorbance at 575 nm increases a couple seconds after the flow stops for an initial [(NH$_4$)$_2$S]$_o$ 6.7 x 10^{-4} M and then remains nearly constant at about 0.05. Further increase in [(NH$_4$)$_2$S]$_o$ results in well-defined increase in absorbance over the time scale of the measurements reported.
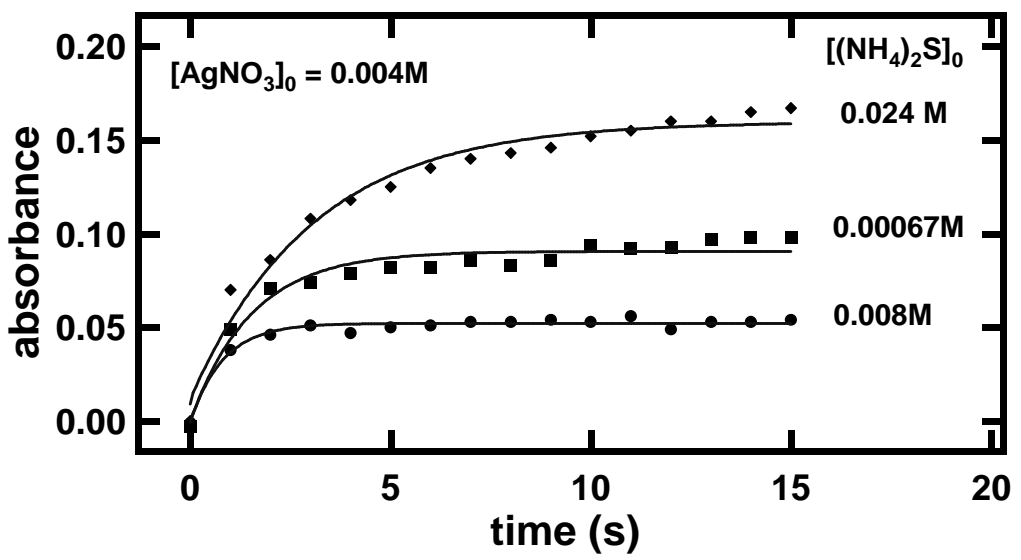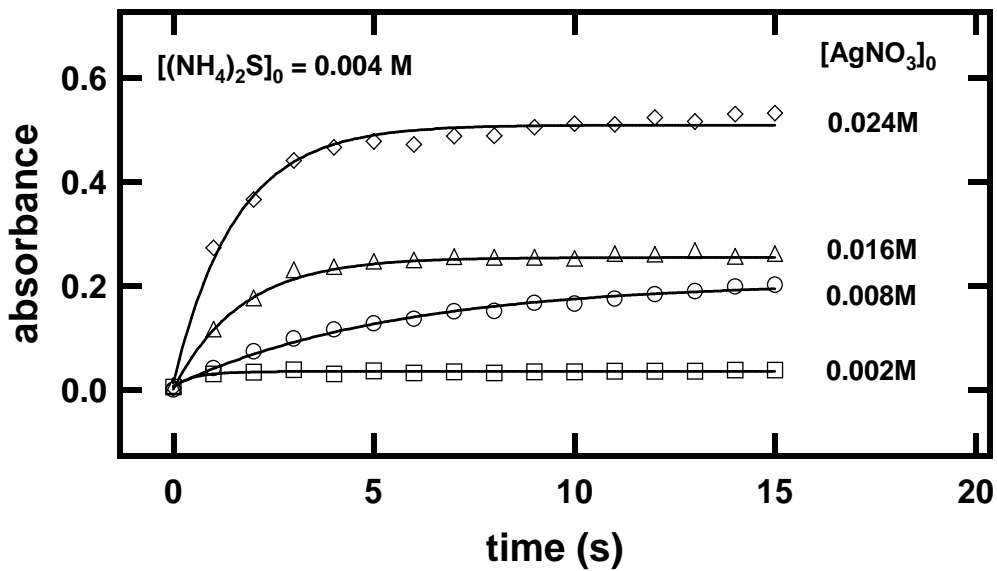
Figure 6.5: Dependence of the absorbance at 575 nm as a function of time for the indicated initial $[(NH_4)_2S]_o$ and $[AgNO_3]_0$ concentrations, respectively. The solid lines are a fit to $A = e^{kt}$, where A is the absorbance, k is a constant and t is time.

The nucleation rate can be determined from the dependence of the absorbance at 575 nm on time. The dependence of the nucleation rate can be divided in two regions. One

61

of these regions is set in the first few seconds, up to about 8 seconds, after the flow stopped.   There is a second region that is characterized by a slower increase in the absorbance near the band edge. This second region is observed at times longer than 5 to 8 seconds after the flow stopped.   Figures 6.6 and 6.7 summarize the dependence of the initial nucleation rate and the nucleation rate determined at times longer than 8 seconds on the initial reactant concentration, respectively.   The nucleation rate, displayed on figure 6.7b, increases by less than 1 % when comparing the values obtained with the largest difference in initial $[AgNO_3]_o$, while it remains nearly constant with initial $[(NH_4)_2S]_o$ concentration.

The initial rates displayed on figure 6.6, on the other hand, have been normalized to the maximum initial rate determined for the indicated initial reactant concentration. The initial nucleation rate does not change significant for initial silver nitrate concentrations that fall between 0.0005 and 0.008 M. It increases with silver nitrate concentration when the $[AgNO_3]_o > 0.008$ M. The initial nucleation rate was also found to depend on initial $[(NH_4)_2S]_o$. The initial nucleation rate was found to increase with $[(NH_4)_2S]_o$ until a $[AgNO_3]_o/[(NH_4)_2S]_o$ of 1 was obtained. Above this ratio, the initial absorbance dropped sharply to between 0.2 and 0.4 for initial $[(NH_4)_2S]_o$ in the 0.008 to 0.024 M range of molar concentrations.

We wish to highlight that the initial nucleation rate appears to split into two regions according to the $[AgNO_3]_o / [(NH_4)_2S]_o$. These regions are highlighted on figure 6.6. Considering first the dependence of the initial rate on initial silver ion concentration, the initial nucleation rate exhibits a significant increase when the $[AgNO_3]_o/[(NH_4)_2S]_o$ larger than 1. Likewise, when the dependence of the initial nucleation rate on the initial $(NH_4)_2S$ concentration is considered, the nucleation rate is observed to increase significantly in those regions where the $[AgNO_3]_o / [(NH_4)_2S]_o$ becomes larger than 1. We conclude that nuclei formation is faster in the presence of a silver excess, which suggests that such nuclei are rich in silver ions.
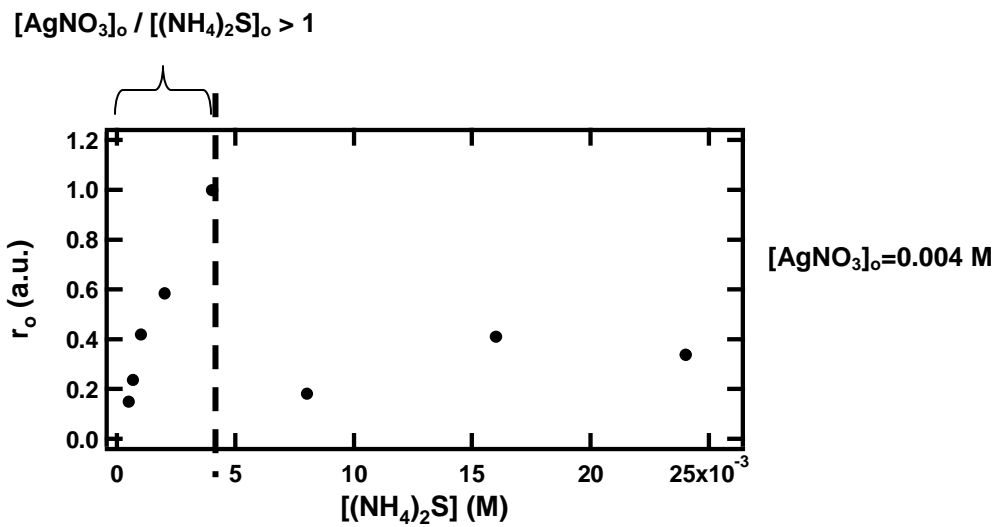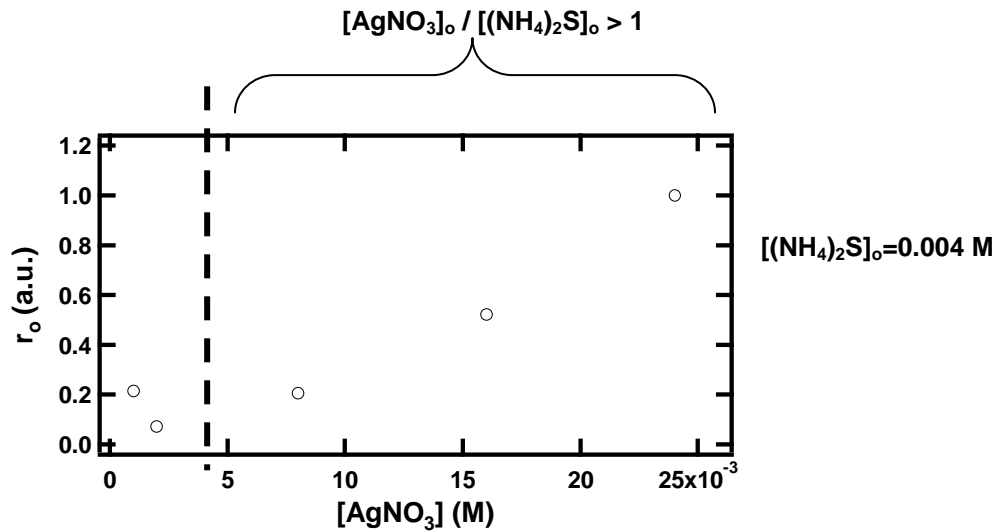
Figure 6.6: Initial nucleation rates (r_o) of Ag_2S NP as a function of $[AgNO_3]_0$ and $[(NH_4)_2S]_o$. The initial concentration of the second reactant is constant at the value indicated on the right hand side of each plot. The regions of increasing initial nucleation rate are highlighted with the $[AgNO_3]_0/ [(NH_4)_2S]_o > 1$.
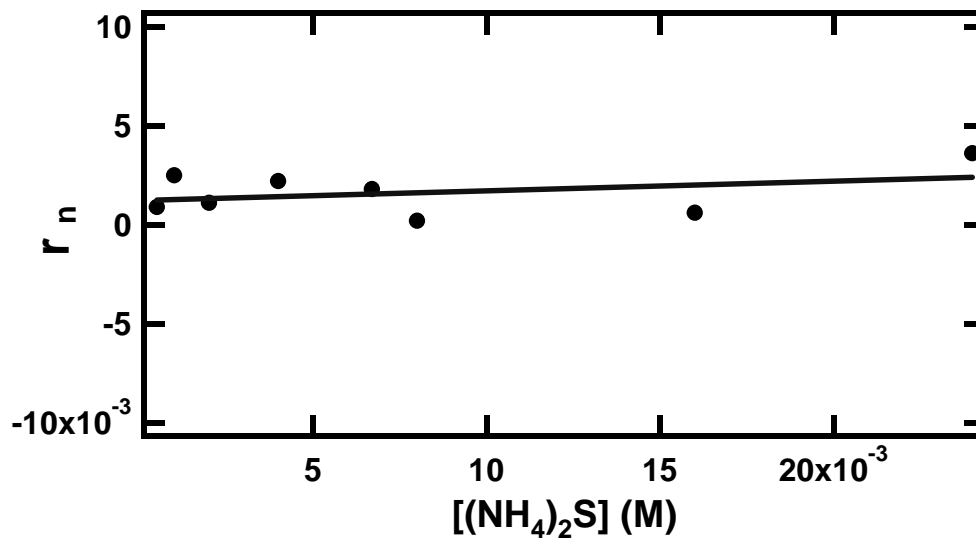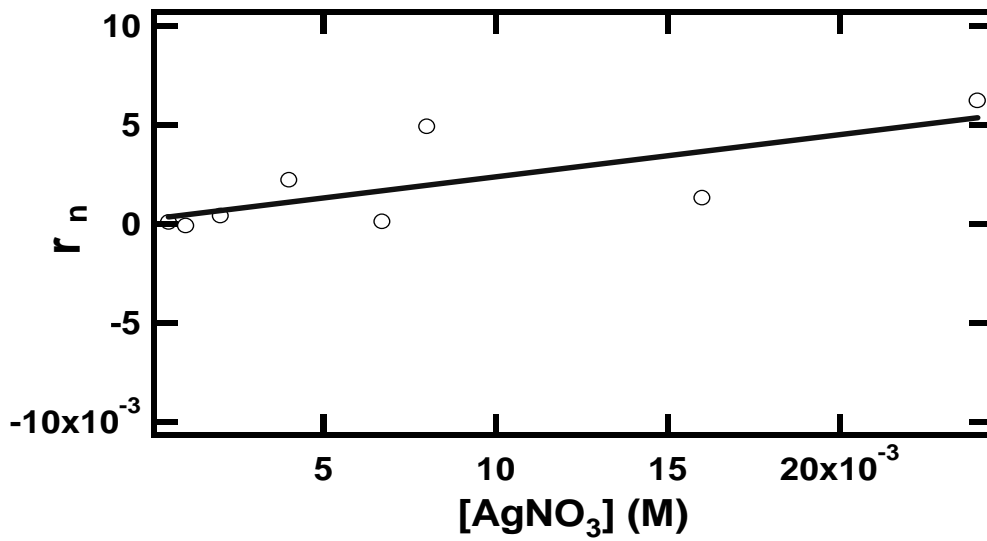
Figure 6.7: The nucleation rate determined t = 5 to 8 seconds after the flow stopped as a function of initial reactant concentration.

6.3.5 Ag$_2$S NP growth

The time profile of the UV visible absorption spectra displayed on figures 6.3 and 6.4 are characterized by a shift in the onset of light absorption with time. As discussed in section 6.3.2, the onset of light absorption shifts toward longer wavelengths with increasing semiconductor nanoparticle size. In this section, we discuss how to obtain particle diameters from the absorption spectra of Ag$_2$S NP. We also discuss the time dependent changes in the onset of light absorption in the context of Ag$_2$S NP growth.

Kryukov [40] has found indirect and direct band gaps in Ag$_2$S NP. Indirect and direct band gap energies are determined by considering the energy at which the absortivity coefficient (α) falls to zero. Rigorously, the intercept in the coordinate axis of plots of $(\alpha E)^{1/2}$ or $(\alpha E)^2$ as a function of incident photon energy (E) represents the indirect or direct band gap energy, respectively. The indirect band gap in Ag$_2$S is located at lower energies (longer wavelengths) than the direct band gap. As a result, indirect band gaps are easier to locate in the optical absorption spectrum. Since the absorbance A is directly proportional to the absortivity coefficient (α), we have taken the energies at which $(AE)^{1/2}$ falls to zero as a measure of the indirect band gap energy. The upper panel in figure 6.8 shows a plot of $(AE)^{1/2}$ as a function of energy (E). The values of $(AE)^{1/2}$ employed to construct the traces displayed on figure 6.8 were obtained from the absorption spectrum of a stopped flow with initial $[AgNO_3]_o$ of 8×10^{-3} M and $[(NH_4)_2]_o$ of 4×10^{-3} M at t =1, 6, 14, 20 and 45 seconds. The indirect band gap energy is obtained from the initial rise in $(AE)^{1/2}$ as a function of energy. For the measurement performed at t=1 second, for instance, we estimate an indirect band gap energy of 1.83 eV or 679 nm. The onset in light absorption is estimated around 660 nm directly from the corresponding absorbance spectrum.

We have used the approach described in the previous paragraph to estimate the indirect band gap energies as a function of time for a set of measurements with initial reactant concentrations of $[AgNO_3]_o=8 \times 10^{-3}$M and $[(NH_4)_2S]_o=4 \times 10^{-3}$ M. The results

are illustrated in the lower panel of figure 6.8. The indirect band gap for this reaction mixture depends on the time of the measurement. Indirect band gap values are found between 670 and 740 nm in the first 15 seconds of reaction.
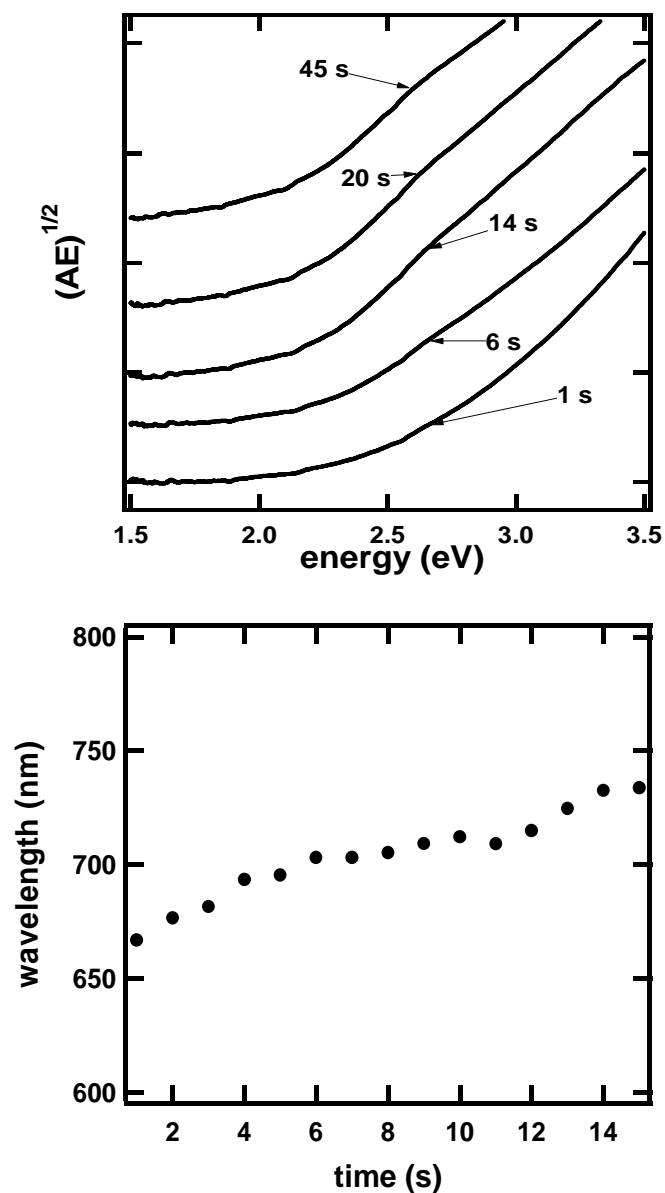
Figure 6.8: The upper graph illustrates the dependence of $(AE)^{1/2}$ as a function of energy for the indicated reactions times. The lower panel illustrates the dependence of the onset of light absorption on time estimated from a time dependent UV-visible absorption profile. The initial concentrations of $[AgNO_3]_o$ and $[(NH_4)_2S]_o$ of 8×10^{-3} M and 4×10^{-3} M throughout, respectively.

There are several models to correlate the direct band gap of a semiconductor nanoparticle with its diameter [41-44]. Such models require knowledge of the effective electron-hole mass and the bulk direct band gap energy. We are not aware of a measurement of the effective electron-hole mass in the case of Ag_2S, although it is known for a few other semiconductor nanoparticles [45-46]. Furthermore, knowledge of the effective mass is of little use in the case of Ag_2S, which has indirect, in addition to direct, band gaps. Quantum confinement effects in the indirect band gap of semiconductor nanostructures have been the subject of a few studies. However, attempts to accommodate experimental observations into a single model may be a difficult task. [55-57] In InP semiconductor NP, a strong quantum confinement has been reported. In that case the quantum confinement effect was observed to significantly reduce the separation between the direct and indirect conduction band states. [55] Short range electron-hole exchange interactions are predicted to play an important role in describing quantum confinement effects in semiconductor NP.[56] In GaAs semiconductor NP, for instance, the band structure experiences significant variations with NP size. [57] It is quite possible that a similar situation also occurs in the case of Ag_2S NP, although variation in phonon mode energies may accompany particle size changes in the electronic structure of the nanoparticles. In passing we note that the difference between the direct and indirect band gap ranges between 1.66 and 1.76 eV for Ag_2S NP prepared with different initial reactant concentrations and in the presence or absence of stabilizers [40]

Fortunately, the contribution from other research groups has resulted in an adequate number of measurements to establish a correlation between Ag_2S particle size and band gap energy. Figure 6.9 shows the dependence of the Ag_2S NP diameter as a function of indirect band gap energy. The data presented in the figure includes data points reported in the earlier works of Motte [32] and Chen [33], as well as three points added by this work in samples prepared in the presence of a surfactant (AOT). In all cases, average particle diameters are estimated from TEM measurements while indirect band gap energies are determined from the onset of light absorption of the corresponding optical absorption spectrum, as described in the previous paragraphs.

There is a linear correlation between Ag_2S NP diameter and band gap energy in the range of particle sizes reported. The dependence of the Ag_2S NP diameter on band gap, taking into account the results reported by Chen [33] and Motte [32] only, is fitted with the equation:

$$d(nm) = 35 - 15\ E_{gap} \qquad\qquad \textbf{equation 6.2}$$

We have used this correlation to estimate the dependence of Ag_2S NP diameter as a function of time. Since the onset of light absorption of large particles appears at longer wavelengths than the onset in smaller particles, the approach we have employed will provide information regarding the growth of the particles with the largest diameter in solution as oppose to the mean or average particle size. [58]
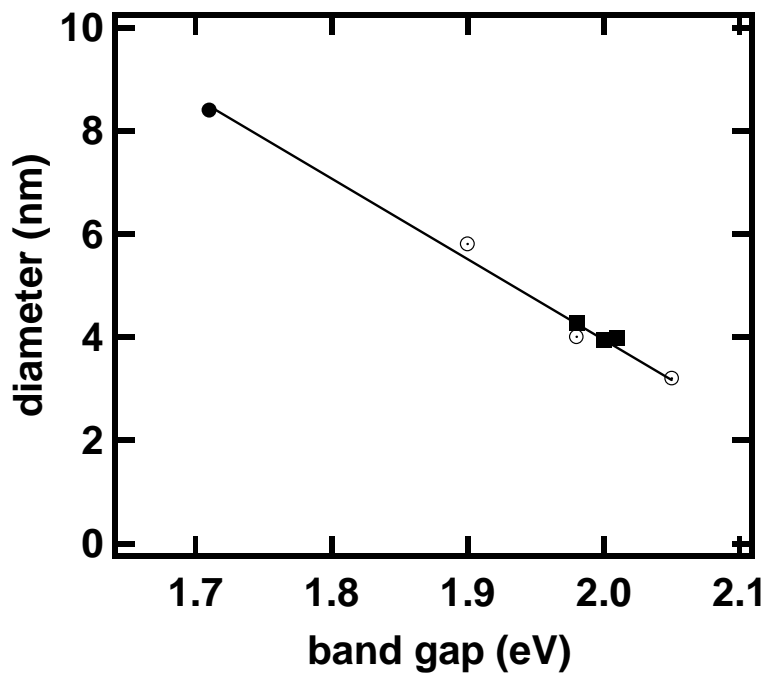
Figure 6.9: Dependence of Ag_2S NP diameter on the indirect band gap energy taken from the work of Chen (closed circle), Motte (open circles) and our work (closed squares).
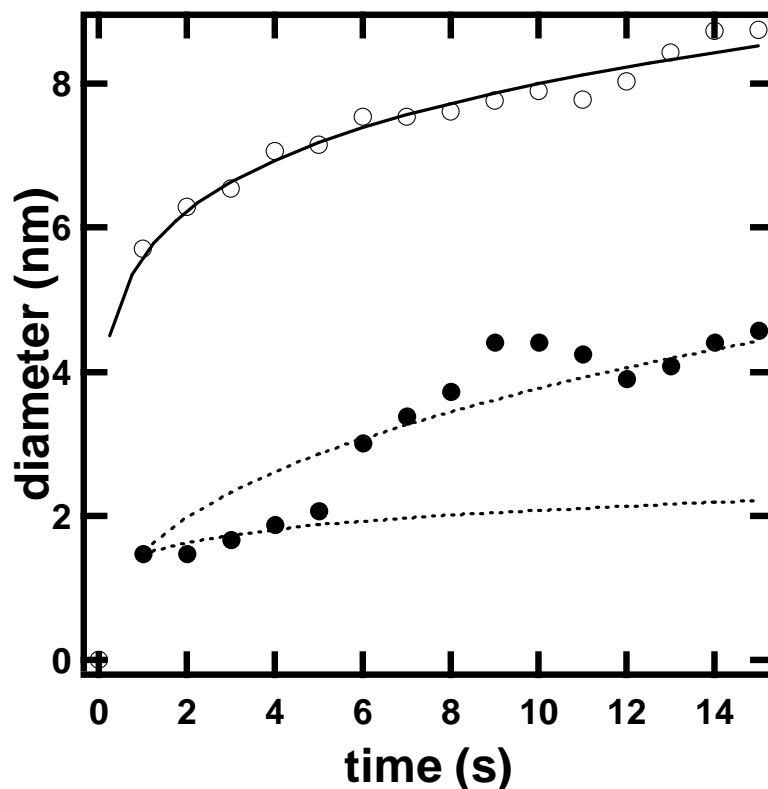
Figure 6.10: Growth curves of Ag_2S NP. The initial reactant concentrations are: open circles $[AgNO_3]_o = 8 \times 10^{-3}$ M and $[(NH_4)_2S]_o = 4 \times 10^{-3}$ M and for the closed circles $[AgNO_3]_o = 4 \times 10^{-3}$ M and $[(NH_4)_2S]_o = 2.4 \times 10^{-2}$ M. The solid and dashed lines represent model fit to the data using equation 6.3 for the two initial reactant concentrations indicated above. The two dotted lines represent attempts to model fit the results for $[AgNO_3]_o = 4 \times 10^{-3}$ M and $[(NH_4)_2S]_o = 2.4 \times 10^{-2}$ M with two different values of α and k.

The open and closed circles in figure 6.10 shows the dependence of the Ag_2S NP diameter on time for a combination of reactants with a $[AgNO_3]_o / [(NH_4)_2S]_o$ ratio of 2 and 0.5, respectively. The Ag_2S NP diameter increases with time in both cases. The solid line in figure 6.10 represents a power plot fit to the data according to:

$$d = kt^{\alpha} \qquad \text{equation 6.3}$$

where k is the growth constant and α represents the power exponent. The fit models the data well for those growth curves with $[AgNO_3]_o$ / $[(NH_4)_2S]_o$ ratio larger than 1, but fails to describe the dependence of the particle size over the entire time scale of the measurements when the $[AgNO_3]_o$ / $[(NH_4)_2S]_o$ ratio is smaller than 1. Since the nucleation rate at long times (figure 6.7) remains nearly constant, it is reasonable to expect the number of nuclei to be constant between t = 8 and 15 seconds. If that is the case, the magnitude of the exponent may be taken as indicative of the process that limits nanoparticle growth. A value of $\alpha = 0.5$ or $\alpha = 1$ represent a growth process limited by the diffusion of the reactants from solution to the surface of the nuclei or by the reactions on the surface of the nuclei, respectively.[52-53] After examining over 10 different initial reactant concentrations values of α between 0.5 and 0.15 were obtained. These values are not those expected for a growth process limited by diffusion or interface reactions, leading us to conclude that other reactions of the ions in solution limit Ag_2S NP growth.

The upper panel on figure 6.11 summarizes initial growth rates as a function of initial $[AgNO_3]_0$ and a constant initial $[(NH_4)_2S]_0$ 0.004 M. The initial growth rate remains nearly constant for the two lowest $[AgNO_3]_0$ concentrations employed and increases when the $[AgNO_3]_0$ is larger than the $[(NH_4)_2S]_0$. Turning to the effect of the sulfide ion in the growth of Ag_2S NP, the initial growth rate increases with $[(NH_4)_2S]_0$ up to about 0.004 M. Further increase in $[(NH_4)_2S]_0$ results in a gradual increase in the initial growth rate. Comparison of the results summarized on figures 6.6 and 6.11 reveal that similar trends are observed in the dependence of the growth and nucleation rates on initial reactant concentration. Both rates exhibit an increase with initial reactant concentration as long as the initial $[AgNO_3]_0$ / $[(NH_4)_2S]_0$ ratio is larger than 1. This similarity leads us to conclude that these processes are facilitated by an excess of silver ions.
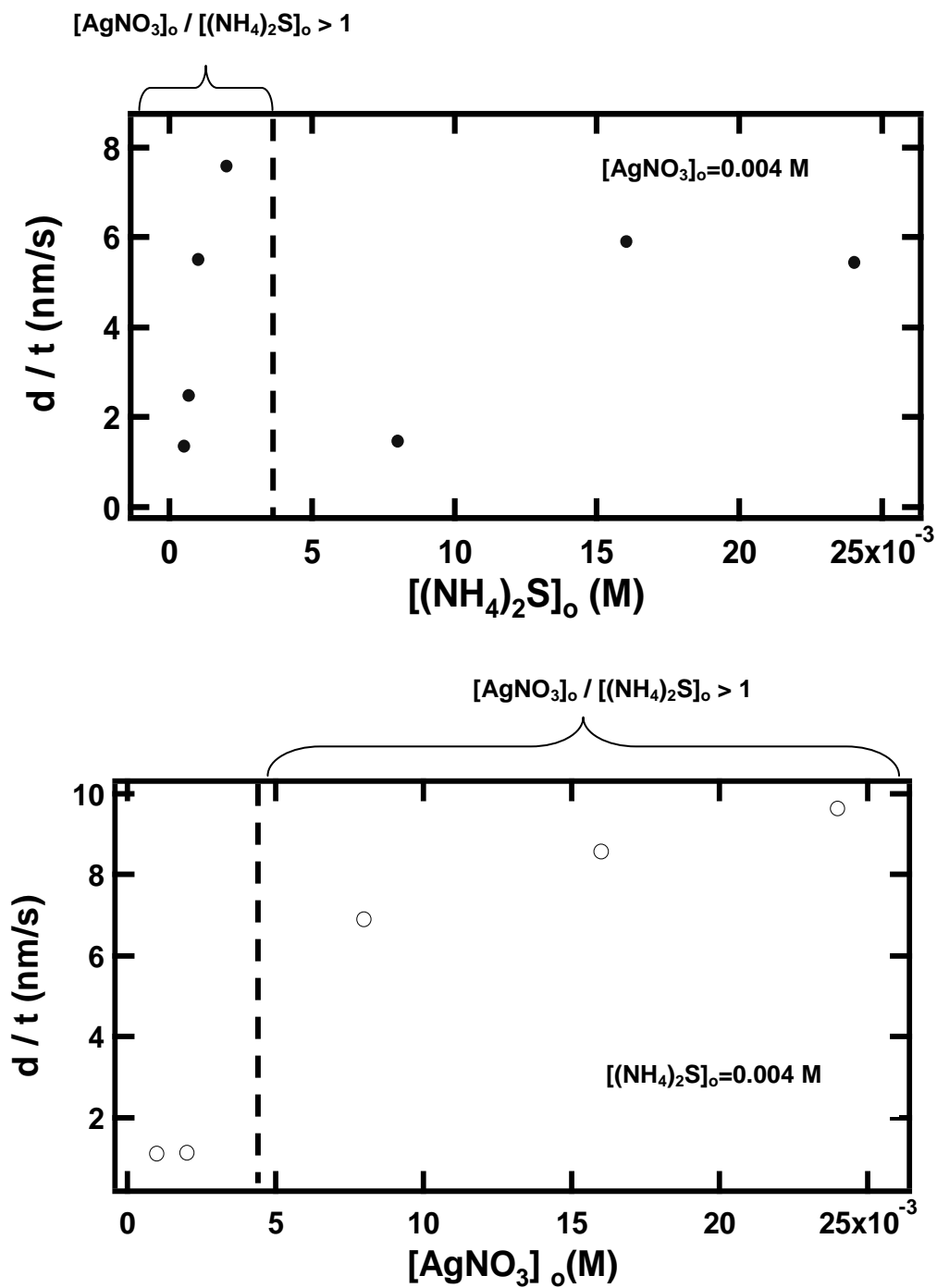
Figure 6.11: Initial growth rates (d/t) of Ag_2S NP as a function of $[AgNO_3]_0$ and $[(NH_4)_2S]_o$. The initial concentration of the second reactant is constant at the value indicated on the graphs. The regions of increasing initial growth rate are highlighted with the $[Ag^+]/[S^{-2}] > 1$.

6.3.6 Theoretical calculations: possible nuclei initiation reactions

$(NH_4)_2S$ is a strong electrolyte and will dissociate in water according to:

$$(NH_4)_2S \rightarrow 2NH_4^+{}_{(aq)} + S^{-2}{}_{(aq)} \qquad \text{reaction 6.1}$$

In solution, the S^{-2} hydrolyzes to form HS^- or H_2S. HS^- is the dominant species at pH values above 7 while strongly acid media is required to have significant H_2S concentrations.[36-39] The solutions of $(NH_4)_2S$ employed for our measurements are basic. For instance, the pH of the $(NH_4)_2S$ solution employed for the measurements displayed on figure 6.3 is around 9.5 and drops to about 9.1 upon mixing the $(NH_4)_2S$ and $AgNO_3$ solutions. At this pH, most of the sulfide is present as $HS^-{}_{(aq)}$:

$$S^{-2}{}_{(aq)} + H_2O \rightarrow OH^-{}_{(aq)} + HS^-{}_{(aq)} \qquad \text{reaction 6.2}$$

Upon mixing the $AgNO_3$ and $(NH_4)_2S$ solutions it is likely that the silver ions react with the HS^- according to:

$$Ag^+{}_{(aq)} + HS^-{}_{(aq)} \rightarrow AgSH_{(aq)} \qquad \text{reaction 6.3}$$

The group directed by Calzaferri has presented strong arguments for the formation of AgSH from the reaction of silver cations with H_2S in Ca-zeolites. [24,54] The AgSH is thought to couple inside the zeolite cage to form Ag_2S monomers according to:

$$2\ AgSH \rightarrow Ag_2S + H_2S \qquad \text{reaction 6.4}$$

In solution, the reactions of silver sulfides may be very different from those that take place inside the cages of zeolites. Besides AgSH and Ag_2S, there are other silver sulfides that may be involved in the early stages of Ag_2S NP nucleation and growth under the experimental conditions employed here. Little is known about the chemistry and physical properties of small silver sulfide clusters. In this regard, theoretical

calculations may provide information on the thermodynamic stability of the different possible silver sulfides involved at the early stages of the reaction. Bagatur'yants [47] and co workers employed ab initio relativistic pseudo potentials to study the stability of silver sulfide monomers and dimers. These authors considered two structural isomers of Ag_2S and six dimers of Ag_2S. The Ag_2S molecules considered by Bagatur'yants have the general Ag-S-Ag structure with bond angles between 78° and 95° for a bent isomer and of 180° for a linear isomer. The bent form of Ag_2S was found to be more stable than the linear isomer. A minimum was found for four Ag_2S dimers studied while imaginary frequencies were found for the two additional dimers studied, indicating that they were either a transition state or saddle point. The work presented below complements these previous efforts by extending theoretical calculations to other silver sulfides that may play relevant roles in the formation of Ag_2S nanostructures.

Table 6.1 summarizes the total energies associated with the optimized structure of various silver sulfides containing one sulfur ion and up to three silver ions. The energies of the indicated molecules were calculated using density functional theory and the DGDZVP basis set. Vibrational frequencies calculated for these molecules and ions at the DFT/B3LYP/DGDZVP level of theory yielded only positive frequencies on the optimized structures. The charge on the sulfur atom is also indicated for each cluster. Since HS^- ions are likely the source of sulfide ions in the reaction between $(NH_4)_2S$ and $AgNO_3$, we have included results for theoretical calculations on AgSH and Ag_2SH^+ in Table 6.1.

Species	Symmetry	Energy (hartrees)	Charge on sulfur
AgS^-	$C^*{}_V$	-5597.683049	-0.913
Ag_2S	C_{2V}	-10797.16583	-0.440
Ag_3S^+	C_{3V}	-15996.47204	-0.421
AgSH	C_S	-5598.26290749	-0.448
Ag_2SH^+	C_S	-10797.54659860	-0.3000

Table 6.1: Energies of silver sulfides with one sulfur ion and up to three silver ions. All results obtained at the DFT/B3LYP/DGDZVP level of theory.

AgSH is found to be more stable than AgS$^-$ by about 0.58 hartrees. AgS$^-$ is found to be strongly ionic, with most of the electron density residing on the sulfur atom. The Ag-S bond in Ag$_2$S and Ag$_3$S$^+$ are found to have a higher covalent character than AgS$^-$ although a significant amount of negative charge still resides on the sulfur atom. The general trend observed is the decrease in energy with the increase in the number of silver cations around the sulfur ion. The addition of each silver ion lowers the sulfide energy by over 5000 hartrees. Of particular interest is the energy of the Ag$_3$S$^+$ cluster, which is over 10,000 and 5000 hartrees lower in energy than the Ag$_2$S molecule and AgS$^-$ ion, respectively. Among those ions considered with a coordination number of three around the sulfur atom, Ag$_3$S$^+$ is found to be more stable than Ag$_2$SH$^+$ by over 5000 hartrees.

Several reactions are possible for the simple sulfides expected to form at the early stages of Ag$_2$S nucleation. Table 6.2 summarizes the change in energy associated with various possible reactions, including those discussed below. For comparison purposes we have included results on reactions leading to the formation of dimers and trimers of Ag$_2$S as well as a linear AgAgS molecule, a linear form of Ag$_2$S with Cs symmetry. The energy released in Ag$_2$S dimerization and trimerization by the routes considered is of the order of 10^2 kJ/mole. However, the formation of Ag$_2$S trimers in a single step, if any, is unlikely.

According to our calculations, reaction 6.4 is slightly endothermic while there are several other reactions that release considerable amounts of energy. AgSH will likely react with hydroxyls to form AgS$^-$ which can undergo stepwise addition of free Ag$^+$ ions thru the following set of thermodynamically downhill reactions to form silver rich sulfide clusters:

AgSH$_{(aq)}$ + OH$^-_{(aq)}$ → AgS$^-_{(aq)}$ + H$_2$O	**reaction 6.5a**
AgS$^-_{(aq)}$ + Ag$^+_{aq)}$ → Ag$_2$S$_{(aq)}$	**reaction 6.5b**
Ag$_2$S$_{(aq)}$ + Ag$^+_{aq)}$ → Ag$_3$S$^+_{(aq)}$	**reaction 6.5c**
2Ag$_2$S → Ag$_4$S$_2$ $_{(aq)}$	**reaction 6.5d**

Reaction	Level of Theory	Energy (kJ/mol)
AgS⁻/AgSH formation and related reactions		
$Ag^+ + S^{-2} \rightarrow AgS^-$	DGDZVP/B3LYP/DFT	-1452.2
$Ag^+ + HS^- \rightarrow AgSH$	DGDZVP/B3LYP/DFT	-743.02
$AgSH + OH- \rightarrow AgS^- + H_2O$	DGDZVP/B3LYP/DFT	-201.4
Ag₂S formation and related reactions		
$Ag^+ + AgS^- \rightarrow AgAgS\ (C_S)$	DGDZVP/RHF	-334.6
$Ag^+ + AgS^- \rightarrow Ag_2S\ (C_{2v})$	DGDZVP/B3LYP/DFT	-747.3
$2Ag^+ + S^{-2} \rightarrow Ag_2S\ (C_{2v})$	DGDZVP/B3LYP/DFT	-2199.5
$2Ag^+ + HS^- \rightarrow Ag_2S\ (C_{2v}) + H^+$	DGDZVP/B3LYP/DFT	+ 48.61
$2\ AgS^- \rightarrow Ag_2S\ (C_{2v}) + S^{-2}$	DGDZVP/B3LYP/DFT	+ 704.9
$2AgSH \rightarrow Ag_2S + H_2S$	DGDZVP/B3LYP/DFT	+ 1.5
$AgSH + Ag^+ \rightarrow Ag_2S + H^+$	DGDZVP/B3LYP/DFT	+ 2875.5
Ag₂SH⁺ formation and related reactions		
$AgSH_{(aq)} + Ag^+_{(aq)} \rightarrow Ag_2SH^+_{(aq)}$	DGDZVP/B3LYP/DFT	-224.7
$Ag_2SH^+_{(aq)} + OH^-(aq) \rightarrow Ag_2S_{(aq)} + H_2O$	DGDZVP/B3LYP/DFT	-724.1
Ag₃S⁺ formation		
$3\ Ag^+ + S^{-2} \rightarrow Ag_3S^+\ (C_{3v})$	DGDZVP/B3LYP/DFT	-2483.2
$3\ Ag^+ + HS^- \rightarrow Ag_3S^+\ (C_{3v}) + H^+$	DGDZVP/B3LYP/DFT	-235.1
$2\ Ag^+ + AgS^- \rightarrow Ag_3S^+\ (C_{3v})$	DGDZVP/B3LYP/DFT	-1031.0
$Ag^+ + Ag_2S\ (C_{2v}) \rightarrow Ag_3S^+\ (C_{3v})$	DGDZVP/B3LYP/DFT	-283.7
Silver Sulfide Dimerization		
$2Ag_2S \rightarrow Ag_4S_2\ (D_{4h})$	DGDZVP/PBEPBE/DFT	-160.4
$2Ag_2S \rightarrow Ag_4S_2\ (C_{2v})$	DGDZVP/PBEPBE/DFT	-197.4
$2Ag_2S \rightarrow Ag_4S_2\ (C_{2h})$	DGDZVP/PBEPBE/DFT	-195.8
Silver Sulfide Trimerization		
$3Ag_2S \rightarrow Ag_6S_3$	LANL2MB/PBEPBE/DFT	-457.6
$Ag_2S\ (D_{4h}) + Ag_4S_2 \rightarrow Ag_6S_3$	LANL2MB/PBEPBE/DFT	-340.7
$Ag_2S\ (C_{2h}) + Ag_4S_2 \rightarrow Ag_6S_3$	LANL2MB/PBEPBE/DFT	-281.3
$Ag_2S\ (C_{2v}) + Ag_4S_2 \rightarrow Ag_6S_3$	LANL2MB/PBEPBE/DFT	-282.7

Table 6.2: Energies associated with the formation of small silver sulfide clusters.

In those cases where the initial $[OH^-]_o \geq [Ag^+]_o$, reaction 6.5a is expected to dominate the observed chemistry. Formation of nuclei from AgS^- will require stepwise addition of free silver ions or self coupling reactions. If the supply of silver ions is limited, then only self coupling reactions of AgS^- can contribute to nuclei formation. According to our calculations, such reactions are thermodynamically uphill, requiring energies of about 700 kJ/mole. Thus it is unlikely that nuclei formation will take place in solutions with $[OH^-]_o \geq [Ag^+]_o$. To test this hypothesis, we performed measurements with an initial $[(NH_4)_2S]_o = 4 \times 10^{-3}$ M and a $[AgNO_3]_o = 10^{-5}$ M. This initial silver nitrate concentration is of the same order of magnitude as the $[OH]^-$ concentration, as revealed by the pH measurements in the $(NH_4)_2S$ solutions. In that case, the UV-visible spectra obtained resembled the one measured for the initial reactants, even after long periods of time, indicating that nuclei formation is unlikely, as expected from the energy associated with the self coupling reaction of AgS^-. As the silver ion concentration is increased, the formation of silver rich sulfide clusters will likely take place thru reactions 6.5b and 6.5c. Alternatively, AgSH may undergo stepwise Ag^+ ion addition and acid-base reactions to form silver rich sulfides according to:

$$AgSH_{(aq)} + Ag^+_{(aq)} \rightarrow Ag_2SH^+_{(aq)} \qquad\qquad \textbf{reaction 6.6a}$$
$$Ag_2SH^+_{(aq)} + OH^-{(aq)} \rightarrow Ag_2S_{(aq)} + H_2O \qquad\qquad \textbf{reaction 6.6b}$$

Formation of silver-rich-sulfide clusters may result from stepwise addition of silver ions to Ag_2S, as described by reaction 6.5c. Ag_2S and AgSH absorb in the UV. [24,54] In the time resolved measurements displayed on figures 6.2, 6.3 and 6.4, we observe bands between 200 and 300 nm that may result from light absorption from these sulfides. However, the quality of the data in this region limits the interpretation of the spectral measurement in the context of the initial reactions that take place upon mixing the reactants. Nevertheless, the trend observed in the nucleation reactions with increasing with the $[AgNO_3]_o/[(NH_4)_2S]_o$ ratio can be accounted for by the formation of stable clusters with a large silver content that may serve as the precursors to nuclei involved in Ag_2S NP formation. In passing we note that among the reactions leading to the formation of the different silver sulfides, including ionic or neutral forms, we found

that the formation of the Ag_3S^+ is energetically feasible by all routes considered, with an associated release of energy in the range of 2500 to 230 kJ/mole. The stability of silver rich sulfide clusters is consistent with the structure of the bulk form of this semiconductor, where the sulfur atoms are coordinated by up to 5 silver ions. The theoretical calculations also lead us to hypothesize that an excess of silver will be present in silver sulfide nanoparticles, even if prepared in the presence of a sulfide ion excess, consistent with recent high resolution transmission electron microscopy measurements on Ag_2S NP reported by Motte. [48]

6.4. Discussion

The reaction of ions in solution results in the formation of nuclei spontaneously or metallic complexes that ultimately result in the formation of nuclei. Overall, the nucleation is given by:

$$x Ag^+_{(aq)} + y HS^-_{(aq)} \rightarrow y H^+_{(aq)} + (Ag_x S_y)^* \qquad \text{reaction 6.7}$$

where $(Ag_x S_y)^*$ represents the nuclei that are formed from the reaction of x Ag^+ ions and y HS^- ions.   Reaction 6.7 represents a phase transition described by an energy change $(\Delta\mu)$:

$$\Delta\mu = \mu (Ag_x S_y)^* - (x \, \mu(Ag^+_{(aq)}) + y \, \mu(HS^-_{(aq)})) \qquad \text{equation 6.4}$$

The results presented in the previous section indicate that there is a significant energy release in the formation of silver rich sulfides. To establish if these species serve as nuclei or embryos to form nuclei is out of the scope of this work. However, the results are consistent with a significant energy release upon the formation of small silver-rich-sulfide clusters.

Energy releases through the formation of chemical bonds is not the only factor driving nuclei formation. The total change in free energy, ΔG, is a delicate balance between the surface free energy, γ, and $\Delta\mu$.[49] While bonding interactions results in a decrease

in $\Delta\mu$, the growth in nuclei size results in an increase in γ: the balance between these terms results in the appearance of a maximum in ΔG with cluster size. The value of the free energy change at this point is usually taken as a measure of the energy barrier, ΔG^*, to form stable nuclei and is given by:[49]

$$\Delta G^* = 16\pi\gamma^3 / (3 |\Delta\mu|^2)$$ **equation 6.5**

 Large values of $\Delta\mu$ effectively reduce the magnitude of the nucleation barrier.   As discussed above, there is an increase in $\Delta\mu$ associated with the formation of silver-rich-sulfide clusters. In the context of this discussion, the increase in initial nucleation rate with initial reactant concentration is observed only when the $[AgNO_3]_0/[(NH_4)_2S]_0$ ratio is larger than 1, in support of our proposal that silver-rich-sulfide clusters play an important role in the nucleation reactions leading to Ag_2S NP formation. Formation of crystalline structures will further increase the magnitude of $\Delta\mu$ and reduce the energy barrier.

Nucleation and growth occur concurrently in the first 5 to 6 seconds after the flow containing the reactants stops. This is evidenced by the dependence of the absorbance and particle diameter on time displayed on figures 6.5 and 6.11**,** respectively.   In general, the largest increase in the absorbance at 575 nm takes place after the flow containing the reactants stopped (t=0 seconds) and about 5 to 8 eight seconds, which is followed by a significantly slower increase in absorbance that extends, depending on initial reactant concentration, to above 15 seconds. The increase in particle diameter occurs over the same time interval where the absorbance increases.   The above discussion lead us to conclude that the nucleation and growth processes are not well separated in the first few seconds of the reaction for the initial concentration range of the study presented here.

Growth may result from coalescence, Ostwald ripening and the reactions of ions with nuclei. Coalescence involves the reaction of two particles: the total particle density is expected to decrease with time. The absorbance near the band edge never decreases in the time scale reported here, indicating that the number of Ag_2S NP does not

decrease. Thus coalescence does not seem to play an important role in Ag_2S NP growth. Ostwald ripening results in the growth of large particles from reactions among smaller particles, leaving the total number of particles the same. Ostwald ripening is a little bit more difficult to distinguish from other growth mechanisms since the total particle density remains nearly the same over time. Ostwald ripening, however, results in a broadening of the nanoparticle distribution over time and an increase in the number of large particle at the expense of a decrease in the number of smaller particles. The distribution of particles displayed on figure 6.1 suggests that ripening may not be important in Ag_2S NP growth under the experimental conditions used here. The most probable diameter at the earliest stages of the reaction is 3 nm. If ripening played an important role in Ag_2S NP growth, then one would have expected the number of larger particles to increase at the expense of the 3 nm particles. This will result in a decrease in the number of 3 nm particles. The most probable diameter does not change significantly over time. Instead, the number of particles with diameters of 3 nm increases over time. We conclude that Ostwald ripening does not play a significant role in Ag_2S NP growth.

Reactions of ions with nuclei, on the other hand, will also result on growth. The results presented on figure 6.2 are consistent with the adsorption of silver ions on the Ag_2S NP surface. The band between 310 and 320 nm appears only when the flow has a $[AgNO_3]_o$ / $[(NH_4)_2S]_o$ ratio larger than 1. The nucleation and growth process are affected over long periods of time by these ions. The dotted trace on figure 6.3 represents the UV visible obtained 45 seconds after a flow containing a $[AgNO_3]_o/[(NH_4)_2S]_o$ ratio of 2 stopped. The absorbance around 310 nm is smaller in the spectrum recorded at 45 seconds than the corresponding absorbance in the spectrum obtained at 15 seconds after the flow stopped. There is a very small increase in the absorbance near the band edge in this time range. This leads us to conclude that the number of Ag_2S NP increases through mechanisms that involve surface reactions. The reactions on the particle surface also represent a growth mechanism. As indicated in the dependence of $(AE)^{1/2}$ as a function of E illustrated on figure 6.8, the onset of light absorption appears around 1.5 eV in measurements performed 45 seconds after the

flow stopped. A quantitative estimate of the diameter of the particles formed for times longer than 15 seconds after the flow stopped cannot be provided since it is difficult to determine the onset of light absorption that are close to 800 nm (1.5 eV) with our spectrometer. However, the onset of light absorption occurs at lower energies 45 seconds after the flow stopped than at earlier times, consistent with the formation of larger particles. Thus the reactions of ions on the particle surface discussed in the previous paragraph results in Ag_2S NP growth. These reactions do not represent the limiting step in the growth process, since the power exponent determined by equation 6.3 fall short of the ideal value of 1 expected for a growth process limited by interface reactions. However, the adsorption of silver ions on the particle surface is consistent with the observations made by previous investigators, in particular, those made by Kryukov and co workers that found Ag_2S NP to catalytically reduce silver in the presence of sulfite ions. Thus a growth mechanism involving the surface reactions of silver ions is consistent with the current body of knowledge related to the chemistry of formation of Ag_2S NP.

6.5 Summary

In summary, real time UV-visible absorption measurements of stopped flows of $AgNO_3$ and $(NH_4)_2S$ are used to monitor the nucleation and growth of silver sulfide nanoparticles (Ag_2S NP). Ag_2S NP, in the size range of 2 to 10 nm, are formed a few seconds after the flow containing the reactants stops. The absorbance near the band edge of the semiconductor nanoparticle is used to monitor the number of particles formed with time and study the nucleation process. The onset in light absorption was used to determine band gap energy of the semiconductor nanoparticle. Transmission electron microscopy measurements, using results from this and previous works, are used to correlate particle size and the indirect band gap energy allowing the use of light absorption measurements to study the growth process. The nucleation and growth process are not well separated in time. The initial nucleation and growth rates are found to increase for $[AgNO_3]_0/[(NH_4)_2S]_0$ ratios larger than 1. The experimental results suggest that silver rich sulfides, particularly ionic forms, are involved in the nucleation

stage and growth process of Ag_2S NP. Density functional calculations for small silver sulfides are consistent with that interpretation: Ag_3S^+ is found to have a lower energy than Ag_2S and AgSH molecules or the AgS^- and Ag_2SH^+ ions.

6.6 References

1. Mahapatra, S. K.; Bogle, K. A.; Dhole, S. D.; Bhoraska, V. N. Synthesis of Gold and Silver Nanoparticles by Electron Irradiation at 5-15 keV Energies. *Nanotechnology* **2007,** *18*, 135602-135607.

2. Eychmüller, A. Structure and Photophysics of Semiconductor Nanocrystals. *J. Phys. Chem. B* **2000**, *104*, 6514-6528.

3. Zhang, J. Z. Interfacial Charge Carrier Dynamics of Semiconductor Nanoparticles. *J. Phys. Chem. B* **2000**, *104*, 7239-7253.

4. Van Dijken, A.; Meulenkamp, E. A.; Vanmaekelbergh, D.; Meijerink A. Identification of the Transition Responsible for the Visible Emission in ZnO Using Quantum Size Effects. *J. Lumin.* **2000**, *90*, 123-128.

5. Lakowicz, J. R.; Gryczynski, I.; Gryczynski, Z.; Murphy, C. J. Luminescence Spectral Properties of CdS Nanoparticles. *J. Phys. Chem. B* **1999**, *103*, 7613-7620.

6. Wilkinson, J. P.; Martin, J. E.; Parsapour, F.; Wiedenman, B.; Kelley, D. F. Photoluminescence from Nanosize Gold Clusters. *J. Chem. Phys.* **1998**, *108*, *21*, 9137-9143.

7. Murray, C. B.; Noms, D. J.; Bawendi, M. G. Synthesis and Characterization of Nearly Monodisperse CdE (E = S, Se, Te) Semiconductor Nanocrystallites. *J. Am. Chem. Soc.* **1993**, *115,* 8706-8715

8. Besson, C.; Finney, E.; Finke, R. Nanocluster Nucleation, Growth, and Then Agglomeration Kinetic and Mechanistic Studies: A More General, Four-Step Mechanism Involving Double Autocatalysis. *Chem. Mater.* **2005**, *17*, 4925-4938.

9. Qu, L.; William Yu, W.; Peng, X. In Situ Observation of the Nucleation and Growth of CdSe Nanocrystals, *Nano Lett.* **2004**, *4*, 465-469.

10. Wang, Z.; Kadohira, T.; Tada, T.; Watanabe, S. Nonequilibrium Quantum Transport Properties of a Silver Atomic Switch, *Nano Lett.* **2007**, *7*, 2688-2692.

11. Liang, C.; Terabe, K.; Hasegawa, T.; Aono, M. Resistance Switching of an Individual Ag_2S/Ag Nanowire Heterostructure. *Nanotechnology* **2007**, *18*, 485202-485207.

12. Akai-Kasaya, M.; Nishihara, K.; Saito, A.; Kuwahara, Y.; Aono, M. Quantum Point-Contact Switches Using Silver Particles. *Appl. Phys. Lett.* **2006**, *88*, 23107-23110.

13. Van Ruitenbeek, J. Device Physics: Silver Nanoswitch, *Nature* **2005**, 433, 21-22.

14. Terabe, K.; Hasegawa, T.; Nakayama, T.; Aono, M. Quantized Conductance Atomic Switch. *Nature* **2005**, *433*, 47-50.

15. Martinez-Castañón, G. A.; Sanchez-Loredo, M. G.; Dorantes, H. J.;.Martinez-Mendoza, J. R; Ortega-Zarzoza, G.;. Ruiz, F. Characterization of Silver Sulfide Nanoparticles Synthesized by a Simple Precipitation Method. *Mater. Lett.* **2005**, *59*, 529-534.

16. Zhang, W.; Zhang, L.; Hui, Z; . Zhang, X.; Qian, Y. Synthesis of Nanocrystalline Ag_2S in Aqueous Solution. *Solid State Ionics*. **2000,** *130,* 111-114.

17. Changqi, X.; Zhicheng, Z.; Qiang, Y. A Novel Facile Method to Metal Sulfide (Metal = Cd, Ag, Hg) Nano-Crystallite. *Mater. Lett.* **2004**, *58*, 1671-1676.

18. Gao, F.; Lu, Q.; Zhao, D. Controllable Assembly of Ordered Semiconductor Ag_2S Nanostructures. *Nano Lett.* **2003**, *3*, 85-88.

19. Schaaff T. G.; Rodinone, A. J. Preparation and Characterization of Silver Sulfide Nanocrystals Generated from Silver (I)-Thiolate Polymers. *J. Phys. Chem. B* **2003,** *107,* 10416-10422.

20. Liu, S. H.; Qian, X. F.; Yin, J.; Hong, L.; Wang, X. L.; Zhu, Z. K. Synthesis and Characterization of Ag_2S Nanocrystals in Hyperbranched Polyurethane at Room Temperature. *J Solid State Chem.* **2002**, *168*, 259-262.

21. Motte, L.; Pileni, M. P. Influence of Length of Alkyl Chains Used to Passivate Silver Sulfide Nanoparticles in Two- and Three-Dimensional Self-Organization. *J. Phys. Chem. B* **1998**, *102*, 4104-4109.

22. Motte, L.; Billoudet, F.; Lacaze, E.; Douin, J.; Pileni, M. P. Self-Organization into 2D and 3D Superlattices of Nanosized Particles by Their Size. *J. Phys. Chem. B* **1997**, *101*, 138-144.

23. Pileni, M. P.; Motte, L.; Billoudet, F.; Lacaze, E.; Mahrt, J.; Willig, F. Nanosized Silver Sulfide Particles: Characterization, Self-Organization into 2D and 3D Superlattices. *Mater. Lett.* **1997**, *31*, 255-260.

24. Brühwiler, D.; Leiggener, C.; Glaus, S.; Calzaferri, G. Luminescent Silver Sulfide Clusters. *J. Phys. Chem. B* **2002**, *106*, 3770-3777.

25. Armelao, L.; Bertoncello, R.; Cattaruzza, E.; Gialanella, S.; Gross, S.; Mattei, G.; Mazzoldie, P.; Tondelloa, E. Chemical and Physical Routes for Composite Materials Synthesis: Ag and Ag_2S Nanoparticles in Silica Glass by Sol-Gel and Ion Implantation Techniques. *J. Mater. Chem.* **2002**, *12*, 2401-2407.

26. Ding, Y.; Xu, B.; Guo, R.; Shen, M. The Preparation of Silver Sulfide Nanoparticles in Lamellar Liquid Crystal and Application to Lubrication. *Mater. Res. Bull.* **2005**, *40,* 575-582.

27. Liu, J.; Raveendran, P.; Shervania, Z.; Ikushima, Y. Synthesis of Ag_2S Quantum Dots in Water-in-CO_2 Microemulsions. *Chem. Commun.* **2004**, *22*, 2582-2583.

28. Mori, J.; Miyashita, Y.; Oliveira, D.; Kasai, H.; Oikawa, H.; Nakanishi, H. Stopped-flow Analysis on the Mechanism of Perylene Nanoparticle Formation by the Reprecipitation Method. *J. Cryst. Growth* **2009**, *311*, 553-555.

29. Moinard-Chécot, D.; Chevalier, Y.; Briançon, S.; Beney, L.; Fessi, H. Mechanism of Nanocapsules. Formation by the Emulsion–Diffusion Process. *J. Colloid Interface Sci.* **2008**, *317*, 458-468.

30. Bremholma, M.; Jensen, H.; Brummerstedt Iversen, S.; Brummerstedt Iversen, B. Reactor Design for *in Situ* X-ray Scattering Studies of Nanoparticle Formation in Supercritical Water Syntheses. *J. Supercrit. Fluid.* **2008**, *44*, 385-390.

31. Tiemann, M.; Marlow, F.; Brieler, F.; Linde´n, M. Early Stages of ZnS Growth Studied by Stopped-Flow UV Absorption Spectroscopy: Effects of Educt Concentrations on the Nanoparticle Formation. *J. Phys. Chem. B* **2006**, *110,* 23142-23147.

32. Motte, L.; Billoudet, F.; Pileni, M. P. Self-Assembled Monolayer of Nanosized Particles Differing by Their Sizes. *J. Phys. Chem. B* **1995**, *99*, 16425-16429.

33. Chen, R.; Nuhfer, N.T.; Moussa, L.; Morris, H. R.; Whitmore, P.M. Silver Sulfide Nanoparticle Assembly Obtained by Reacting an Assembled Silver Nanoparticle Template with Hydrogen Sulfide Gas. *Nanotechnology* **2008**, *19*, 1-11.

34. Núñez Rodriguez, A.; Nair, M.T.S.; Nair, P. K. Structural, Optical and Electrical Properties of Chemically Deposited Silver Sulfide Thin Films, *Semicond. Sci. Technol.* **2005**, *20*, 576-585.

35. Meherzi-Maghraoui, H.; Dachraoui, M.; Belgacem, S.; Buhre, K. D.; Kunst, R.; Cowache, P.; Lincot, D. Structural, Optical and Transport Properties of Ag_2S Films Deposited Chemically from Aqueous Solution. *Thin Solid Films* **1996**, *288*, 217-223.

36. Roig , B.; Chalmin, E.; Touraud, E.; Thomas, O. Spectroscopic Study of Dissolved Organic Sulfur (DOS): A Case Study of Mercaptans. *Talanta* **2002**, *56*, 585-590.

37. Guenther, E. A.; Johnson, K. S.; Coale, K. H. Direct Ultraviolet Spectrophotometric Determination of Total Sulfide and Iodide in Natural Waters. *Anal. Chem.* **2001,** *73*, 3481-3487.

38. Johnson, K. S.; Coletti, L. J. In Situ Ultraviolet Spectrophotometry for High Resolution and Long-term Monitoring of Nitrate, Bromide and Bisulfide in the Ocean. *Deep-Sea Research I* **2002**, *49*, 1291-1305.

39. Zuma, P.; Szafranskl, W. Ultraviolet Spectra of Hydroxide, Alkoxide, and Hydrogen Sulfide Anions. *Anal. Chem.* **1976,** *48*, 2162-263.

40. Kryukov, A. I.; Zin'chuk, N. N.; Korzhak A. V.; Ya. Kuchmil, S. Quantum Size Effects and Nature of Photoprocesses in Nanoparticles of Ag_2S. *Theor. Exp. Chem.* **2001**, *37*, 296-303.

41. Murphy, C. J.; Copper, J. L. Quantum Dots: A Primer. *Appl. Spectrosc.* **2002**, *56*, 16A-36A.

42. Bawendi, M. G.; Steigerwald, M. L.; Brus, L. E. The Quantum Mechanics of Larger Semiconductor Clusters ("Quantum Dots"). *Annu. Rev. Phys. Chem.* **1990**, *41*, 477-496.

43. Steigerwald M. L.; Brus, L. E. Synthesis, Stabilization, and Electronic Structure of Quantum Semiconductor Nanoclusters. *Annu. Rev. Mater. Sci.* **1989**, *19*, 471-495.

44. Yoffe, A. D. Semiconductor Quantum Dots and Related Systems: Electronic, Optical, Luminescence and Related Properties of Low Dimensional Systems. *Adv. Phys.* **2001**, *50*, 1-208.

45. Reithmaier, J. P. Strong Exciton–Photon Coupling in Semiconductor Quantum Dot Systems. *Semicond. Sci. Technol.* **2008**, *23*, 123001-123019.

46. Wang, Y.; Herron, N. Quantum Size Effects on the Exciton Energy of CdS Clusters. *Phys. Rev. B.* **1990**, *42*, 7253-7255.

47. Bagatur'yants, A. A.; Safonov, A. A.; Stoll, H.; Werner, H. J. Ab Initio Relativistic Pseudopotential Study of Small Silver and Gold Sulfide Clusters $(M_2S)_n$, n=1 and 2. *J. Chem. Phys.* **1998**, *109*, 3096-3108.

48. Motte, L.; Urban, J. Silver Clusters on Silver Sulfide Nanocrystals: Synthesis and Behavior After Electron Beam Irradiation. *J. Phys. Chem. B*, **2005**, *109*, 21499-21501.

49. Wang, C. X.; Yang, G. W. Thermodynamics of Metastable Phase Nucleation at the Nanoscale. *Mat. Sci. Eng. R* **2005**, *49*, 157-202.

50. Tobler, D. J.; Shaw, S. ; Benning, L. G. Quantification of Initial Steps of Nucleation and Growth of Silica Nanoparticles: An *in-situ* SAXS and DLS Study*. Geochim. Cosmochim. Ac.* **2009**, *73*, 5377-5393.

51. Abe´cassis, B.; Testard, F.; Spalla, O.; Barboux, P. Probing In Situ the Nucleation and Growth of Gold Nanoparticles by Small-Angle X-ray Scattering. *Nano Lett.* **2007**, *7*, 1723-1727.

52. Rizza, G.; Ramjauny, Y.; Gacoin, T.; Vieille, L.; Henry, S. Chemically Synthesized Gold Nanoparticles Embedded in a SiO_2 Matrix: A Model System to Give Insights into Nucleation and Growth Under Irradiation. *Phys. Rev. B,* **2007**, *76*, 245414-245423.

53. Nozawa, K.; Hélène Delville, M.; Ushiki, H.; Panizza, P.; Pierre Delville, J. Growth of Monodisperse Mesoscopic Metal-Oxide Colloids Under Constant Monomer Supply. *Phys. Rev. E* **2005**, *72*, 011404-011412.

54. Brühwiler, D.; Leiggener, C.; Calzaferri, G. Luminescence Properties of Ag_2S and Ag_4S_2 in Zeolite A. *J. Mater. Chem.* **2003**, *13*, 1969-1977.

55. Menoni, C. S.; Miao, L.; Patel, D.; Mic'ic', O. I.; Nozik, A. J. Three-Dimensional Confinement in the Conduction Band Structure of InP. *Phys. Rev. Lett.* **2000**, *84*, 4168-4171.

56. Luo, J. W.; Franceschetti, A.; Zunger, A. Direct-Bandgap InAs Quantum-Dots Have Long-Range Electron–Hole Exchange Whereas Indirect Gap Si Dots Have Short-Range Exchange. *Nano Lett.* **2009**, *9*, 2648-2653.

57. Luo, J. W.; Franceschetti, A.; Zunger, A. Quantum-Size-Induced Electronic Transitions in Quantum Dots: Indirect Band-Gap GaAs. *Phys. Rev. B* **2008**, *78*, 035306-035314.

58. Privman, V. Diffusional Nucleation of Nanocrystals and Their Self-Assembly into Uniform Colloids. *J. Optoelectronics Adv. Mater.* **2008**, *10*, 2827-2839.

59. León-Velázquez, M.; Irizarry, R.; Castro-Rosario, M. Nucleation and Growth of Silver Sulfide Nanoparticles; *J. Phys. Chem. C,* **2010**, *114*, 5839–5849.

CHAPTER 7: CONCLUSIONS

In summary, we have presented the synthesis of silver sulfide nanoparticles via a stop flow reactor that allows the formation of a homogeneous mixture of reactants in a flow prior to the reaction: it avoids the formation of concentrations gradients in the solution. $AgNO_3$ and $(NH_4)_2S$ are used as the source of silver (Ag^+) and sulfide ions and (S^{-2}) ions. Real time conductivity and UV-visible absorption measurements were employed to learn about the nucleation and growth of this reaction mixture. Kinetics measurements reveal that the rate law is directly proportional to the S^{-2} concentration while it is inversely proportional to Ag^+ concentration.

Ionic conductivity measurements provide qualitative information related to the process occurring in the early stages of the reaction but does not provided information related to the identity of the clusters or embryos chemistry. These measurements suggest the formation of non stoichiometric ionic Ag_2S species, rather of neutral Ag_2S, in the early stages of the reaction mixture. Comparison of the configuration interaction single calculations on structures of several silver sulfide clusters optimized at the density functional level with the optical absorption spectra of reaction mixtures obtained in the early stages of the reaction lead us to conclude that the dependence of the optical absorption spectra on time in the first few milliseconds after the flow stops is consistent with formation of AgS^- and Ag_3S^+ cluster ions. Bands that can be attributed to the formation of larger silver sulfide clusters – including Ag_4S_2 and Ag_6S_3 - are observed at longer reaction times. The study of the effect of AOT surfactant in the reaction mixture shows that at large amounts of AOT inhibit the nucleation process and stabilize a D_4h Ag_2S_4 cluster.

The UV-visible absorption measurements at longer times revealed that the nucleation and growth process are not well separated in time. The initial nucleation and growth rates are found to increase with initial $[AgNO_3]_0/[(NH_4)_2S]_0$ ratios larger than 1. Silver ions play a central role in the nucleation and growth process. The experimental results suggest that silver-rich-sulfides are involved in the nucleation stage and growth process of Ag_2S NP.

CHAPTER 8: FUTURE WORKS

The study of the nucleation and growth of silver sulfide nanoparticles provide the foundation to continue studies in the area of identification and possible isolation of clusters in the early stages of the reaction and theoretical studies of the kinetics of reaction.

The study of the identification and possible isolation of clusters in the early stages of the reaction study can be performed by using other types of surfactants or stabilizers. In addition in these early stages of the reaction supplementary kinetics studies can be performed using fastest methods of data acquisition. Supplementary, the studies of the kinetics of reaction can be complemented by performing theoretical simulations using Simulated Dynamic Optical Response Strategy (SDOR). This model has been used before for the simulation of the kinetics for silver and gold nanoparticles [1].

There are several models to correlate the band gap of a semiconductor nanoparticle with its diameter by making a relation between the size of the nanoparticles with the length and the energy of the particle in the box quantum model. These models were ineffective to predict the relation between the energy and the size for the silver sulfide nanoparticles presented above. Fortunately, our findings and the contribution from other research groups has resulted in an adequate number of measurements to establish a correlation between Ag_2S particle size and band gap energy. The result establishes a linear correlation between Ag_2S NP diameter and band gap energy. The result suggests that a simple particle in a box model, where the edge is predicted to depend on $1/r^2$, may not be adequate to describe the dependence of indirect band gap on particle size. This observation may have important implications on the role of vibrational motion in quantum confinement effects, a subject that may be pursued theoretically in the future.

8.1. References

1. Irizarry, R. Simulated Dynamic Optical Response Strategy for Model Identification of Metal Colloid Synthesis. *Ind. Eng. Chem. Res*., **2010**, *49,* 5588–5602.

CHAPTER 9: GENERAL REFERENCES

1. León-Velázquez, M. S.; Morales, M.; Irizarry, R.; Castro, M. Conduction in Collodial Systems: A Kinetic Study of Ag_2S Semiconductor. Nanoparticles: Synthesis, Stabilization, Passivation, and Functionalization, Chapter 15, **2008,** pp 203-213, *ACS Symposium Series*, Volume 996.

2. León-Velázquez, M. S.; Morales, M.; Carbo, M.; Sepúlveda, W.; González, M. Rivera, D.; Irizarry, R.; Castro, M. Inhibition of Ag_2S Nucleation by AOT micelles. Submitted to Materials Letters.

3. León-Velázquez, M.; Irizarry, R.; Castro-Rosario, M. Nucleation and Growth of Silver Sulfide Nanoparticles; *J. Phys. Chem. C*, **2010**, *114*, 5839–5849.

4. Lakowicz, J. R.; Gryczynski, I.; Gryczynski, Z.; Murphy, C. J. Luminescence Spectral Properties of CdS Nanoparticles. *J. Phys. Chem. B,* **1999**, *103*, 7613-7620.

5. Murray, C. B.; Noms, D. J.; Bawendi, M. G. Synthesis and Characterization of Nearly Monodisperse CdE (E = **S,** Se, Te) Semiconductor Nanocrystallites. *J. Am. Chem. Soc.* **1993**, *115,* 8706-8715.

6. Mu, J.; Gu, D.; Xu, Z. Synthesis and stabilization of ZnS nanoparticles embedded in silica nanospheres. *Applied Physics A –Materials Science & Processing,* **2004.**

7. van Dijken, A.; Meulenkamp, E.A.; Vanmaekelbergh, D.; Meijerink, A. Identification of the transition responsible for the visible emission in ZnO using quantum size effects. Journal of Luminescence, **2000**, 90, 123-128.

8. Wang, Z.; Kadohira, T.; Tada, T.; Watanabe, S. Nonequilibrium Quantum Transport Properties of a Silver Atomic Switch., *Nano Lett.* **2007**, *7*, 2688-2692.

9. Liang, C.; Terabe, K.; Hasegawa, T.; Aono, M. Resistance Switching of an Individual Ag_2S/Ag Nanowire Heterostructure. *Nanotechnology*, **2007**, *18*, 485202-485207.

10. Akai-Kasaya, M.; Nishihara, K.; Saito, A.; Kuwahara, Y.; Aono, M. Quantum Point-Contact Switches Using Silver Particles. *Appl. Phys. Lett.* **2006**, *88*, 23107-23110.

11. Van Ruitenbeek, J. Device Physics: Silver Nanoswitch, *Nature* **2005**, *433*, 21-22.

12. Terabe, K.; Hasegawa, T.; Nakayama, T.; Aono, M. Quantized Conductance Atomic Switch. *Nature* **2005**, *433*, 47-50.

13. Liu, S. H.; Qian, X. F.; Yin, J.; Hong, L.; Wang, X. L.; Zhu, Z. K. Synthesis and Characterization of Ag_2S Nanocrystals in Hyperbranched Polyurethane at Room Temperature. *J Solid State Chem.* **2002**, *168*, 259-262.

14. Meziani, M. J; Sun,Y. Protein-Conjugated Nanoparticles from Rapid Expansion of Supercritical Fluid Solution into Aqueous Solution. *J. Am. Chem. Soc,* **2003**, *125*, 8015-8018.

15. Motte, L.; Pileni, M. P. Influence of Length of Alkyl Chains Used to Passivate Silver Sulfide Nanoparticles in Two- and Three-Dimensional Self-Organization. *J. Phys. Chem. B* **1998**, *102*, 4104-4109.

16. Brelle, M. C.; Zhang, J. Z.; Nguyen, L.; Mehra, R. K. Synthesis and Ultrafast Study of Cysteine- and Glutathione-Capped Ag_2S Semiconductor Colloidal Nanoparticles. *J. Phys. Chem. A,* **1999**, *103,* 10194-10201

17. Eychmüller, A. Structure and Photophysics of Semiconductor Nanocrystals. *J. Phys. Chem. B* **2000**, *104*, 6514-6528.

18. Martinez-Castañón, G. A.; Sanchez-Loredo, M. G.; Dorantes, H. J.;.Martinez-Mendoza, J. R; Ortega-Zarzoza, G.;. Ruiz, F. Characterization of Silver Sulfide Nanoparticles Synthesized by a Simple Precipitation Method. *Mater. Lett.* **2005**, *59*, 529-534.

19. Zhang, W.; Zhang, L.; Hui, Z. ; Zhang, X.; Qian, Y. Synthesis of Nanocrystalline Ag_2S in Aqueous Solution. *Solid State Ionics.* **2000,** *130*, 111-114.

20. Liu, J.; Raveendran, P.; Shervania, Z.; Ikushima, Y. Synthesis of Ag_2S Quantum Dots in Water-in-CO_2 Microemulsions. *Chem. Commun.* **2004**, *22*, 2582-2583

21. Schaaff T. G.; Rodinone, A. J. Preparation and Characterization of Silver Sulfide Nanocrystals Generated from Silver (I)-Thiolate Polymers. *J. Phys. Chem. B* **2003,** *107,* 10416-10422.

22. Changqi, X.; Zhicheng, Z.; Qiang, Y. A Novel Facile Method to Metal Sulfide (Metal = Cd, Ag, Hg) Nano-Crystallite. *Mater. Lett.* **2004**, *58*, 1671-1676.

23. Brühwiler, D.; Leiggener, C.; Glaus, S.; Calzaferri, G. Luminescent Silver Sulfide Clusters. *J. Phys. Chem. B* **2002**, *106*, 3770-3777.

24. Armelao, L.; Bertoncello, R.; Cattaruzza, E.; Gialanella, S.; Gross, S.; Mattei, G.; Mazzoldie, P.; Tondelloa, E. Chemical and Physical Routes for Composite Materials Synthesis: Ag and Ag_2S Nanoparticles in Silica Glass by Sol-Gel and Ion Implantation Techniques. *J. Mater. Chem.* **2002**, *12*, 2401-2407.

25. Ding, Y.; Xu, B.; Guo, R.; Shen, M. The preparation of silver sulfide nanoparticles in lamellar liquid crystal and application to lubrication. *Materials Research Bulletin,* **2005**, *40,* 575–582.

26. Xiao, J.; Xie, Y.; Tang, R.; Luo, W. Template-based synthesis of nanoscale Ag_2E (E ~ S, Se) dendrites. *J. Mater. Chem.*, **2002**, *12*, 1148–1151.

27. Wu, M.; Pan, X.; Qian, X.; Yin, J; Zhu, Z. Solution-phase synthesis of Ag_2S hollow and concave nanocubes. *Inorganic Chemistry Communications* **2004**, *7*, 359–362

28. Hernandez, E. ; Posada, B.; Irizarry, R.; Castro, M..E. The role of hydrogen bonding interactions in directing one dimensional-thiol assisted growth of silver based nanofibers *J. Phys. Chem. B,* **2005**, *109,* 7251-7257

29. Besson, C.; Finney, E. E.; Finke, R. G. Nanocluster Nucleation, Growth and the Agglomeration Kinetic and Mechanistic Studies: A more general, four-step mechanism involving double autocatalysis. *Chem. Mater.*, **2005**, *17*, 4925-4938.

30. Jana, N. R.; Gearheart, L.; Murphy, C. J. Seeding Growth for Size Control of 5-40 nm Diameter Gold Nanoparticles. *Langmuir*, **2001**, *17*, 6782-6786.

31. Privman, V.; Goia, D. V.; Park, J.; Matijevic, E. Mechanism of Formation of Monodispersed Colloids by Aggregation of Nanosize Precursors, *Journal of Colloid and Interface Science*, **1999**, *213*, 36- 45.

32. Murillo, L.E.; Viera, O.; Briano, J. G.; Castro, M. E.; Ishikawa, Y.; Irizarry, R.; Solá, L. Growth kinetics of gold nanoparticles. Proceedings of the International Conference on Computational Nanoscience and Nanotechnology, Chapter 16, *Materials and Nanostructures Studies*, **2002***, 435-438.

33. Qu, L.; Yu, W.; Peng, X. In Situ Observation of the Nucleation and Growth of CdSe Nanocrystals. *Nanoletters*, **2004**, *4*, 465-469.

34. Moskovits, M.; Vlckova, B. Adsorbate-Induced Silver Nanoparticle Aggregation Kinetics. *J. Phys. Chem. B.* **2005**, *109*, 14755-14758.

35. Rodriguez-Sanchez, M. L.; Rodriguez, M. J.; Blanco, M. C.; Rivas, J.; Lopez-Quintela, M. A. Kinetics and Mechanism of the Formation of Ag Nanoparticles by Electrochemical Techniques: A Plasmon and Cluster Time-Resolved Spectroscopic Study. *J. Phys Chem. B.* **2005**, *109*, 1183-1191.

36. Zhang, Z.; Patel, R. C.; Kothari, R.; Johnson, C. P.; Friberg, S. E.; Aikens, P. A. Stable Silver Clusters and Nanoparticles Prepared in Polyacrylate and Inverse Micellar Solutions. *J. Phys. Chem. B*, **2000**, *104*, 1176 -1182.

37. Meneses, C. T.; Flores, W. H.; Sasaki, J. M. Direct Observation of the Formation of Nanoparticles by in situ time-resolved X-ray absorption spectroscopy. *Chem. Mater.* **2007**, *19* , 1024 -1027.

38. Kryukov, A.I.; Stroyuk, A.L.; Zin'chuk, N.N.; Korzhak A.V.; Kuchmii, S.Y.; Optical and catalytic properties of Ag_2S nanoparticles. *Journal of Molecular Catalysis A: Chemical*, **2004**, *221*, 209–221.

39. Calzaferri, G.; Brühwiler, D.; Glaus, S.; Schürch, D.; Currao, A.; Leiggener, C. Quantum-Sized Silver, Silver Chloride and Silver Sulfide Clusters. *Journal of Imaging Science and Technology* , **2001**, *45*, 331–339.

40. Kryukov, A. I.; Zin'chuk, N. N.; Korzhak A. V.; Ya. Kuchmil, S. Quantum Size Effects and Nature of Photoprocesses in Nanoparticles of Ag_2S. *Theor. Exp. Chem.* **2001**, *37*, 296-303

41. Brühwiler, D.; Leiggener, C.; Calzaferri, G. Luminescence Properties of Ag_2S and Ag_4S_2 in Zeolite A. *J. Mater. Chem.* **2003**, *13*, 1969-1977.

42. Motte, L.; Billoudet, F.; Lacaze, E.; Douin, J.; Pileni, M. P. Self-Organization into 2D and 3D Superlattices of Nanosized Particles by Their Size. *J. Phys. Chem. B* **1997**, *101*, 138-144.

43. Electrochemical methods fundamentals and applications, Bard, A. and Faulkner L., 2nd edition (2001), John Wiley & Sons, Inc.

44. Physical Chemistry, Atkins, P. and de Paula J., 7th edition (2002), Oxford University Press Inc., New York.

45. Nayak, A.; Tamura, T.; Tsuruoka, T.; Terabe, K.; Hosaka, S.; Hasegawa,T.; Aono, M. Rate-Limiting Processes Determining the Switching Time in a Ag_2S Atomic Switch. *J. Phys. Chem. Lett.* **2010**, *1*, 604–608.

46. Lu, X.; Li, L.; Zhang, W.; Wang, C. Preparation and characterization of Ag_2S nanoparticles embedded in polymer fibre matrices by electrospinning. *Nanotechnology.* **2005**, *16*, 2233 - 2237.

47. Núñez Rodriguez, A.; Nair, M.T.S.; Nair, P. K. Structural, Optical and Electrical Properties of Chemically Deposited Silver Sulfide Thin Films, *Semicond. Sci. Technol.* **2005**, *20*, 576-585.

48. Meherzi-Maghraoui, H.; Dachraoui, M.; Belgacem, S.; Buhre, K. D.; Kunst, R.; Cowache, P.; Lincot, D. Structural, Optical and Transport Properties of Ag_2S Films Deposited Chemically from Aqueous Solution. *Thin Solid Films* **1996**, *288*, 217-223.

49. Motte, L.; Billoudet, F.; Pileni, M. P. Self-Assembled Monolayer of Nanosized Particles Differing by Their Sizes. *J. Phys. Chem. B* **1995**, *99*, 16425-16429.

50. Tian, C.; Kang, Z.; Wang, E.; Mao, B.; Li, S.; Su, Z.; Xu, L. 'One-step' controllable synthesis of Ag and Ag_2S nanocrystals on a large scale. *Nanotechnology.* **2006**, *17*, 5681 – 5685.

51. Gao, F.; Lu, Q.; Zhao, D. Controllable Assembly of Ordered Semiconductor Ag_2S Nanostructures. *Nano Lett.* **2003**, *3*, 85-88.

52. Pileni, M. P.; Motte, L.; Billoudet, F.; Lacaze, E.; Mahrt, J.; Willig, F. Nanosized Silver Sulfide Particles: Characterization, Self-Organization into 2D and 3D Superlattices. *Mater. Lett.* **1997**, *31*, 255-260.

53. Bagatur'yants, A. A.; Safonov, A. A.; Stoll, H.; Werner, H. J. Ab Initio Relativistic Pseudopotential Study of Small Silver and Gold Sulfide Clusters $(M_2S)_n$, n=1 and 2. *J. Chem. Phys.* **1998**, *109*, 3096-3108.

54. Leiggener, C.; Calzaferri, G. Synthesis and Luminescence Properties of Ag_2S and PbS Clusters in Zeolite *A. Chem. Eur. J.* **2005**, *11*, 7191 -7198.

55. Harris, D. C. *Quantitative Chemical Analysis*, 6th Ed., W.H. Freeman, New York, NY, **2002.**

56. Bujan, M.; Sikiric, M.; Filipovic-Vincekovic, N.; Vdovic, N; Garti, N., Furedi-Milhofer, H. Effect of Anionic Surfactants on Crystal Growth of Calcium Hydrogen Phosphate Dihydrate, *Langmuir,* **2001,** *17,* 6461-6470.

57. Chatterjee, A.; Moulik, S. P.; Sanyal, S. K.; Mishra, B. K.; Puri, P. M. Thermodynamics of Micelle Formation of Ionic Surfactants: A Critical Assessment for Sodium Dodecyl Sulfate, Cetyl Pyridinium Chloride and Dioctyl Sulfosuccinate (Na Salt) by Microcalorimetric, Conductometric, and Tensiometric Measurements**,** *J. Phys. Chem. B,* **2001,** *105,* 12823-12831.

58. Fan, Y.; Li, Y.; Yuan, G.; Wang, Y.; Wang, J.; Han, C. C.; Yan, H. Comparative Studies on the Micellization of Sodium Bis(4-phenylbutyl) Sulfossuccinate and Sodium Bis(2-ethylhexyl) Sulfosuccinate and Their Interaction with Hydrophobically Modified Poly(acrylamide). *Langmuir*, **2005**, *21*, 3814-3820.

59. Datwani, S. S.; Stebe, K. J. Surface Tension of an Anionic Surfactant: Equilibrium, Dynamics, and Analysis for Aerosol-OT. *Langmuir*, **2001**, *17*, 4287-4296.

60. Kashida, .S.; Watanabe, N.; Hasewaga, T.; Iida, H.; Mori, M.; Savrasov, S. Electronic structure of Ag_2S, band calculation and photoelectron spectroscopy. *Solid State Ionics*. **2003**, *158*, 167- 175. Mahapatra, S. K.; Bogle, K. A.; Dhole, S. D.; Bhoraska, V. N. Synthesis of Gold and Silver Nanoparticles by Electron Irradiation at 5-15 keV Energies. *Nanotechnology* **2007,** *18*, 135602-135607.

61. Zhang, J. Z. Interfacial Charge Carrier Dynamics of Semiconductor Nanoparticles. *J. Phys. Chem. B* **2000**, *104*, 7239-7253.

62. Wilkinson, J. P.; Martin, J. E.; Parsapour, F.; Wiedenman, B.; Kelley, D. F. Photoluminescence from Nanosize Gold Clusters. *J. Chem. Phys.* **1998**, *108*, *21*, 9137-9143.

63. Mori, J.; Miyashita, Y.; Oliveira, D.; Kasai, H.; Oikawa, H.; Nakanishi, H. Stopped-flow Analysis on the Mechanism of Perylene Nanoparticle Formation by the Reprecipitation Method. *J. Cryst. Growth*. **2009**, *311*, 553-555.

64. Moinard-Chécot, D.; Chevalier, Y.; Briançon, S.; Beney, L.; Fessi, H. Mechanism of Nanocapsules. Formation by the Emulsion–Diffusion Process. *J. Colloid Interface Sci.* **2008**, *317*, 458-468.

65. Bremholma, M.; Jensen, H.; Brummerstedt Iversen, S.; Brummerstedt Iversen, B. Reactor Design for in Situ X-ray Scattering Studies of Nanoparticle Formation in Supercritical Water Syntheses. *J. Supercrit. Fluid.* **2008**, *44*, 385-390.

66. Tiemann, M.; Marlow, F.; Brieler, F.; Linde´n, M. Early Stages of ZnS Growth Studied by Stopped-Flow UV Absorption Spectroscopy: Effects of Educt Concentrations on the Nanoparticle Formation. *J. Phys. Chem. B* **2006**, *110,* 23142-23147.

67. Chen, R.; Nuhfer, N.T.; Moussa, L.; Morris, H. R.; Whitmore, P.M. Silver Sulfide Nanoparticle Assembly Obtained by Reacting an Assembled Silver Nanoparticle Template with Hydrogen Sulfide Gas. *Nanotechnology* **2008**, *19,* 1-11.

68. Roig , B.; Chalmin, E.; Touraud, E.; Thomas, O. Spectroscopic Study of Dissolved Organic Sulfur (DOS): A Case Study of Mercaptans. *Talanta* **2002**, *56*, 585-590.

69. Guenther, E. A.; Johnson, K. S.; Coale, K. H. Direct Ultraviolet Spectrophotometric Determination of Total Sulfide and Iodide in Natural Waters. *Anal. Chem.* **2001,** *73*, 3481-3487.

70. Johnson, K. S.; Coletti, L. J. In Situ Ultraviolet Spectrophotometry for High Resolution and Long-term Monitoring of Nitrate, Bromide and Bisulfide in the Ocean. *Deep-Sea Research I* **2002**, *49*, 1291-1305.

71. Zuma, P.; Szafranskl, W. Ultraviolet Spectra of Hydroxide, Alkoxide, and Hydrogen Sulfide Anions. *Anal. Chem.* **1976,** *48*, 2162-263.

72. Murphy, C. J.; Copper, J. L. Quantum Dots: A Primer. *Appl. Spectrosc.* **2002**, *56*, 16A-36A.

73. Bawendi, M. G.; Steigerwald, M. L.; Brus, L. E. The Quantum Mechanics of Larger Semiconductor Clusters ("Quantum Dots"). *Annu. Rev. Phys. Chem.* **1990**, *41*, 477-496.

74. Steigerwald M. L.; Brus, L. E. Synthesis, Stabilization, and Electronic Structure of Quantum Semiconductor Nanoclusters. *Annu. Rev. Mater. Sci.* **1989**, *19*, 471-495.

75. Yoffe, A. D. Semiconductor Quantum Dots and Related Systems: Electronic, Optical, Luminescence and Related Properties of Low Dimensional Systems. *Adv. Phys.* **2001**, *50*, 1-208.

76. Reithmaier, J. P. Strong Exciton–Photon Coupling in Semiconductor Quantum Dot Systems. Semicond. *Sci. Technol.* **2008**, *23*, 123001-123019.

77. Wang, Y.; Herron, N. Quantum Size Effects on the Exciton Energy of CdS Clusters. *Phys. Rev. B.* **1990**, *42*, 7253-7255.

78. Motte, L.; Urban, J. Silver Clusters on Silver Sulfide Nanocrystals: Synthesis and Behavior After Electron Beam Irradiation. J. Phys. Chem. B, **2005**, 109, 21499-21501.

79. Wang, C. X.; Yang, G. W. Thermodynamics of Metastable Phase Nucleation at the Nanoscale. *Mat. Sci. Eng. R* **2005**, *49*, 157-202.

80. Tobler, D. J.; Shaw, S. ; Benning, L. G. Quantification of Initial Steps of Nucleation and Growth of Silica Nanoparticles: An *in-situ* SAXS and DLS Study. *Geochim. Cosmochim. Ac.* **2009**, *73*, 5377-5393.

81. Abe´cassis, B.; Testard, F.; Spalla, O.; Barboux, P. Probing In Situ the Nucleation and Growth of Gold Nanoparticles by Small-Angle X-ray Scattering. *Nano Lett.* **2007**, *7*, 1723-1727.

82. Rizza, G.; Ramjauny, Y.; Gacoin, T.; Vieille, L.; Henry, S. Chemically Synthesized Gold Nanoparticles Embedded in a SiO_2 Matrix: A Model System to Give Insights into Nucleation and Growth Under Irradiation. *Phys. Rev. B*, **2007**, *76*, 245414-245423.

83. Nozawa, K.; Hélène Delville, M.; Ushiki, H.; Panizza, P.; Pierre Delville, J. Growth of Monodisperse Mesoscopic Metal-Oxide Colloids Under Constant Monomer Supply. *Phys. Rev. E* **2005**, *72*, 011404-011412.

84. Menoni, C. S.; Miao, L.; Patel, D.; Mic'ic', O. I.; Nozik, A. J. Three-Dimensional Confinement in the Conduction Band Structure of InP. *Phys. Rev. Lett.* **2000**, *84*, 4168-4171.

85. Luo, J. W.; Franceschetti, A.; Zunger, A. Direct-Bandgap InAs Quantum-Dots Have Long-Range Electron–Hole Exchange Whereas Indirect Gap Si Dots Have Short-Range Exchange. *Nano Lett.* **2009**, *9*, 2648-2653.

86. Luo, J. W.; Franceschetti, A.; Zunger, A. Quantum-Size-Induced Electronic Transitions in Quantum Dots: Indirect Band-Gap GaAs. *Phys. Rev. B* **2008**, *78*, 035306-035314.

87. Privman, V. Diffusional Nucleation of Nanocrystals and Their Self-Assembly into Uniform Colloids. *J. Optoelectronics Adv. Mater.* **2008**, *10*, 2827-2839.

88. Irizarry, R. Simulated Dynamic Optical Response Strategy for Model Identification of Metal Colloid Synthesis. *Ind. Eng. Chem. Res.*, **2010**, *49,* 5588–5602.